https://ntrs.nasa.gov/search.jsp?R=19820007202 2020-03-21T09:42:59+00:00Z

NASA
TP
1360
c.1

NASA Technical Paper 1360

LOAN COPY: RETURN TO
AFWL TECHNICAL LIBRARY
KIRTLAND AFB, N. M.

TECH LIBRARY KAFB, NM
0134372

Longitudinal and Lateral Static Stability and Control Characteristics of a 1/6-Scale Model of a Remotely Piloted Research Vehicle With a Supercritical Wing

Thomas A. Byrdsong and James B. Hallissy

MAY 1979

FOR EARLY DOMESTIC DISSEMINATION

Because of its significant early commercial potential, this information, which has been developed under a U.S. Government program, is being disseminated within the United States in advance of general publication. This information may be duplicated and used by the recipient with the express limitation that it not be published. Release of this information to other domestic parties by the recipient shall be made subject to these limitations.

Foreign release may be made only with prior NASA approval and appropriate export licenses. This legend shall be marked on any reproduction of this information in whole or in part.

Date for general release December 31, 1980

14 MAY 1979
Technical Library

errata made
2-20-81 dw

ERRATA

NASA Technical Paper 1360

LONGITUDINAL AND LATERAL STATIC STABILITY AND CONTROL CHARACTERISTICS OF A 1/6-SCALE MODEL OF A REMOTELY PILOTED RESEARCH VEHICLE WITH A SUPERCRITICAL WING

Thomas A. Byrdsong and James B. Hallissy

May 1979

Please make the following corrections:

Page 58, figure 11(b): In the key, the value corresponding to the test-point symbol Δ should be -6

Page 77, figure 21: The ordinate scale values should be 0, -.02, -.04, -.06, -.08, -.10

ISSUED SEPTEMBER 1979

FEDD DOCUMENT

Note that this document bears the label "FEDD," an acronym for "FOR EARLY DOMESTIC DISSEMINATION." The FEDD label is affixed to documents that may contain information having high commercial potential.

The FEDD concept was developed as a result of the desire to maintain U.S. leadership in world trade markets and encourage a favorable balance of trade. Since the availability of tax-supported U.S. technology to foreign business interests could represent an unearned benefit, research results that may have high commercial potential are being distributed to U.S. industry in advance of general release.

The recipient of this report must treat the information it contains according to the conditions of the FEDD label on the front cover.

TECH LIBRARY KAFB, NM

0134372

NASA Technical Paper 1360

Longitudinal and Lateral Static Stability and Control Characteristics of a 1/6-Scale Model of a Remotely Piloted Research Vehicle With a Supercritical Wing

Thomas A. Byrdsong and James B. Hallissy
Langley Research Center
Hampton, Virginia

NASA
National Aeronautics
and Space Administration

Scientific and Technical
Information Office

1979

SUMMARY

An investigation has been conducted in the Langley 8-foot transonic pressure tunnel to determine the longitudinal and lateral-directional static stability and control characteristics of a 1/6-scale force model of a remotely piloted research vehicle. The model was equipped with a supercritical wing and employed elevons for pitch and roll control. Test conditions were as follows: Reynolds number of about 6.6×10^6 per meter, variations of sideslip from about -6° to 6°, elevon deflection angle (symmetrically and asymmetrically) from -9° to 3°, and rudder deflection angle from 0° to -10°.

The model was longitudinally statically stable at angles of attack up to about 7°, which is significantly greater than the angle of attack for the cruise condition (approximately 4°). In the range of test Mach numbers, the model was directionally stable and had positive effective dihedral, sufficient pitch control, and positive effectiveness of roll and yaw control. The drag-divergence Mach number (defined as the Mach number where $\partial C_D/\partial M = 0.10$ where C_D and M represent drag coefficient and Mach number, respectively) decreased slightly as lift coefficient was increased.

INTRODUCTION

The National Aeronautics and Space Administration has initiated a flight-test program to evaluate an active control-flutter suppression system and to obtain transonic flight-load measurements for a flexible, supercritical wing. The program utilizes an existing target drone (Teledyne Ryan Firebee II) modified for use as a test-bed aircraft. The Firebee II is a highly maneuverable, supersonic aircraft designed for relatively high load factors and equipped with elevons for pitch and roll control. For the flight test program the production wing of the test-bed aircraft will be replaced with a new aeroelastic research wing that was designed to flutter within the flight envelope of the research vehicle. The geometry of the research wing is a scaled version of the supercritical wing used in the flight-test program reported in reference 1.

A wind-tunnel investigation was conducted to provide data for the assessment of stability and control characteristics and for the design of the flight-vehicle control system to ensure the success of the proposed flight tests. In addition, these data are needed to provide vehicle flight characteristics to a computer simulation program that provides assistance in planning and execution of specific flight-research missions and for the assessment of structural loadings at critical points in the flight envelope.

The purpose of this paper is to document the results, with limited analysis, of wind-tunnel measurements of the total aerodynamic forces and moments for a 1/6-scale force model of the Firebee II aircraft equipped with an NASA supercritical wing. The wind-tunnel tests were conducted in the Langley 8-foot transonic pressure tunnel at Mach numbers from 0.400 to 0.980, angles of attack

from approximately -4° to 12°, angles of sideslip from approximately 6° to -6°, and at a Reynolds number of approximately 6.6×10^{6} per meter.

SYMBOLS

All data presented herein are referenced to a stability-axis system (ref. 2). Total force and moment data have been reduced to conventional coefficient form based on the geometry of the reference wing planform, that is, the planform produced by extending the straight leading and trailing edges of the outboard sections of the wing to the fuselage center line. The total pitching-moment coefficients are referenced to the quarter-chord point of the mean geometric chord of the reference wing panel. This point is located at model station 0.76 m. All dimensions are given in SI units; however, measurements and calculations were made in U.S. Customary Units.

b wing span

c streamwise local chord of wing (includes leading-edge glove and trailing-edge extension)

$\bar{c}$ wing mean geometric chord

$\bar{c}_t$ elevon mean geometric chord

C_D drag coefficient (corrected for fuselage base pressure and duct internal flow), $\frac{\text{Drag}}{qS}$

$C_{D,i}$ duct internal drag force coefficient, $\frac{\text{Internal drag force}}{qS}$

C_{D_u} effect of speed on drag coefficient, $M \frac{\partial C_D}{\partial M}$

C_{D_α} slope of drag curve, per deg

C_L lift coefficient, $\frac{\text{Lift}}{qS}$

C_{L_u} effect of speed on lift coefficient, $\frac{M^2}{1 - M^2} C_L$

C_{L_α} slope of lift curve (measured in angle-of-attack range from 1° to 5°), per deg

$C_{L_{\delta_e}}$ effect of symmetric elevon deflection on lift coefficient, $\frac{\partial C_L}{\partial \delta_e}$, per deg

C_l rolling-moment coefficient, $\frac{\text{Rolling moment}}{qSb}$

C_{l_β} effective dihedral parameter, $\frac{\partial C_l}{\partial \beta}$, per deg

$C_{l_{\delta_a}}$ asymmetric elevon effectiveness parameter, $\frac{\partial C_l}{\partial \delta_a}$, per deg

$C_{l_{\delta_r}}$ effect of rudder deflection on rolling-moment coefficient $\frac{\Delta C_l}{\Delta \delta_r}$

C_m pitching-moment coefficient, $\frac{\text{Pitching moment}}{qS\bar{c}}$

$C_{m,o}$ pitching-moment coefficient at zero lift

C_{m_u} effect of speed on pitching-moment coefficient, $M \frac{\partial C_m}{\partial M} + \rho u^2 \frac{\partial C_m}{\partial q}$

$C_{m_{C_L}}$ slope of pitching-moment coefficient against lift-coefficient curve, $\frac{\partial C_m}{\partial C_L}$

C_{m_α} slope of pitching-moment coefficient against angle-of-attack curve, per deg

$C_{m_{\delta_e}}$ elevon effectiveness in pitch parameter, $\frac{\partial C_m}{\partial \delta_e}$, per deg

C_n yawing-moment coefficient, $\frac{\text{Yawing moment}}{qSb}$

C_{n_β} directional-stability parameter, $\frac{\partial C_n}{\partial \beta}$, per deg

$C_{n_{\delta_a}}$ effect of asymmetric elevon deflection on yawing-moment coefficient, $\frac{\partial C_n}{\partial \delta_a}$, per deg

$C_{n_{\delta_r}}$ rudder-effectiveness parameter, $\frac{\Delta C_n}{\Delta \delta_r}$, per deg

$C_{p,b}$ fuselage base-pressure coefficient, $\frac{p_b - p}{q}$

C_Y side-force coefficient, $\frac{\text{Side force}}{qS}$

C_{Y_β} side-force parameter, $\frac{\partial C_Y}{\partial \beta}$, per deg

$C_{Y_{\delta_a}}$ effect of asymmetric elevon deflection on side-force coefficient, $\frac{\partial C_Y}{\partial \delta_a}$, per deg

$C_{Y_{\delta_r}}$ effect of rudder deflection on side-force coefficient, $\frac{\Delta C_Y}{\Delta \delta_r}$, per deg

M free-stream Mach number

m local airfoil slope, $\frac{dz}{dx}$

p free-stream static pressure

p_b static pressure at fuselage base

q free-stream dynamic pressure

R free-stream Reynolds number per meter

S planform area of basic wing panels (including fuselage intercept)

t local wing thickness

t_{te} airfoil trailing-edge thickness

u forward speed

x streamwise distance measured from leading edge of total wing planform, positive toward wing trailing edge

y spanwise distance measured normal to model plane of symmetry, zero at fuselage center line

z vertical distance from wing reference chord

z_w vertical location of wing reference chord line at fuselage plane of symmetry; water line, 0.024 m (fig. 1(c))

α angle of attack relative to fuselage reference line (see fig. 1(c)), deg

β angle of sideslip, deg

δ_a effective asymmetric elevon-deflection angle (positive trailing edge down), $\frac{\delta_{HL} - \delta_{HR}}{2}$, deg

δ_e symmetric elevon deflection angle (positive trailing edge down), deg

$\delta_{e\alpha}$ symmetric elevon-control sensitivity, $\frac{C_{m_\alpha}}{C_{m_{\delta_e}}}$

δ_{HL} left elevon deflection angle (positive trailing edge down), deg

δ_{HR} right elevon deflection angle (positive trailing edge down), deg

δ_r rudder deflection angle (positive trailing edge left), deg

$\delta_{r\beta}$ rudder-control sensitivity, $-\frac{\Delta C_n/\Delta\beta}{\Delta C_n/\Delta\delta_r}$

θ angle of twist of local airfoil section (angle between the wing reference chord line and a line through the nose and a point midway between the upper and lower surfaces at the airfoil maximum thickness), deg

ρ test-medium density

APPARATUS AND PROCEDURE

Model Description

The wind-tunnel investigation utilized a 1/6-scale force model of the test-bed aircraft with a scaled-down version of the NASA supercritical wing developed for the F-8 flight-test program (ref. 1). The general arrangement of

the wind-tunnel model is shown in figure 1(a); some pertinent dimensions are shown in figure 1(b); and variation of fuselage cross-sectional shape is shown in figure 1(c); and photographs of the model mounted in the wind tunnel are shown in figure 2. The wing had an aspect ratio of 6.8, a taper ratio of 0.36, and a sweepback angle of the quarter-chord line of 42.24°. Nondimensional coordinates used to fabricate the model wing are presented in table I. An airfoil shape and a typical variation of shape and upper and lower surface slopes are shown in figure 3. These data were obtained from coordinates presented in table I and from measurements of the wing at the 70-percent-semispan station. Wing twist distributions are shown in figure 4. Variations of wing thickness-to-chord ratio and trailing-edge thickness are shown in figure 5. As shown in figure 5(b) the trailing edge for the model wing was squared to facilitate fabrication, whereas the wing trailing edge for the flight vehicle was beveled (table I); this alteration was not expected to have a noticeable effect on the wing aerodynamics. The angle of incidence of the wing reference chord at the fuselage center line was 0°.

The model fuselage was equipped with a single flow-through duct that simulated the intake and exit engine ducts. The aft end of the fuselage was modified to allow for the wind-tunnel sting support. (See fig. 6.) The modification deleted approximately 18 cm of the aft fuselage to provide a 5.1-cm-diameter clearance hole through the fuselage to the balance cavity for the sting support. Four static-pressure orifices were located on the exit duct wall near the base, and two static-pressure orifices were located in the fuselage balance cavity. The exit-duct static-pressure orifices complemented a 16-tube total-pressure rake that provided measurements of internal drag and mass-flow data. A photograph of the rake attached to the aft-fuselage exit duct is presented in figure 2(b). The keel and parachute riser housing of the full-scale vehicle were also simulated on the model (figs. 2 and 6).

Deflected rudder data were obtained by using rudders that were fabricated to predetermined deflection angles of 0° and -10°. The right and left elevons were attached in a manner which allowed manually variable independent deflections of each elevon in the range from -15° to 9°. The range of rudder deflection for the flight vehicle is from -10° to 10°, and the range of elevon deflection is from -12° to 7°.

Test Facility

The investigation was conducted in the Langley 8-foot transonic pressure tunnel (ref. 3). This facility is a continuous-flow, single-return, slotted-throat tunnel having controls that allow for the independent variation of Mach number, density, temperature, and dewpoint. The test section is square in cross section with the upper and lower walls axially slotted (each wall having an open ratio of approximately 0.06) to permit changing the test-section Mach number continuously through the transonic speed range. The stagnation pressure in the tunnel can be varied from a minimum value of about 0.25 atmosphere at all test Mach numbers to a maximum value of approximately 1.5 atmospheres at transonic Mach numbers and to approximately 2.0 atmospheres at Mach numbers of 0.400 or less.

Boundary-Layer Transition

Boundary-layer transition on the model was determined with the aid of references 4 and 5 and from experience gained with similar wind-tunnel models. Fixed-transition strips were used that consisted of 0.25-cm-wide bands of carborundum grains embedded in a plastic adhesive. The size and location of the transition strips are presented in figure 7. The outboard portion of the wing upper surface strip was positioned in a conventional location near the leading edge (10 percent c), and the lower surface strip was positioned well aft (22 percent c) of the leading edge to prevent an unrealistically thick boundary-layer buildup ahead of the trailing-edge cusp region. The more forward locations of the inboard portions of the wing upper surface strip were based on previous investigations (ref. 1). The surface forward of the strips on all regions of the model was kept exceptionally smooth to maintain laminar flow.

Measurements and Test Conditions

Measurements were obtained to evaluate the longitudinal and lateral-directional characteristics for the model over ranges of angle of attack from about -4° to 12°, angle of sideslip from about -6° to 6°, and Mach number from about 0.400 to 0.980, all for a Reynolds number of approximately 6.6×10^{6} per meter. Static aerodynamic force and moment measurements were obtained by means of an internally mounted six-component strain-gage balance which, in turn, was rigidly mounted to a tapered sting-support system. Basic longitudinal data were obtained for all control surfaces undeflected. In addition, yaw-control data were obtained by rudder deflection, and pitch- and roll-control data were obtained by symmetric and asymmetric elevon deflections, respectively.

The static pressures in the balance cavity and in the plane of the model base were recorded for determination of the base drag by using differential-pressure transducers referenced to the free-stream static pressure. The internal-drag coefficients were determined from measurements of the total-pressure distribution and the static pressure in the duct exit area.

Accuracies and Corrections

The maximum allowable loadings for the six-component balance used in this investigation were as follows: normal force, 1890 N; axial force, 378 N; side force, 1779 N; pitching moment, 226 N-m; rolling moment, 23 N-m; and yawing moment, 113 N-m. The accuracy of each component of the balance was estimated to be half of 1 percent of the maximum value.

The differential-pressure transducers used with the scanning-valve units for the static and rake total pressures had a maximum range of 17.2 kN/m^2. The estimated accuracy of these transducers was 1 percent of the maximum range.

The measured angles of attack have been corrected for deflections of the model support sting and balance which occurred as a result of aerodynamic loads

on the model. Further corrections to the measured angles of attack were made for the tunnel airflow angularity. At the maximum lift coefficients, the angles of attack are estimated to be within $\pm 0.1^{\circ}$; and near cruise lift coefficients, the angles of attack are estimated to be within $\pm 0.05^{\circ}$. The accuracies for the angles of sideslip are estimated to be approximately 0.1°.

The drag results presented herein have been corrected for the internal drag of the engine air duct (see fig. 8) and for the fuselage base pressure $C_{p,b}$. No corrections have been applied to the data for sting-interference effects other than exclusion of the base drag from the total measured drag. However, the model support sting was selected on the basis of reference 6 to minimize sting interference at near-sonic Mach numbers. Furthermore, no corrections have been applied to the data for the effects of either solid wake blockage or lift interference due to wall effects. The estimated accuracy of Mach number was 0.003.

PRESENTATION OF RESULTS

The results of this investigation are presented in the following figures:

	Figure
Basic longitudinal aerodynamic characteristics:	
Longitudinal aerodynamic characteristics at two angles of sideslip; $\delta_e = 0^{\circ}$; $0.400 \leq M \leq 0.980$	9
Effect of sideslip on longitudinal aerodynamic coefficients for two angles of attack; $\delta_e = 0^{\circ}$; $0.400 \leq M \leq 0.980$	10
Effect of symmetric elevon deflection on longitudinal aerodynamic characteristics	11
Summary of longitudinal aerodynamic characteristics:	
Variation of pitch-up angle of attack $\left(C_{m_\alpha} = 0\right)$ with Mach number; $\delta_e = 0^{\circ}$	12
Variation of drag coefficient with Mach number for three values of lift coefficient; $\delta_e = 0^{\circ}$	13
Variation of drag-divergence Mach number with lift coefficient	14
Variation of zero-lift pitching-moment coefficient with Mach number; $\delta_e = 0^{\circ}$	15
Variation of $C_{m_{C_L}}$ with Mach number; $\delta_e = 0^{\circ}$	16
Variation of untrimmed lift-curve slope with Mach number; $\delta_e = 0^{\circ}$	17
Variation of pitching-moment-curve slope with Mach number; $\delta_e = 0^{\circ}$	18
Variation of drag-curve slope with Mach number for five angles of attack; $\delta_e = 0^{\circ}$	19
Variation of the lift effectiveness $C_{L_{\delta_e}}$ with Mach number	20
Variation of pitch-control power $C_{m_{\delta_e}}$ with Mach number	21
Variation of pitch-control sensitivity δ_{e_α} with Mach number	22

Figure

Variation of the derivative $\partial C_L/\partial M$ with Mach number for three symmetric elevon deflections at three angles of attack 23
Variation of the derivative $\partial C_m/\partial M$ with Mach number for three symmetric elevon deflections at three angles of attack 24
Variation of the derivative $\partial C_D/\partial M$ with Mach number for three symmetric elevon deflections at three angles of attack 25

Basic lateral-directional aerodynamic characteristics:
Lateral-directional aerodynamic characteristics at two angles of attack; $\delta_e = 0^\circ$ 26
Effect of angle of attack on lateral-directional aerodynamic characteristics at two angles of sideslip; $\delta_e = 0^\circ$ 27
Effect of asymmetric elevon deflection on lateral-directional aerodynamic characteristics; $\beta = 0^\circ$ 28
Effect of rudder deflection on lateral-directional aerodynamic characteristics; $\beta = 0^\circ$ 29
Effect of rudder deflection on lateral-directional aerodynamic characteristics; $\alpha = 2.2^\circ$ 30

Summary of lateral-directional aerodynamic characteristics:
Variation of lateral-directional stability characteristics with Mach number at two angles of attack 31
Variation of lateral-directional aileron-control (asymmetric elevon) derivatives with Mach number at three angles of attack; $\beta = 0^\circ$ 32
Variation of lateral-directional rudder-control derivatives with Mach number at three angles of attack 33
Variation of rudder-control sensitivity with Mach number; average α, 2.2° 34

DISCUSSION OF RESULTS

Longitudinal Aerodynamic Characteristics

The longitudinal aerodynamic characteristics of the model are presented in figure 9 as a function of angle of attack for sideslip angles of 0° and 2.2° and for 0° elevon deflection. The data indicate that differences of more than a few percent for corresponding values of the coefficients do not appear until a Mach number of 0.950 is obtained. There was very little difference in the longitudinal aerodynamic characteristics for sideslip angles of 0° and 2.2° over the range of Mach numbers investigated.

The longitudinal aerodynamic characteristics of the model are presented in figure 10 as a function of sideslip. The data show variations of the longitudinal coefficients over a range of sideslip angles from approximately -6° to 6° for average angles of attack of 2.2° (range from 2.1° to 2.3°) and 5.6° (range from 5.3° to 5.7°) in the test Mach number range. The data show a negligible effect of sideslip on the lift and drag coefficients and a more

noticeable effect of sideslip on the pitching-moment coefficient. A minimum pitching-moment coefficient was generally developed for a sideslip angle near or slightly greater than 0°. As the Mach number was increased, the effect of sideslip on the pitching-moment coefficient also increased. In addition, the data indicate that the effect of sideslip on the pitching-moment coefficient was larger for an average angle of attack of 5.6° than the effect of sideslip for an average angle of attack of 2.2° throughout the Mach number range except for a Mach number of 0.900 where limited data were obtained.

The effect of symmetric elevon deflection on the longitudinal aerodynamic characteristics is presented in figure 11. Data are presented for deflection angles of -6°, -3°, 0°, and 3° and for the tail-off condition. The data indicate that the lift coefficient increased and the pitching-moment coefficient decreased as elevon deflection was varied from -6° to 3°. In general, the results indicate that the model could have been trimmed throughout the range for Mach numbers for low to moderate angles of attack for a relatively small, symmetric elevon deflection angle.

The variation with Mach number of the angle of attack at which a pitch-up condition occurs is shown in figure 12 for the basic data presented in figure 9. Included in the figure are data from previous investigations of similar wing designs (refs. 7 and 8). The data of figure 12 indicate an approximate pitch-up angle of attack of about 7° for Mach numbers from about 0.700 to 0.950. At Mach numbers below and above this range, the pitch-up angle of attack is indicated to be substantially higher. The angle of attack at the cruise condition for this flight configuration was determined to be approximately 4° based on the results from a previous feasibility study (ref. 9) and figure 9(f) (for the following cruise conditions: $C_L = 0.36$; $M = 0.980$; altitude, 13.72 km; and $R = 3.33 \times 10^6$, full scale). This value for angle of attack is substantially smaller than the pitch-up angle of attack shown by the results of figure 12. Pitch-up will not be a problem for the research flights planned for the flight vehicle since angle of attack will be held to less than 6°. However, for flight conditions at angles of attack larger than 6° the addition of underwing leading-edge vortex generators can be used to postpone the pitch-up angle of attack to higher values (ref. 10).

The drag characteristics for the model are presented in figure 13 as a function of Mach number for lift coefficients of 0.20, 0.36, and 0.50. The data show a characteristic drag rise at the higher Mach numbers (from 0.800 to 0.980). The drag-divergence Mach number (drag-divergence Mach number is defined as the Mach number at which $\partial C_D/\partial M = 0.10$) as a function of lift coefficient is presented in figure 14. The data of figure 14 indicate a maximum drag-divergence Mach number for a lift coefficient of about 0.15 and a slight reduction in the value of the drag-divergence Mach number for other values of lift coefficient. At the design lift coefficient of 0.36, the data indicate a drag-divergence Mach number of approximately 0.94. This value corresponds to a drag-divergence Mach number of 0.96 which was obtained for the F-8 configuration reported in reference 1.

(It is of interest to note the significant difference in the primary wing-design emphasis between the F-8 configuration (ref. 1) and the Firebee II research vehicle of this investigation. The F-8 configuration was designed to

demonstrate optimum cruise condition (C_L = 0.40; M = 0.970; altitude, 6.4 km) for a supercritical wing representative of that for an advanced transport designed for near-sonic flight. The Firebee II was configured with the supercritical wing used on the F-8 configuration without effort to optimize the performance on the Firebee vehicle. The primary purposes of the present tests are to aid in the development and analysis of active control systems for flutter suppression and to obtain measurements of aerodynamic loadings for this aeroelastic research wing at high subsonic and transonic Mach numbers at load factors up to 2.5g. The full-scale Reynolds number (based on the wing mean aerodynamic chord) for the F-8 configuration was approximately 10.6×10^6 at the design condition; for the Firebee II configuration, the full-scale Reynolds number is estimated to be about 3.7×10^6 (ref. 9).)

The variation of zero-lift pitching-moment coefficient with Mach number is shown in figure 15 for 0° elevon deflection. The data indicate a small change in the magnitude of the zero-lift pitching-moment coefficient in the Mach number range from 0.400 to 0.925 and a substantial increase in the magnitude of the pitching-moment coefficient at higher Mach numbers. A positive value for the zero-lift pitching-moment coefficient is indicated throughout the range of Mach numbers.

Variation of the derivative $C_{m_{C_L}}$ with Mach number is presented in figure 16 for an elevon deflection of 0°. Data are presented for a range of lift coefficients from 0 to 0.50. The data indicate negative values for $C_{m_{C_L}}$ in the range of test Mach numbers and a significant increase (negative) in the magnitude of $C_{m_{C_L}}$ for Mach numbers greater than 0.900. This rapid change in the value of the derivative $C_{m_{C_L}}$ is primarily attributed to the change in pitching moment associated with a rearward shift in the position of the wing center of pressure with increasing Mach number.

Variation of the lift-curve slope with Mach number is presented in figure 17 for an angle-of-attack range from 1° to 5° and an elevon deflection of 0°. The data show a gradually increasing lift-curve slope with a greater rate of increase for Mach numbers greater than 0.800 and a maximum lift-curve slope at a Mach number of 0.950.

Variation of the pitching-moment-curve slope with Mach number is presented in figure 18. These data show that the model was statically stable in the range of test numbers, with a significant increase in the static stability for Mach numbers between 0.800 and 0.980. This increase in longitudinal stability with Mach number was accompanied by a positive increase of the zero-lift pitching-moment coefficient (fig. 15) which tends to offset the pitching-moment-coefficient trim increment resulting from increased stability.

Variation of the drag-curve slope with Mach number is presented in figure 19. These data which were obtained from the results of figure 9 are presented for angles of attack from 1° to 5° and for 0° elevon deflection. Large variations of the drag-curve slope are indicated for the range of Mach numbers

from 0.800 to 0.980. The angle of attack for minimum drag (i.e., when $C_{D_\alpha} = 0$) is shown to increase from a value slightly larger than 1° at Mach numbers in the range from 0.400 to about 0.700 or 0.800 to an angle of attack of 2° at a Mach number of 0.970. Both angle of attack and Mach number have considerable effect on the drag-curve slope.

Variations of elevon effectiveness on lift and pitching moment and variation of elevon-control sensitivity with Mach number are presented in figures 20, 21, and 22, respectively. These data were obtained for an angle-of-attack range from 2° to 6° and symmetric elevon deflections of -6°, -3°, 0°, and 3°. The lift effectiveness (fig. 20) and the pitching-moment effectiveness (fig. 21) increased gradually as Mach number was increased from 0.400 to 0.980. The lift effectiveness increased about 33 percent and the pitching-moment effectiveness increased about 40 percent. The symmetric elevon-control sensitivity (fig. 22) increased slightly for Mach numbers up to about 0.900. As Mach number was varied from 0.900 to 0.980, the elevon-control sensitivity more than doubled in magnitude. The data (fig. 22) indicate that at the higher Mach numbers (Mach numbers greater than 0.900) a larger change of symmetric elevon deflection is required to effect a given degree of change of angle of attack than at the lower Mach numbers.

The rate of change of the lift, pitching moment, and drag relative to Mach number are presented in figures 23, 24, and 25 as a function of Mach number, respectively. Data are shown for angles of attack of 2°, 3°, and 4° and for symmetric elevon deflections of -6°, 0°, and 3°. These data are useful in determining the speed derivatives C_{L_u}, C_{m_u}, and C_{D_u} which are required for dynamic-stability analysis of the flight configuration. The data, in general, indicate a relative insensitivity to Mach number in the low-speed range (i.e., for Mach numbers between 0.400 and 0.800); however, for Mach numbers greater than 0.800, all those derivatives vary rapidly with increasing Mach number and approach very large magnitudes.

Lateral-Directional Aerodynamic Characteristics

Variations of the lateral-directional aerodynamic coefficient with angle of sideslip are presented in figure 26 for average angles of attack of 2.2° and 5.6° (ranges from 2.1° to 2.3° and 5.3° to 5.7°, respectively) and for a range of Mach numbers from 0.400 to 0.980. The data indicate a nearly linear variation of the lateral-directional aerodynamic coefficients with angle of sideslip. A sizable effect of angle of attack is indicated for the rolling moments and a small or negligible effect of angle of attack is indicated for the yawing moment and side force throughout the Mach number range.

Variations of the lateral-directional aerodynamic coefficients with angle of attack are presented in figure 27 for sideslip angles of 0° and 2°. The data indicate a small or negligible effect of angle of attack on the rolling-moment coefficient for a sideslip angle of 0° and for an angle-of-attack range from about -2° to 6°. At angles of attack above 6° and for Mach numbers of 0.400 and 0.980, the data show that the rolling-moment coefficient became larger

as angle of attack was increased. A significant effect of angle of attack on the rolling-moment coefficient for a sideslip angle of 2° is shown throughout the Mach number range. In several cases, peaks are observed in the curve of rolling-moment coefficient at or near the angle of attack where a break occurs in the lift curve and where pitch-up is also indicated. (See, for example, fig. 27(c) and fig. 9(c).) This effect can be expected with asymmetric flow conditions at angles of sideslip other than 0°. A small effect of angle of attack is also shown for the yawing-moment coefficient (fig. 27). A gradual reduction of yawing-moment coefficient with increasing angle of attack characterizes the data for sideslip angles of 0° and 2° in the Mach number range from 0.800 to 0.980. The side-force coefficient shows a negligible effect of angle of attack at sideslip angles of 0° and 2° throughout the Mach number range.

The effect of asymmetric elevon deflection on the lateral-directional aerodynamic characteristics is presented in figure 28. These data show variations of the rolling-moment, yawing-moment, and side-force coefficients with angle of attack for three asymmetric elevon deflections of 0°, 3°, and 6°, and a sideslip angle of 0° in the range of test Mach numbers. The offsets of the coefficients for undeflected elevons are attributed to asymmetry of the model. The variation of the coefficients with angle of attack is generally smooth; however, data for the rolling-moment coefficient at the higher Mach numbers of 0.900 and 0.980 (figs. 28(c) and 28(d), respectively) show significant nonlinear variations near angles of attack where a pitch-up condition ($C_m = 0$) occurs (fig. 9). These variations are considered to be primarily associated with asymmetric wing stall (an effect also noted in ref. 11, which reports on a similar study for the research of ref. 1) and occur at lift coefficients that are well beyond the operating range of the flight vehicle. The data also show a general reduction of yawing-moment coefficient due to roll control with increasing angle of attack in the test Mach number range. A change from positive to negative yawing-moment coefficients is indicated for Mach numbers of 0.900 and 0.980 at the higher angles of attack.

The effect of rudder deflection on the lateral-directional aerodynamic characteristics is presented in figures 29 and 30. The data show variations of the rolling-moment, yawing-moment, and side-force coefficients with angle of attack (fig. 29) and angle of sideslip (fig. 30) for rudder deflections of 0° and -10° (trailing edge to the right). The primary effect of rudder deflection is indicated by the relatively large positive yawing moments for the ranges of angle of attack, angle of sideslip, and Mach number. The data of figure 29 also indicate that the effect of rudder deflection on the rolling-moment coefficient is decreased as the angle of attack is increased, and there is a negligible influence of angle of attack on the yawing-moment and side-force coefficients. The results of figures 29 and 30 indicate that rudder deflection provides significant positive directional control and smaller side effects of rolling moment and side force.

Variations of the static lateral-directional stability characteristics with Mach number for two angles of attack are presented in figure 31. The data show that the model had positive effective dihedral (negative values of the rolling-moment derivative) and was directionally stable (positive values of the yawing-moment derivative). Large variations of the rolling-moment derivative

are shown for Mach numbers greater than 0.800, with the more severe excursion shown for the larger angle of attack. The yawing-moment derivative (the directional stability derivative) and the side-force derivative generally show a very small effect of angle of attack.

Variations of the roll-control derivatives (asymmetric elevon) with Mach number are presented in figure 32 for three angles of attack. These data were obtained for effective asymmetric elevon deflections of 0° ($\delta_{HL} = 0^{\circ}$, $\delta_{HR} = 0^{\circ}$), 3° ($\delta_{HL} = 3^{\circ}$, $\delta_{HR} = -3^{\circ}$), and 6° ($\delta_{HL} = 3^{\circ}$, $\delta_{HR} = -9^{\circ}$) for 0° sideslip. The data show that roll-control effectiveness was positive (positive values of the rolling-moment derivative) for angles of attack of 0°, 2°, and 4°. Near-constant values of roll-control effectiveness were developed for Mach numbers up to about 0.900, and larger values of roll-control effectiveness were developed at the higher Mach numbers (about 0.900) for angles of attack of 2° and 4°. The data also show that the cross-control derivative (yawing moment due to asymmetric control) was positive for angles of attack of 0°, 2°, and 4° and that the derivative decreased slightly with increasing angle of attack. The cross-control derivative also increased as the Mach number was increased. Negative values of the side-force derivative were developed for the ranges of angle of attack and Mach number, and larger negative values of side-force derivative were developed as Mach number was increased.

Variations of the rudder-control derivatives with Mach number are presented in figure 33 for three angles of attack. The data show that the rudder-control derivatives were not significantly affected by angles of attack of 0°, 2°, and 4°. The rolling-moment derivative was positive and essentially unchanged in the Mach number range. The data also indicated positive rudder effectiveness (negative values of the yawing-moment derivative). The yawing-moment derivative increased only slightly (to larger negative values) as Mach number was increased. The side force due to directional control was positive also and increased only slightly as Mach number was increased.

Variation of the rudder-control sensitivity with Mach number is presented in figure 34 for an average angle of attack of 2.2° (2.1° to 2.3°). The data show that the rudder-control sensitivity was approximately constant for the test condition.

CONCLUDING REMARKS

A wind-tunnel investigation has been conducted to determine the longitudinal and lateral static stability and control characteristics of a 1/6-scale force model of a remotely piloted research vehicle with a supercritical wing. The model was tested at Mach numbers from 0.400 to 0.980, at angles of attack from about -4° to 12°, and at angles of sideslip from about -6° to 6°.

The model exhibited a pitch-up characteristic at an angle of attack of approximately 7° for Mach numbers from 0.700 to 0.950. However, the pitch-up angle of attack was significantly greater for Mach numbers of 0.400 and 0.980. In general, the drag-divergence Mach number (defined as the Mach number where $\partial C_D/\partial M = 0.10$ where C_D and M represent drag coefficient and Mach number,

respectively) decreased slightly as lift coefficient was increased. The model exhibited longitudinal characteristics that were statically stable at angles of attack up to and significantly greater than that for the cruise condition. Elevon effectiveness was shown to be sufficient to trim the model throughout the Mach number range. The model was directionally stable and had positive effective dihedral throughout the Mach number range. Positive effectiveness of the roll and yaw control was demonstrated throughout the Mach number range.

Langley Research Center
National Aeronautics and Space Administration
Hampton, VA 23665
January 26, 1979

REFERENCES

1. Supercritical Wing Technology - A Progress Report on Flight Evaluations. NASA SP-301, 1972.

2. Gainer, Thomas G.; and Hoffman, Sherwood: Summary of Transformation Equations of Motion Used in Free-Flight and Wind-Tunnel Data Reduction and Analysis. NASA SP-3070, 1972.

3. Schaefer, William T., Jr.: Characteristics of Major Active Wind Tunnels at the Langley Research Center. NASA TM X-1130, 1965.

4. Braslow, Albert L.; and Knox, Eugene C.: Simplified Method for Determination of Critical Height of Distributed Roughness Particles for Boundary-Layer Transition at Mach Numbers From 0 to 5. NACA TN 4363, 1958.

5. Blackwell, James A., Jr.: Preliminary Study of Effects of Reynolds Number and Boundary-Layer Transition Location on Shock-Induced Separation. NASA TN D-5003, 1969.

6. Lee, George; and Summers, James L.: Effects of Sting-Support Interference on the Drag of an Ogive-Cylinder Body With and Without a Boattail at 0.6 to 1.4 Mach Number. NACA RM A57109, 1957.

7. Re, Richard J.: Stability and Control Characteristics, Including Aileron Hinge Moments, of a Model of a Supercritical-Wing Research Airplane. NASA TM X-2929, 1974.

8. Bartlett, Dennis W.; and Harris, Charles D.: Aerodynamic Characteristics of an NASA Supercritical-Wing Research Airplane Model With and Without Fuselage Area-Rule Additions at Mach 0.25 to 1.00. NASA TM X-2633, 1972.

9. James, H. A.: Feasbility Study of Modifications to BQM-34E Drone for NASA Applications. NASA CR-112323, 1972.

10. Bartlett, Dennis W.; Harris, Charles D.; and Kelly, Thomas C.: Wind-Tunnel Development of Underwing Leading-Edge Vortex Generators on an NASA Supercritical-Wing Research Airplane Configuration. NASA TM X-2808, 1973.

11. Bartlett, Dennis W.: Effects of Differential and Symmetrical Aileron Deflection on the Aerodynamic Characteristics of an NASA Supercritical-Wing Research Airplane Model. NASA TM X-3231, 1975.

TABLE I.- WING COORDINATES ALONG STREAMWISE CHORDS

(a) Sketch showing semispan stations for wing coordinates

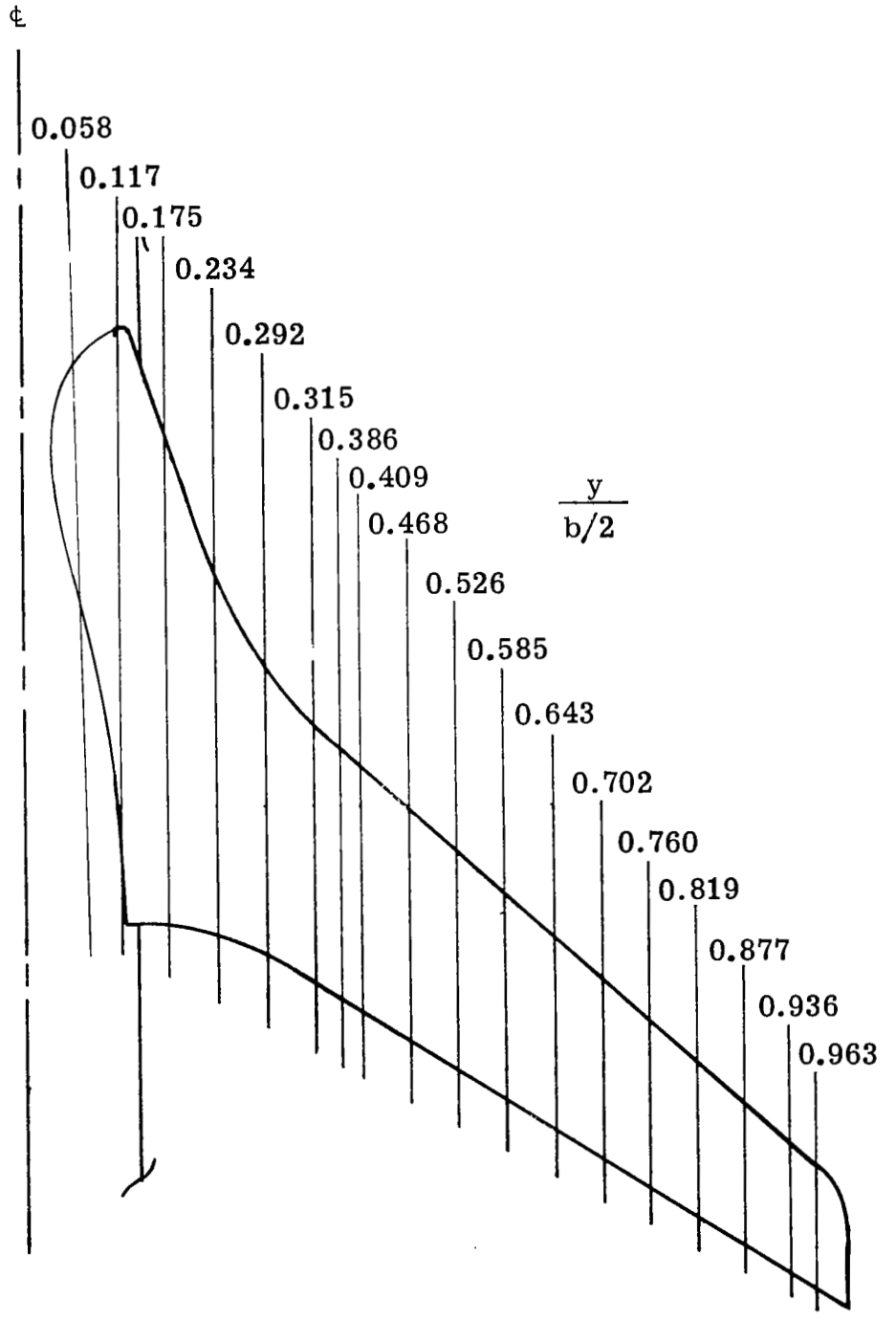

TABLE I.- Continued

(b) $\frac{y}{b/2} = 0.058$ to 0.175

$\frac{y}{b/2} = 0.058$; c = 204.710 cm

x/c	z/c	
	Upper surface	Lower surface
.0000	.0206	.0206
.0006	.0241	.0171
.0013	.0255	.0157
.0025	.0275	.0137
.0038	.0290	.0122
.0050	.0303	.0109
.0075	.0324	.0087
.0100	.0342	.0069
.0150	.0371	.0039
.0200	.0395	.0015
.0250	.0415	-.0005
.0375	.0457	-.0044
.0500	.0492	-.0075
.0750	.0550	-.0124
.1000	.0595	-.0161
.1500	.0663	-.0214
.1750	.0688	-.0231
.2000	.0708	-.0245
.2500	.0733	-.0262
.3000	.0739	-.0269
.3500	.0730	-.0265
.4000	.0712	-.0250
.4500	.0689	-.0222
.5000	.0662	-.0184
.5500	.0633	-.0136
.6000	.0604	-.0081
.6500	.0571	-.0021
.7000	.0535	.0042
.7500	.0496	.0107
.8000	.0454	.0165
.8500	.0405	.0204
.9000	.0344	.0216
.9250	.0315	.0213
.9500	.0283	.0205
.9750	.0245	.0191
.9913	.0216	.0177
1.0000		.0168

$\frac{y}{b/2} = 0.117$; c = 166.043 cm

x/c	z/c	
	Upper surface	Lower surface
0.0000	.0245	.0245
.0006	.0283	.0206
.0012	.0299	.0190
.0025	.0322	.0167
.0037	.0338	.0150
.0050	.0353	.0136
.0075	.0376	.0112
.0100	.0396	.0092
.0150	.0428	.0059
.0200	.0454	.0032
.0250	.0477	.0010
.0375	.0523	-.0034
.0500	.0560	-.0067
.0750	.0622	-.0120
.1000	.0670	-.0158
.1500	.0740	-.0212
.1750	.0766	-.0230
.2000	.0786	-.0243
.2500	.0811	-.0259
.3000	.0818	-.0264
.3500	.0811	-.0257
.4000	.0795	-.0237
.4500	.0774	-.0204
.5000	.0749	-.0162
.5500	.0722	-.0111
.6000	.0693	-.0052
.6500	.0660	.0014
.7000	.0623	.0082
.7500	.0582	.0153
.8000	.0539	.0219
.8500	.0489	.0265
.9000	.0426	.0282
.9250	.0396	.0281
.9500	.0361	.0274
.9750	.0323	.0260
.9913	.0292	.0246
1.0000		.0237

$\frac{y}{b/2} = 0.175$; c = 129.524 cm

x/c	z/c	
	Upper surface	Lower surface
.0000	.0293	.0293
.0006	.0334	.0253
.0013	.0351	.0235
.0025	.0376	.0211
.0037	.0394	.0192
.0050	.0410	.0176
.0075	.0435	.0151
.0100	.0456	.0129
.0150	.0489	.0095
.0200	.0516	.0068
.0250	.0538	.0044
.0375	.0584	-.0001
.0500	.0621	-.0035
.0750	.0680	-.0085
.1000	.0724	-.0120
.1500	.0788	-.0164
.1750	.0810	-.0178
.2000	.0827	-.0189
.2500	.0848	-.0199
.3000	.0856	-.0197
.3500	.0856	-.0183
.4000	.0849	-.0156
.4500	.0838	-.0119
.5000	.0823	-.0076
.5500	.0806	-.0024
.6000	.0783	.0033
.6500	.0754	.0098
.7000	.0723	.0168
.7500	.0686	.0242
.8000	.0647	.0313
.8500	.0606	.0367
.9000	.0550	.0394
.9250	.0522	.0399
.9500	.0490	.0395
.9750	.0455	.0385
.9913	.0430	.0373
1.0000		.0364

TABLE I.- Continued

(c) $\frac{y}{b/2} = 0.234$ to 0.351

$\frac{y}{b/2} = 0.234$; $c = 99.604$ cm

x/c	z/c	
	Upper surface	Lower surface
0.0000	.0349	.0349
.0006	.0392	.0307
.0013	.0411	.0288
.0025	.0438	.0262
.0038	.0457	.0241
.0050	.0474	.0225
.0075	.0500	.0198
.0100	.0522	.0177
.0150	.0556	.0143
.0200	.0582	.0115
.0250	.0603	.0092
.0375	.0646	.0048
.0500	.0679	.0017
.0750	.0729	-.0026
.1000	.0768	-.0053
.1500	.0823	-.0082
.1750	.0844	-.0091
.2000	.0860	-.0097
.2500	.0888	-.0099
.3000	.0910	-.0088
.3500	.0924	-.0067
.4000	.0931	-.0039
.4500	.0931	-.0004
.5000	.0924	.0038
.5500	.0913	.0088
.6000	.0894	.0146
.6500	.0873	.0216
.7000	.0853	.0291
.7500	.0827	.0372
.8000	.0799	.0452
.8500	.0764	.0517
.9000	.0722	.0557
.9250	.0694	.0566
.9500	.0665	.0564
.9750	.0634	.0554
.9913	.0613	.0540
1.0000		.0530

$\frac{y}{b/2} = 0.292$; $c = 82.446$ cm

x/c	z/c	
	Upper surface	Lower surface
.0000	.0375	.0375
.0006	.0415	.0337
.0012	.0432	.0319
.0025	.0457	.0295
.0037	.0475	.0277
.0050	.0489	.0263
.0075	.0513	.0240
.0100	.0531	.0222
.0150	.0563	.0191
.0200	.0590	.0168
.0250	.0612	.0150
.0375	.0656	.0114
.0500	.0690	.0087
.0750	.0745	.0052
.1000	.0788	.0027
.1500	.0851	-.0006
.1750	.0877	-.0014
.2000	.0900	-.0017
.2500	.0937	-.0013
.3000	.0964	-.0000
.3500	.0981	.0021
.4000	.0993	.0050
.4500	.0998	.0085
.5000	.0996	.0128
.5500	.0991	.0180
.6277	.0985	.0242
.6500	.0978	.0319
.7000	.0969	.0405
.7500	.0954	.0499
.8000	.0934	.0592
.8500	.0907	.0666
.9000	.0870	.0709
.9250	.0845	.0716
.9500	.0816	.0710
.9750	.0781	.0691
.9913	.0756	.0669
1.0000		.0654

$\frac{y}{b/2} = 0.351$; $c = 73.703$ cm

x/c	z/c	
	Upper surface	Lower surface
.0000	.0387	.0387
.0006	.0428	.0347
.0013	.0444	.0331
.0025	.0468	.0307
.0037	.0485	.0291
.0050	.0498	.0277
.0075	.0520	.0256
.0100	.0538	.0240
.0150	.0567	.0214
.0200	.0591	.0195
.0250	.0612	.0179
.0375	.0654	.0150
.0500	.0688	.0126
.0750	.0744	.0093
.1000	.0787	.0069
.1500	.0854	.0042
.1750	.0881	.0038
.2000	.0905	.0036
.2500	.0943	.0042
.3000	.0972	.0057
.3501	.0995	.0080
.4001	.1011	.0110
.4501	.1022	.0146
.5001	.1030	.0191
.5501	.1036	.0246
.6001	.1041	.0313
.6501	.1042	.0396
.7001	.1040	.0495
.7501	.1032	.0601
.8001	.1018	.0703
.8500	.0998	.0779
.9000	.0964	.0817
.9250	.0941	.0820
.9500	.0912	.0808
.9750	.0875	.0779
.9913	.0846	.0749
1.0000		.0733

TABLE I.- Continued

(d) $\frac{y}{b/2}$ = 0.386 to 0.468

$\frac{y}{b/2}$ = 0.386; c = 70.912 cm

x/c	z/c	
	Upper surface	Lower surface
0.0000	.0394	.0394
.0006	.0436	.0352
.0013	.0457	.0336
.0025	.0476	.0313
.0038	.0494	.0295
.0050	.0507	.0282
.0075	.0529	.0260
.0100	.0547	.0244
.0150	.0575	.0220
.0200	.0598	.0201
.0250	.0618	.0186
.0375	.0659	.0157
.0500	.0692	.0135
.0750	.0745	.0102
.1000	.0787	.0080
.1500	.0853	.0059
.1750	.0879	.0057
.2000	.0902	.0056
.2500	.0939	.0063
.3000	.0971	.0080
.3500	.0997	.0104
.4000	.1017	.0136
.4500	.1032	.0173
.5000	.1044	.0218
.5500	.1055	.0274
.6000	.1062	.0343
.6500	.1066	.0429
.7000	.1066	.0530
.7500	.1059	.0639
.8000	.1048	.0743
.8500	.1030	.0819
.9000	.0997	.0856
.9250	.0975	.0857
.9500	.0946	.0843
.9750	.0909	.0812
.9913	.0880	.0781
1.0000		.0765

$\frac{y}{b/2}$ = 0.409; c = 69.518 cm

x/c	z/c	
	Upper surface	Lower surface
0.0000	.0398	.0398
.0006	.0440	.0356
.0012	.0456	.0341
.0025	.0480	.0317
.0037	.0497	.0300
.0050	.0510	.0286
.0075	.0532	.0265
.0100	.0550	.0249
.0150	.0578	.0225
.0200	.0601	.0206
.0250	.0620	.0191
.0375	.0662	.0163
.0500	.0695	.0141
.0750	.0747	.0109
.1000	.0789	.0088
.1500	.0856	.0068
.1750	.0883	.0067
.2000	.0905	.0067
.2500	.0944	.0075
.3000	.0976	.0093
.3500	.1003	.0118
.4000	.1024	.0150
.4500	.1040	.0187
.5000	.1055	.0233
.5500	.1067	.0289
.6000	.1075	.0359
.6500	.1080	.0445
.7000	.1082	.0547
.7500	.1076	.0657
.8000	.1066	.0761
.8500	.1048	.0837
.9000	.1016	.0875
.9250	.0994	.0876
.9500	.0965	.0862
.9750	.0928	.0830
.9913	.0899	.0800
1.0000		.0783

$\frac{y}{b/2}$ = 0.468; c = 66.033 cm

x/c	z/c	
	Upper surface	Lower surface
0.0000	.0408	.0408
.0006	.0449	.0368
.0013	.0465	.0352
.0025	.0489	.0329
.0038	.0506	.0312
.0050	.0519	.0299
.0075	.0541	.0277
.0100	.0558	.0262
.0150	.0586	.0238
.0200	.0608	.0220
.0250	.0628	.0206
.0375	.0669	.0178
.0500	.0702	.0157
.0750	.0754	.0128
.1000	.0796	.0109
.1500	.0864	.0094
.1750	.0891	.0093
.2000	.0914	.0095
.2500	.0955	.0106
.3000	.0990	.0127
.3500	.1020	.0153
.4000	.1044	.0187
.4500	.1065	.0226
.5000	.1083	.0274
.5500	.1098	.0331
.6000	.1110	.0402
.6500	.1119	.0490
.7000	.1124	.0593
.7500	.1122	.0705
.8000	.1114	.0809
.8500	.1098	.0887
.9000	.1067	.0925
.9250	.1044	.0926
.9500	.1016	.0912
.9750	.0978	.0880
.9913	.0948	.0849
1.0000		.0831

TABLE I.- Continued

(e) $\frac{y}{b/2} = 0.526$ to 0.643

$\frac{y}{b/2} = 0.526$; c = 62.548 cm

x/c	z/c	
	Upper surface	Lower surface
0.0000	.0420	.0420
.0006	.0460	.0380
.0013	.0475	.0365
.0025	.0499	.0341
.0038	.0516	.0325
.0050	.0529	.0312
.0075	.0550	.0291
.0100	.0567	.0276
.0150	.0594	.0253
.0200	.0617	.0236
.0250	.0637	.0222
.0375	.0677	.0194
.0500	.0710	.0175
.0750	.0762	.0149
.1000	.0804	.0133
.1500	.0872	.0121
.1750	.0900	.0122
.2000	.0924	.0126
.2500	.0968	.0141
.3000	.1005	.0165
.3500	.1038	.0193
.4000	.1067	.0228
.4500	.1091	.0269
.5000	.1114	.0319
.5500	.1132	.0378
.6000	.1149	.0451
.6500	.1161	.0539
.7000	.1170	.0645
.7500	.1172	.0758
.8000	.1167	.0862
.8500	.1152	.0942
.9000	.1123	.0980
.9250	.1101	.0981
.9500	.1072	.0967
.9750	.1034	.0935
.9913	.1003	.0904
1.0000		.0885

$\frac{y}{b/2} = 0.585$; c = 59.063 cm

x/c	z/c	
	Upper surface	Lower surface
0.0000	.0433	.0433
.0006	.0472	.0394
.0013	.0487	.0379
.0025	.0511	.0356
.0038	.0527	.0340
.0050	.0540	.0327
.0075	.0560	.0307
.0100	.0577	.0292
.0150	.0604	.0270
.0200	.0627	.0253
.0250	.0646	.0239
.0375	.0687	.0213
.0500	.0719	.0195
.0750	.0771	.0172
.1000	.0813	.0160
.1500	.0882	.0152
.1750	.0910	.0155
.2000	.0936	.0161
.2500	.0982	.0181
.3000	.1022	.0207
.3500	.1058	.0238
.4000	.1092	.0274
.4500	.1121	.0317
.5000	.1149	.0369
.5500	.1171	.0429
.6000	.1192	.0505
.6500	.1209	.0595
.7000	.1222	.0702
.7500	.1229	.0817
.8000	.1226	.0922
.8500	.1214	.1004
.9000	.1186	.1042
.9250	.1164	.1043
.9500	.1135	.1030
.9750	.1097	.0997
.9913	.1064	.0965
1.0000		.0945

$\frac{y}{b/2} = 0.643$; c = 55.577 cm

x/c	z/c	
	Upper surface	Lower surface
0.0000	.0448	.0448
.0006	.0486	.0410
.0012	.0501	.0395
.0025	.0524	.0373
.0037	.0541	.0357
.0050	.0553	.0344
.0075	.0573	.0325
.0100	.0589	.0311
.0150	.0616	.0290
.0200	.0638	.0273
.0250	.0657	.0260
.0375	.0698	.0234
.0500	.0730	.0218
.0750	.0782	.0199
.1000	.0824	.0190
.1500	.0893	.0188
.1750	.0922	.0193
.2000	.0949	.0201
.2500	.0998	.0225
.3000	.1041	.0254
.3500	.1082	.0288
.4000	.1120	.0326
.4500	.1155	.0372
.5000	.1188	.0425
.5500	.1215	.0488
.6000	.1241	.0566
.6500	.1263	.0657
.7000	.1280	.0767
.7500	.1292	.0884
.8000	.1293	.0999
.8500	.1282	.1073
.9000	.1257	.1112
.9250	.1235	.1112
.9500	.1206	.1100
.9750	.1167	.1067
.9913	.1133	.1034
1.0000		.1012

TABLE I.- Continued

(f) $\frac{y}{b/2}$ = 0.702 to 0.819

$\frac{y}{b/2}$ = 0.702; c = 52.092 cm

x/c	z/c	
	Upper surface	Lower surface
0.0000	.0472	.0472
.0006	.0508	.0434
.0012	.0523	.0420
.0025	.0545	.0398
.0037	.0562	.0383
.0050	.0574	.0370
.0075	.0593	.0351
.0100	.0609	.0337
.0150	.0636	.0317
.0200	.0658	.0301
.0250	.0677	.0288
.0375	.0717	.0264
.0500	.0750	.0249
.0750	.0801	.0234
.1000	.0843	.0227
.1500	.0913	.0230
.1750	.0943	.0237
.2000	.0971	.0247
.2500	.1023	.0276
.3000	.1069	.0309
.3500	.1113	.0345
.4000	.1157	.0386
.4500	.1197	.0433
.5000	.1235	.0489
.5500	.1266	.0554
.6000	.1297	.0634
.6500	.1323	.0727
.7000	.1346	.0839
.7500	.1362	.0957
.8000	.1366	.1062
.8500	.1358	.1149
.9000	.1335	.1189
.9250	.1313	.1189
.9500	.1285	.1177
.9750	.1246	.1144
.9913	.1211	.1112
1.0000		.1088

$\frac{y}{b/2}$ = 0.760; c = 48.607 cm

x/c	z/c	
	Upper surface	Lower surface
0.0000	.0506	.0506
.0006	.0541	.0469
.0012	.0556	.0455
.0025	.0578	.0434
.0037	.0594	.0419
.0050	.0606	.0407
.0075	.0625	.0388
.0100	.0640	.0375
.0150	.0667	.0356
.0200	.0689	.0340
.0250	.0708	.0328
.0375	.0748	.0304
.0500	.0781	.0290
.0750	.0832	.0278
.1000	.0875	.0274
.1500	.0946	.0282
.1750	.0977	.0291
.2000	.1005	.0303
.2500	.1060	.0335
.3000	.1108	.0371
.3500	.1156	.0410
.4000	.1204	.0454
.4500	.1248	.0504
.5000	.1291	.0563
.5500	.1326	.0629
.6000	.1361	.0712
.6500	.1392	.0807
.7000	.1418	.0919
.7500	.1439	.1038
.8000	.1447	.1143
.8500	.1442	.1232
.9000	.1422	.1274
.9250	.1401	.1275
.9500	.1373	.1263
.9750	.1334	.1230
.9913	.1299	.1199
1.0000		.1175

$\frac{y}{b/2}$ = 0.819; c = 45.122 cm

x/c	z/c	
	Upper surface	Lower surface
0.0000	.0556	.0556
.0006	.0590	.0519
.0012	.0604	.0505
.0025	.0625	.0484
.0037	.0641	.0470
.0050	.0653	.0458
.0075	.0671	.0441
.0100	.0687	.0428
.0150	.0713	.0409
.0200	.0736	.0394
.0250	.0755	.0382
.0375	.0795	.0360
.0500	.0827	.0347
.0750	.0879	.0336
.1000	.0923	.0334
.1500	.0995	.0346
.1750	.1027	.0356
.2000	.1056	.0370
.2500	.1112	.0405
.3000	.1163	.0444
.3500	.1214	.0486
.4000	.1264	.0533
.4500	.1313	.0587
.5000	.1358	.0648
.5500	.1398	.0716
.6000	.1436	.0800
.6500	.1471	.0897
.7000	.1501	.1010
.7500	.1525	.1128
.8000	.1537	.1233
.8500	.1536	.1324
.9000	.1519	.1369
.9250	.1499	.1371
.9500	.1472	.1360
.9750	.1433	.1328
.9913	.1398	.1297
1.0000		.1274

TABLE I.- Concluded

(g) $\frac{y}{b/2}$ = 0.877 to 0.963

$\frac{y}{b/2}$ = 0.877; c = 41.637 cm

x/c	z/c	
	Upper surface	Lower surface
0.0000	.0624	.0624
.0006	.0657	.0587
.0013	.0671	.0573
.0025	.0691	.0553
.0038	.0707	.0540
.0050	.0719	.0529
.0075	.0737	.0512
.0100	.0753	.0500
.0150	.0779	.0481
.0200	.0802	.0466
.0250	.0821	.0455
.0375	.0861	.0434
.0500	.0894	.0421
.0750	.0947	.0410
.1000	.0991	.0409
.1500	.1066	.0424
.1750	.1098	.0436
.2000	.1128	.0451
.2500	.1185	.0489
.3000	.1238	.0530
.3500	.1290	.0575
.4000	.1342	.0626
.4500	.1393	.0683
.5000	.1440	.0747
.5500	.1483	.0818
.6000	.1525	.0903
.6500	.1562	.1001
.7000	.1595	.1114
.7500	.1621	.1229
.8000	.1638	.1335
.8500	.1642	.1427
.9000	.1629	.1476
.9250	.1611	.1480
.9500	.1585	.1471
.9750	.1547	.1439
.9913	.1514	.1411
1.0000		.1389

$\frac{y}{b/2}$ = 0.936; c = 38.152 cm

x/c	z/c	
	Upper surface	Lower surface
0.0000	.0717	.0717
.0006	.0750	.0679
.0013	.0763	.0665
.0025	.0782	.0647
.0037	.0798	.0635
.0050	.0809	.0624
.0075	.0828	.0608
.0100	.0844	.0596
.0150	.0871	.0577
.0200	.0894	.0563
.0250	.0913	.0553
.0375	.0954	.0533
.0500	.0988	.0520
.0750	.1042	.0506
.1000	.1088	.0505
.1500	.1165	.0522
.1750	.1198	.0536
.2000	.1228	.0551
.2500	.1285	.0589
.3000	.1338	.0632
.3500	.1391	.0681
.4000	.1444	.0737
.4500	.1494	.0798
.5000	.1542	.0865
.5500	.1588	.0937
.6000	.1630	.1023
.6500	.1669	.1123
.7000	.1703	.1234
.7500	.1732	.1344
.8000	.1753	.1450
.8500	.1763	.1543
.9000	.1755	.1598
.9250	.1739	.1605
.9500	.1714	.1598
.9750	.1678	.1568
.9913	.1648	.1543
1.0000		.1524

$\frac{y}{b/2}$ = 0.963; c = 36.496 cm

x/c	z/c	
	Upper surface	Lower surface
0.0000	.0772	.0772
.0006	.0805	.0734
.0013	.0818	.0720
.0025	.0836	.0703
.0038	.0852	.0690
.0050	.0863	.0680
.0075	.0883	.0665
.0100	.0899	.0653
.0150	.0926	.0634
.0200	.0949	.0620
.0250	.0969	.0610
.0375	.1010	.0591
.0500	.1044	.0578
.0750	.1099	.0561
.1000	.1146	.0559
.1500	.1225	.0578
.1750	.1257	.0591
.2000	.1287	.0607
.2500	.1344	.0644
.3000	.1397	.0688
.3500	.1450	.0739
.4000	.1502	.0797
.4500	.1551	.0860
.5000	.1599	.0929
.5500	.1645	.1002
.6000	.1688	.1088
.6500	.1727	.1189
.7000	.1761	.1298
.7500	.1790	.1405
.8000	.1814	.1510
.8500	.1827	.1603
.9000	.1821	.1663
.9250	.1807	.1672
.9500	.1784	.1665
.9750	.1748	.1636
.9913	.1721	.1614
1.0000		.1597

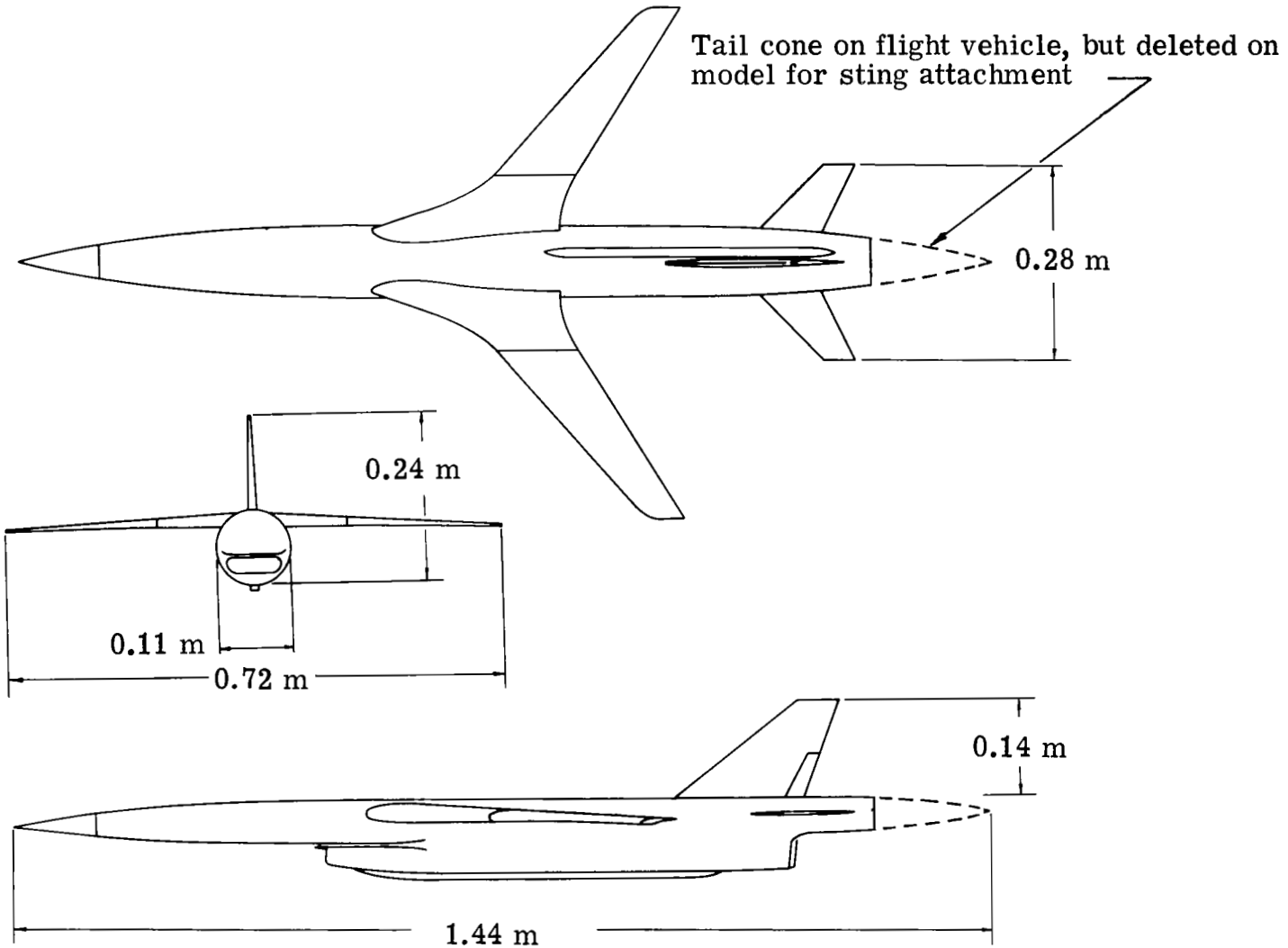

(a) General arrangement.

Figure 1.- Wind-tunnel model configuration.

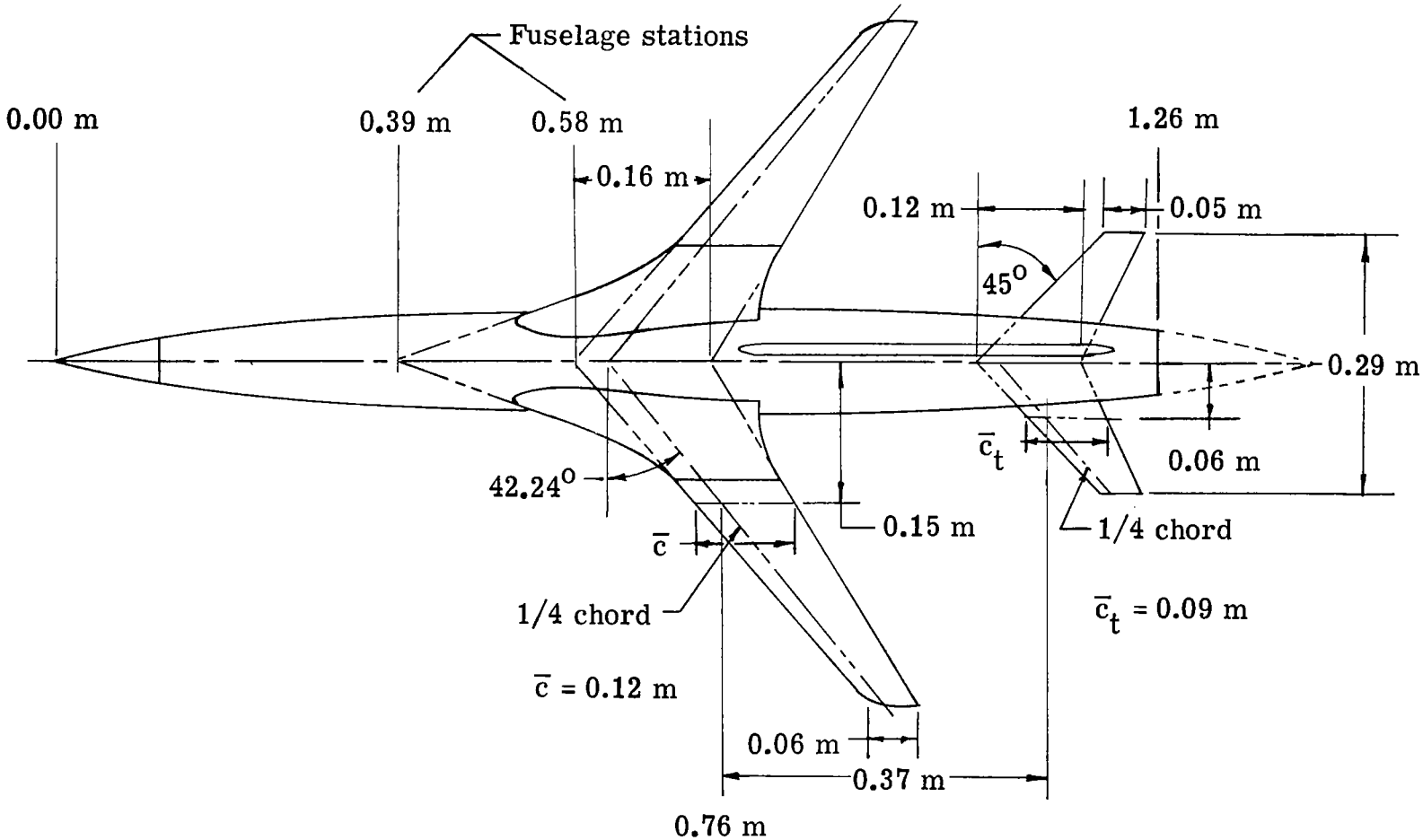

(b) Model planform.

Figure 1.- Continued.

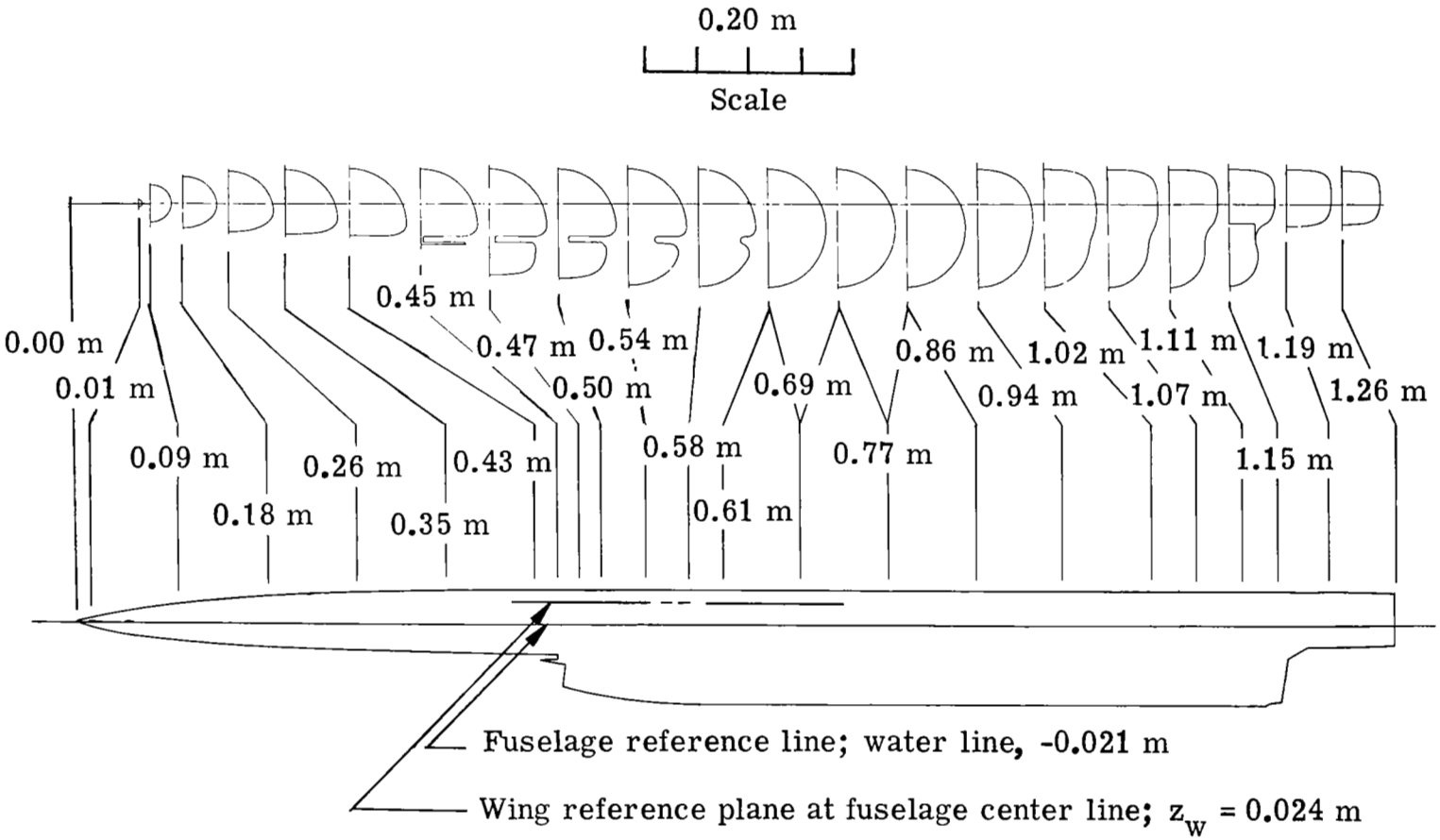

(c) Cross-sectional views of fuselage geometry.

Figure 1.- Concluded.

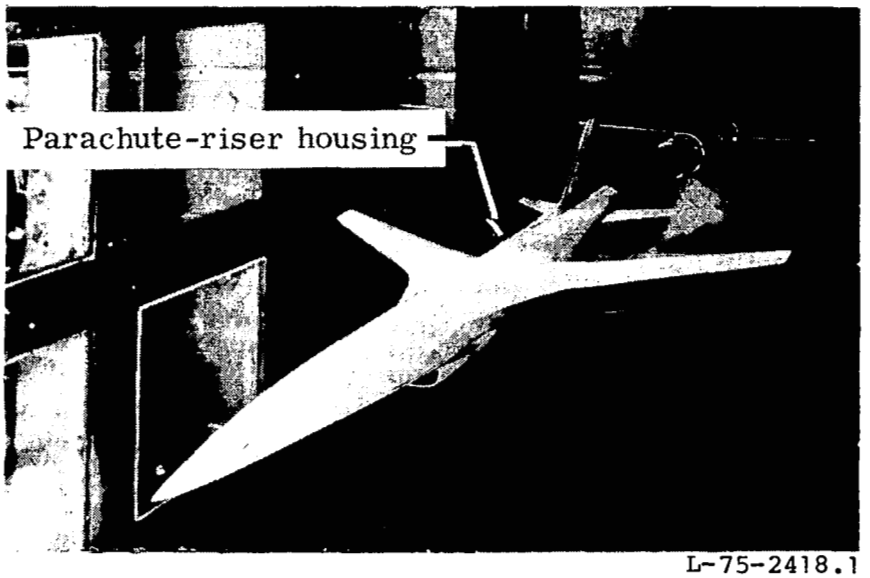

L-75-2418.1

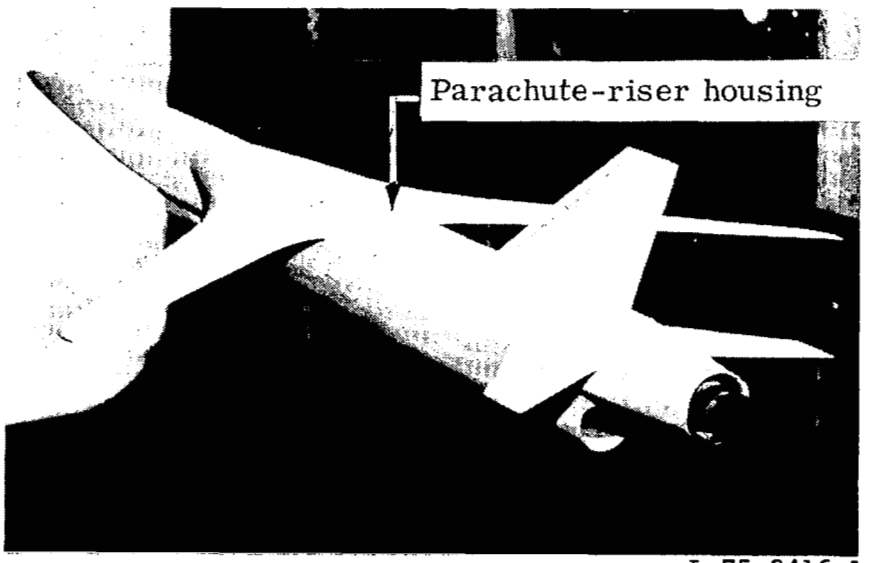

L-75-2416.1

(a) Views of model mounted in keel section.

Figure 2.- Photographs of 1/6-scaled wind-tunnel model.

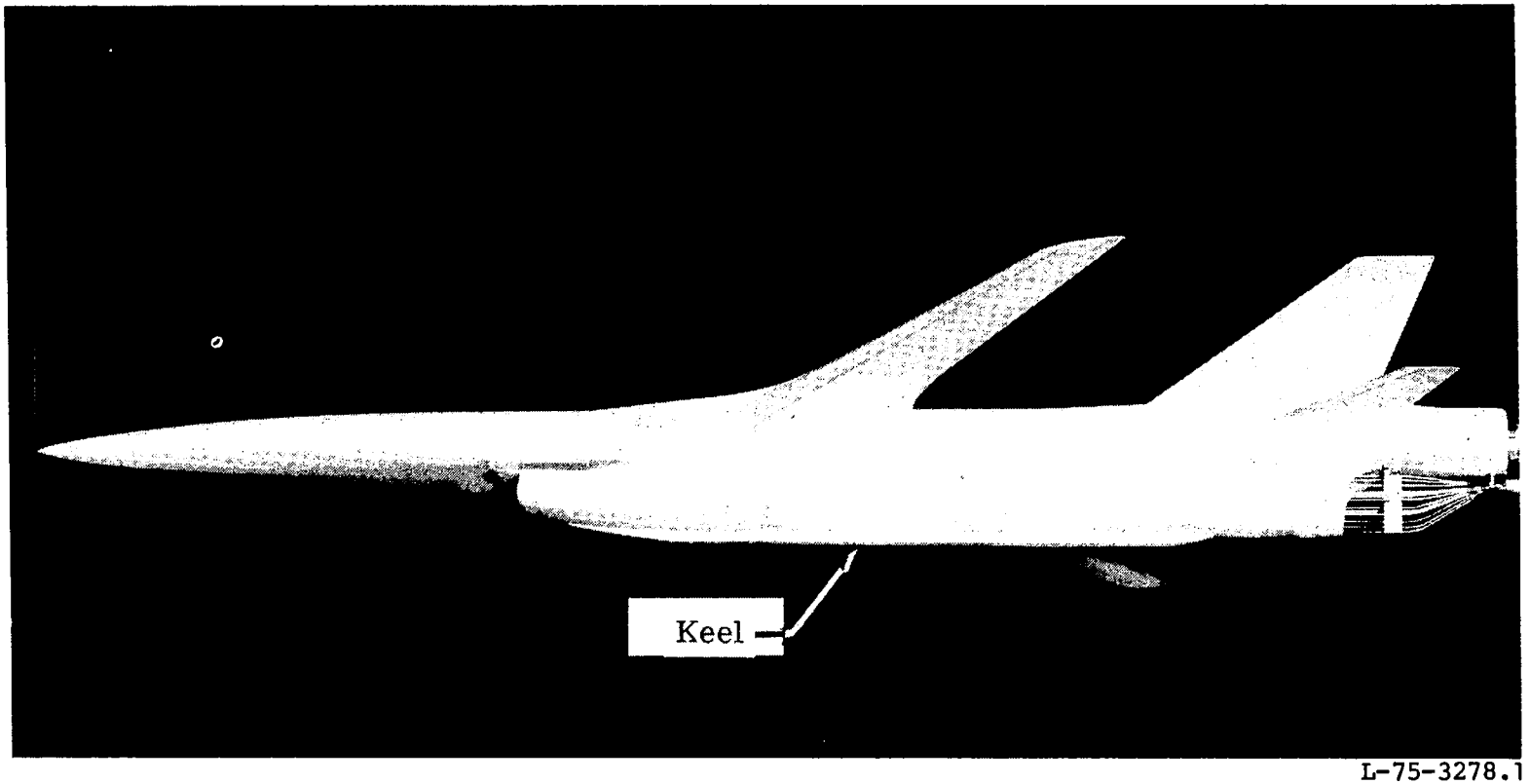

L-75-3278.1

(b) Views of model and rake installation.

Figure 2.- Concluded.

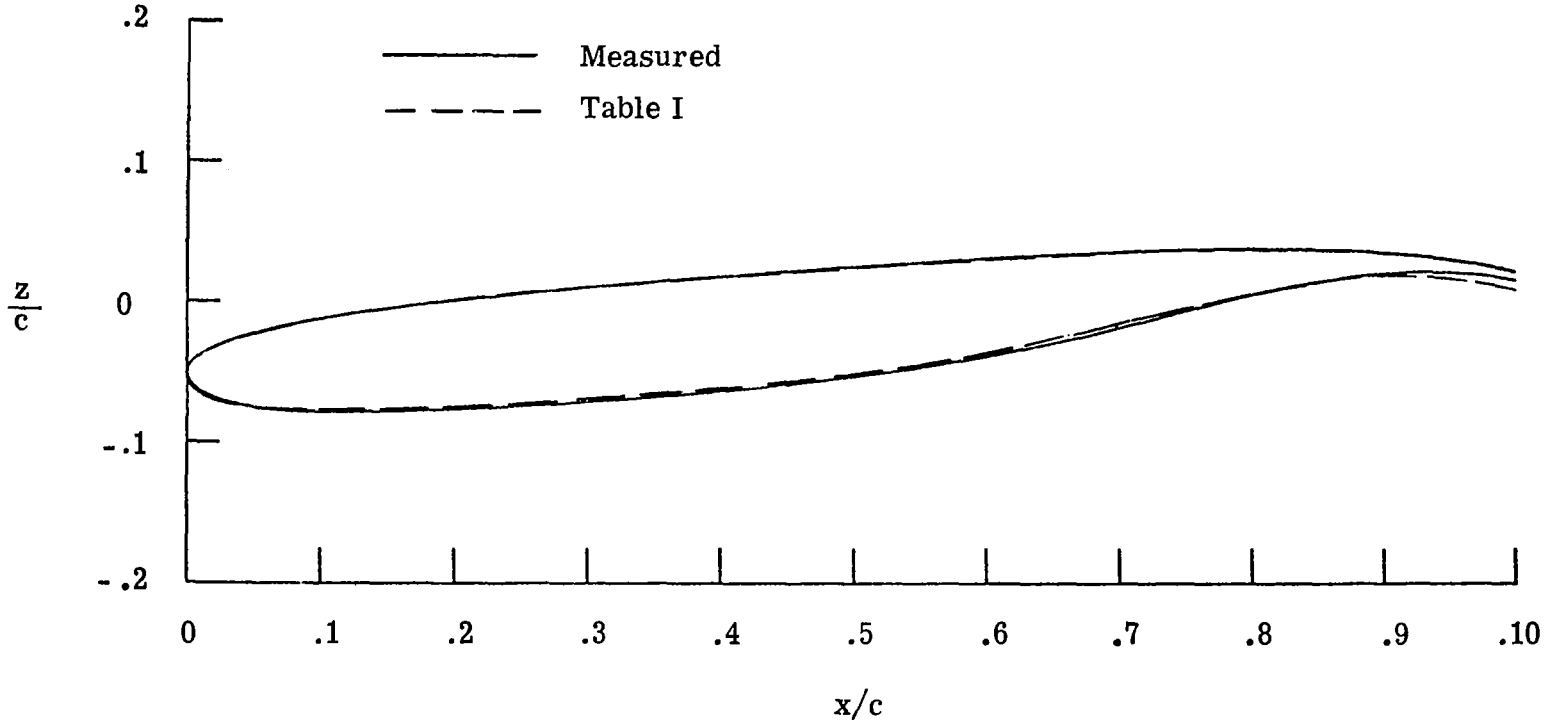

(a) Wing station at $\frac{y}{b/2} = 0.70$.

Figure 3.- Typical airfoil geometry.

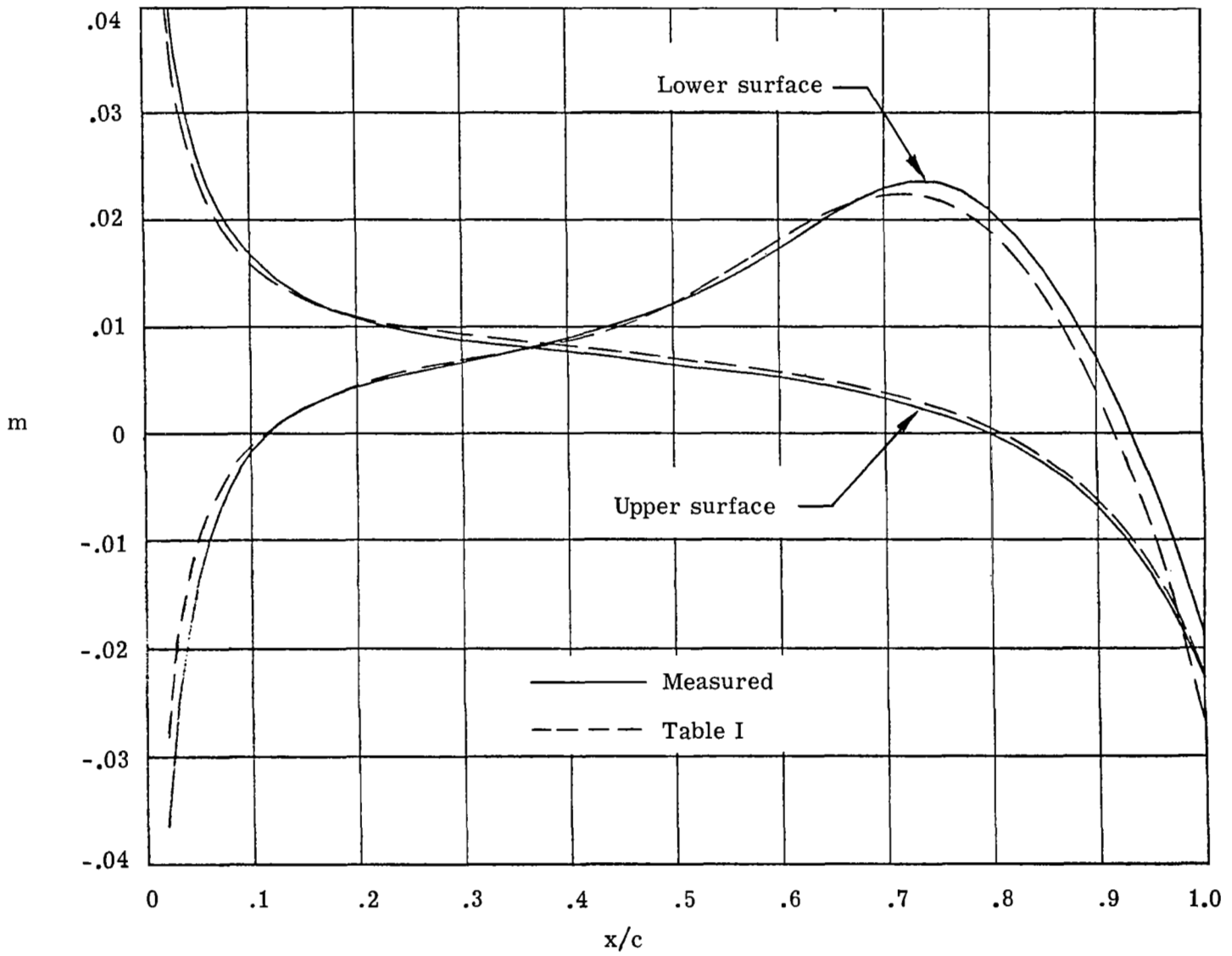

(b) Streamwise variation of wing upper and lower surface slopes at $\frac{y}{b/2} = 0.70$.

Figure 3.- Concluded.

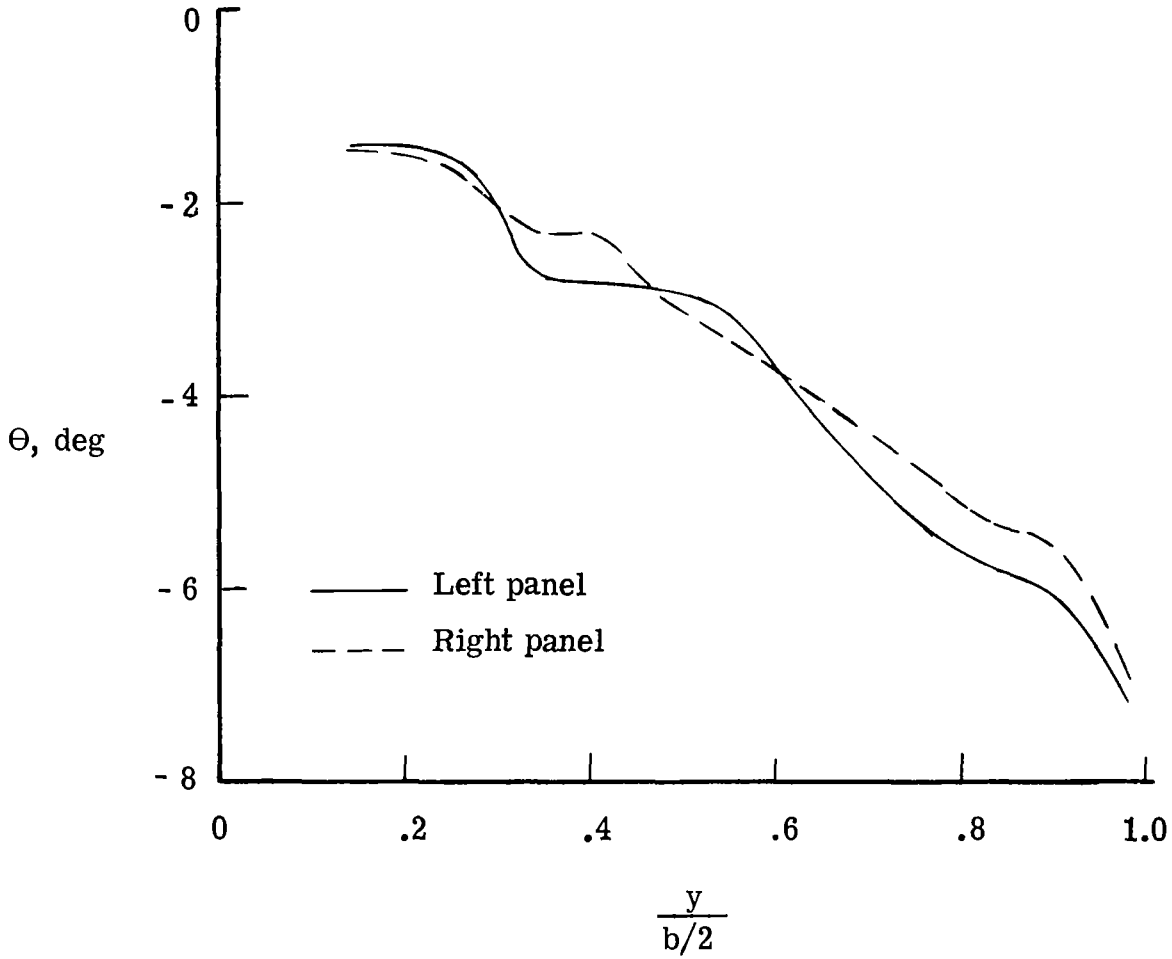

Figure 4.- Measured twist distribution for model wing.

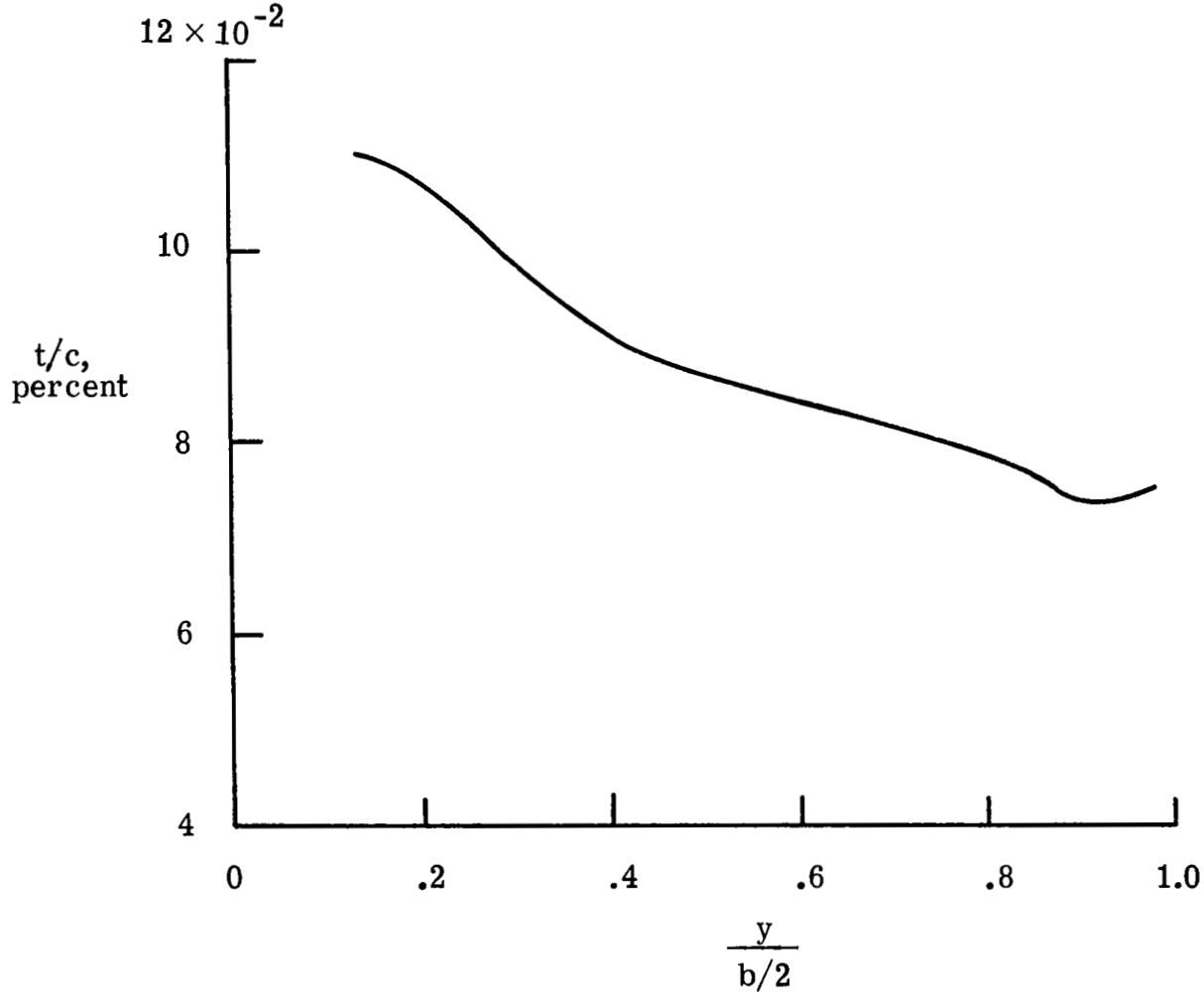

(a) Measured thickness-to-chord ratio for model wing.

Figure 5.- Measured wing thickness for model.

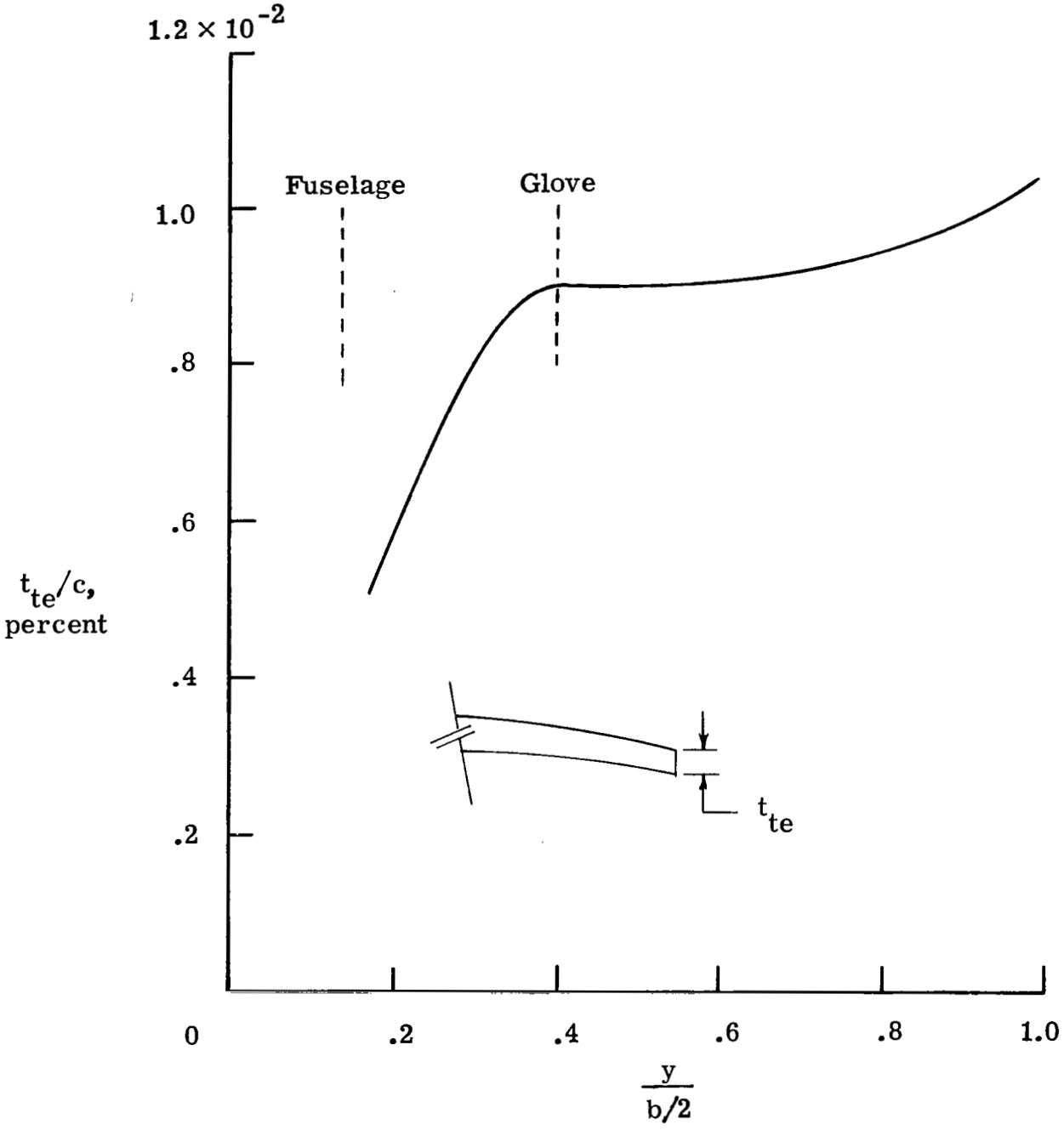

(b) Variation of trailing-edge thickness with semispan for model wing.

Figure 5.- Concluded.

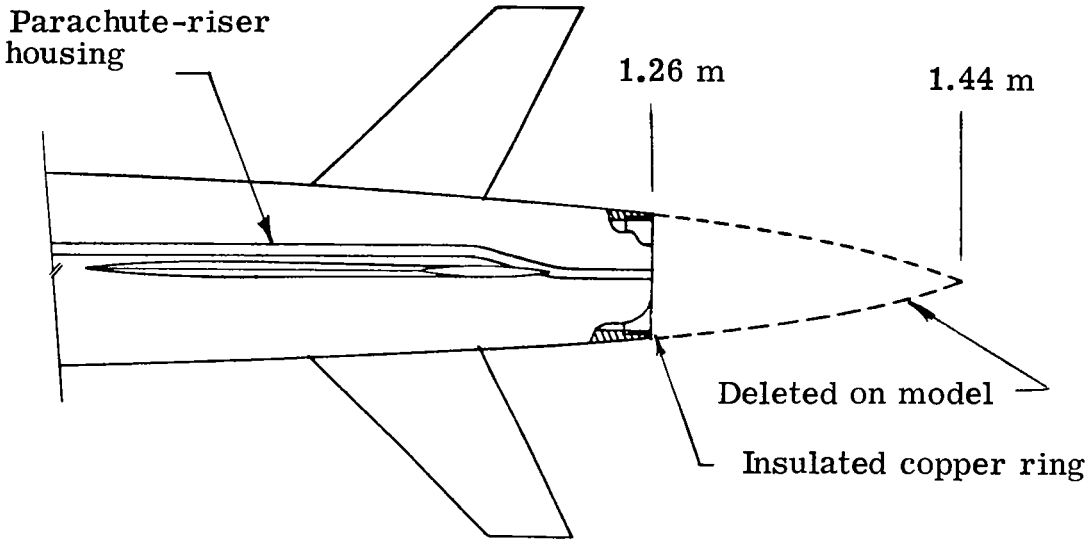

(a) Top view.

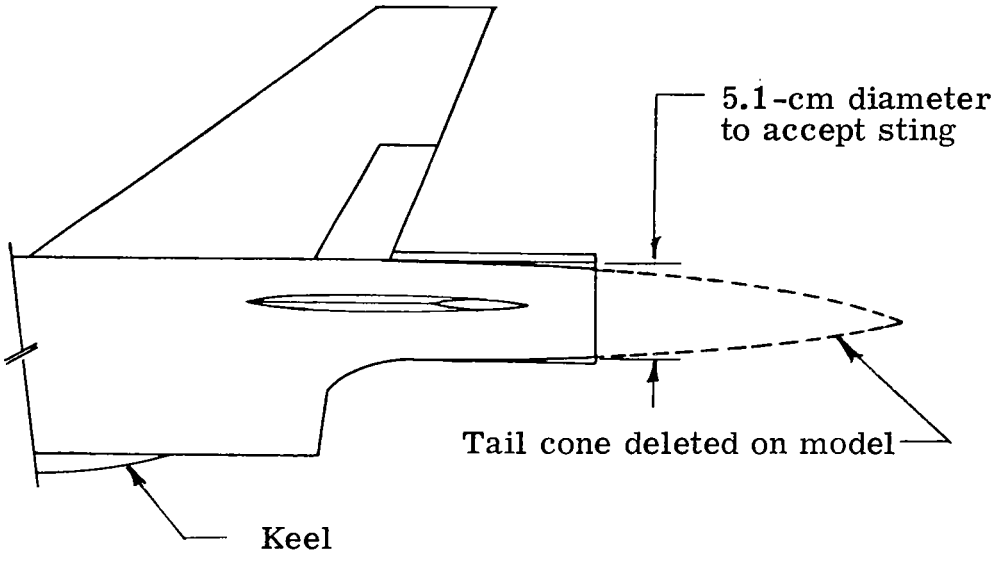

(b) Side view.

Figure 6.- Modification of aft end of fueslage.

Carborundum-grain size (Streamwise location in percent chord)					
Upper wing surface				Lower wing surface	
A	B	C	D	E	F
100 (10)	100 (10)	90 ---	80 ---	80 (22)	60 (22)

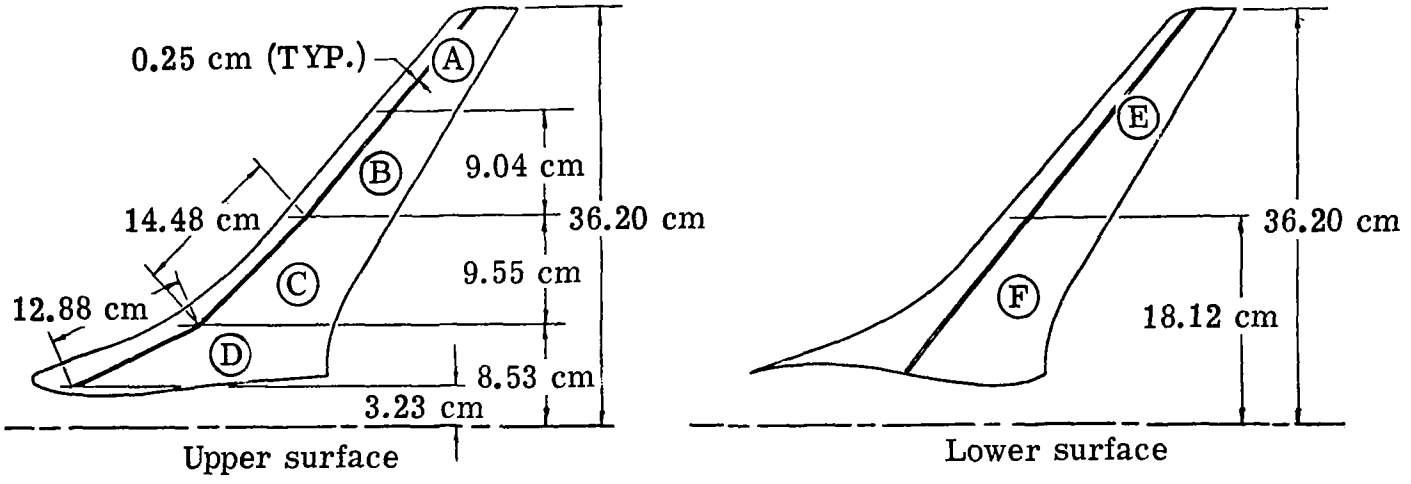

(a) Wing-flow transition-strip patterns.

Figure 7.- Boundary-layer transition-strip locations and carborundum-grain sizes for model.

Component	Carborundum-grain size
Nose	60
Nacelle	80
Fin	80
Elevon	80

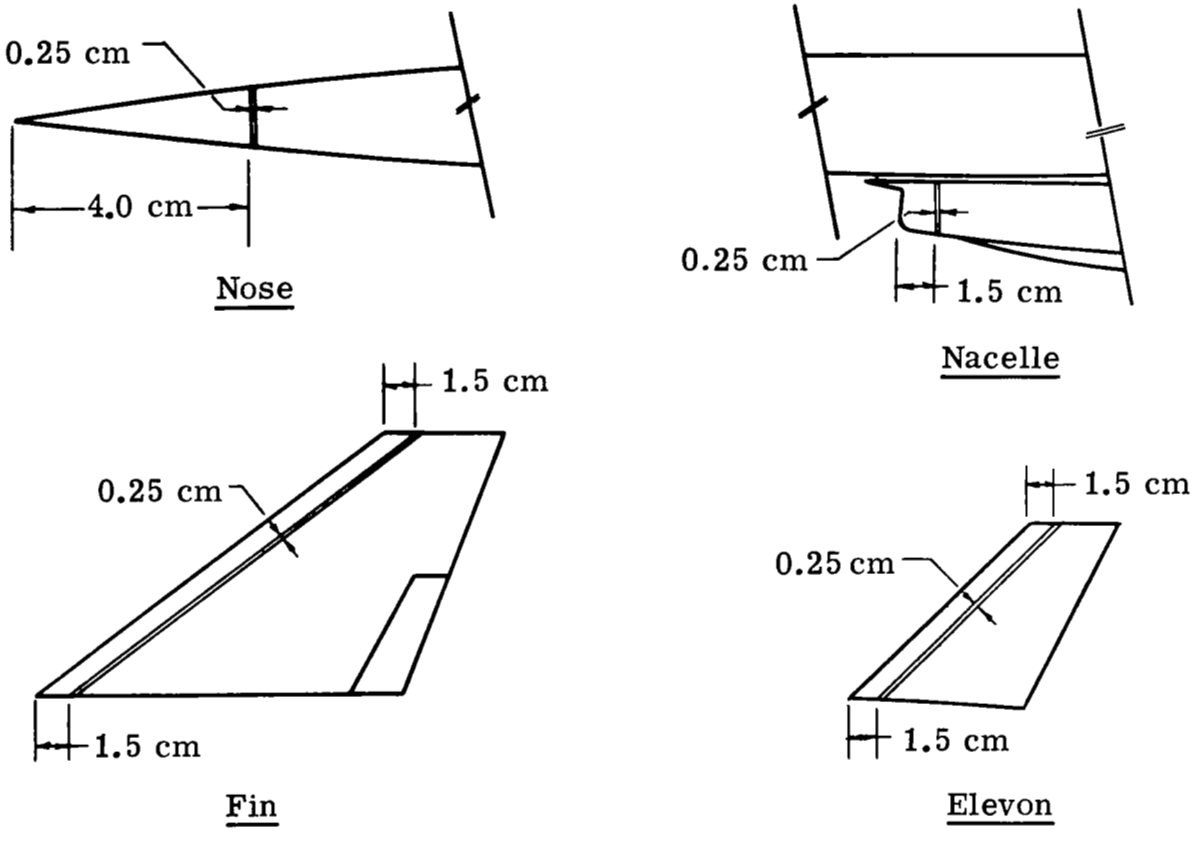

(b) Flow transition-strip patterns for fuselage and control surface.

Figure 7.- Concluded.

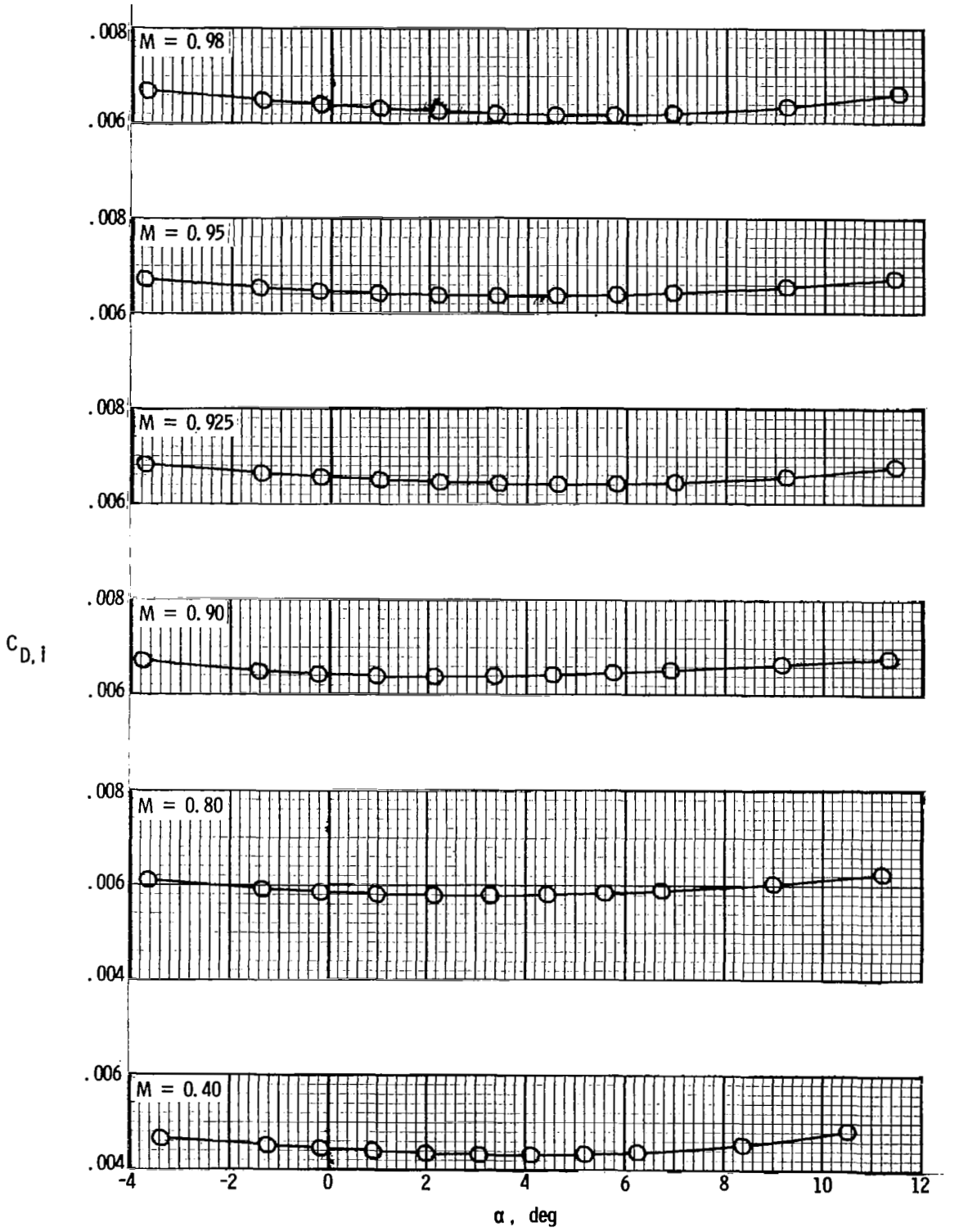

Figure 8.- Model internal-drag characteristics. $\beta = 0^{\circ}$.

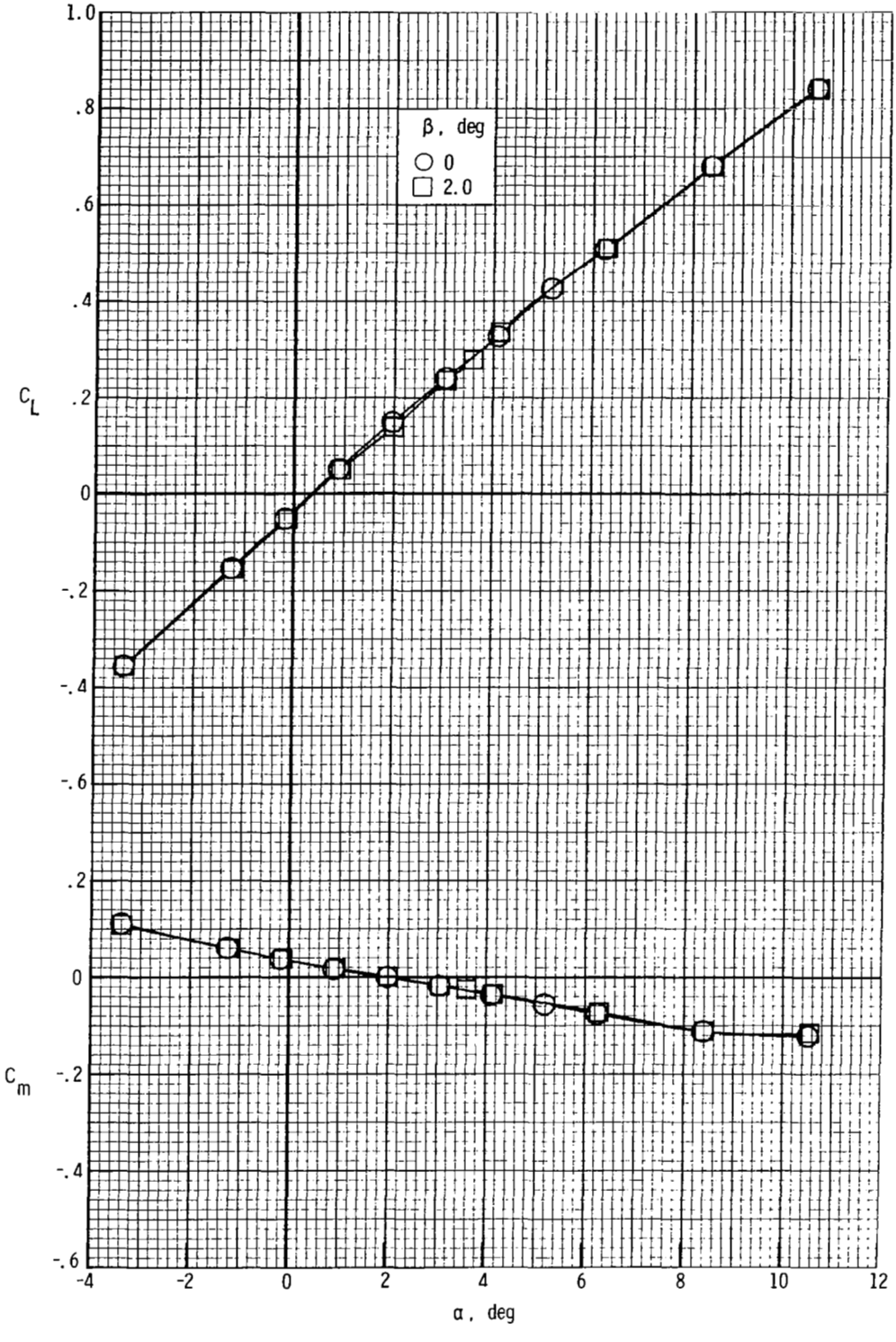

(a) M = 0.400.

Figure 9.- Variation of longitudinal aerodynamic characteristics with angle of attack at two angles of sideslip. $\delta_e = 0^o$.

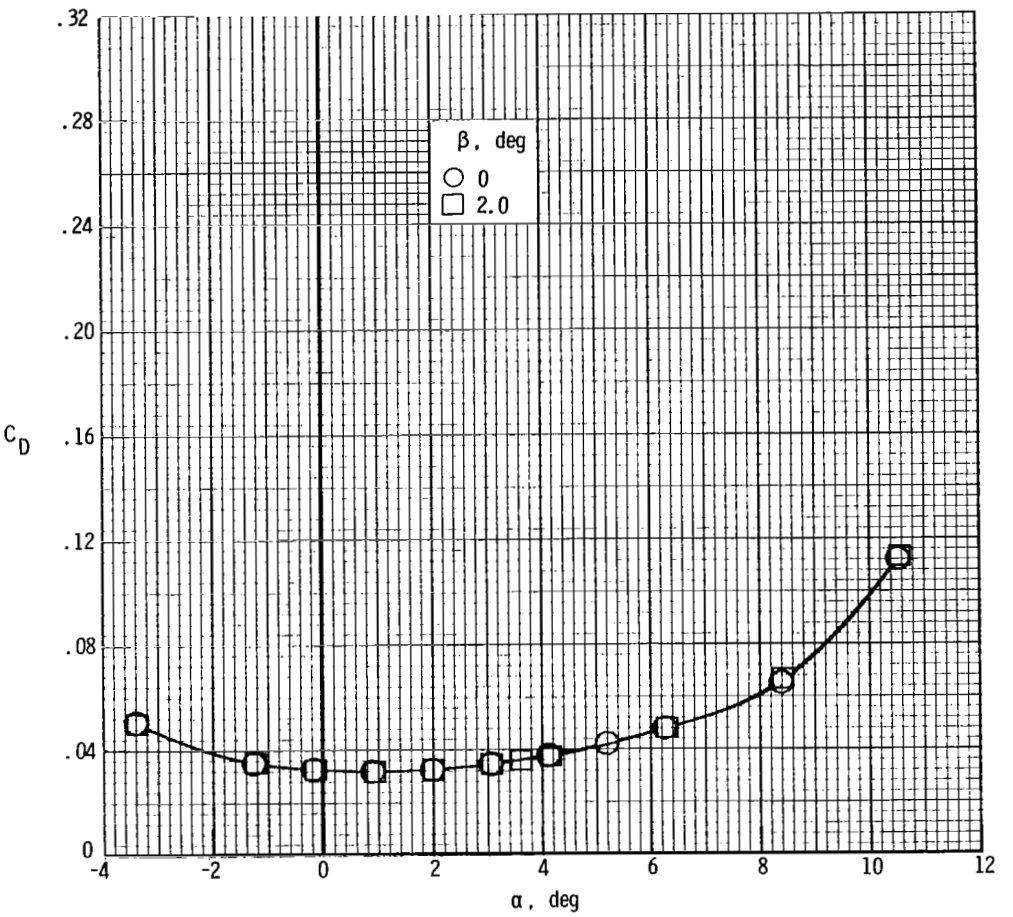

(a) M = 0.400. Concluded.

Figure 9.- Continued.

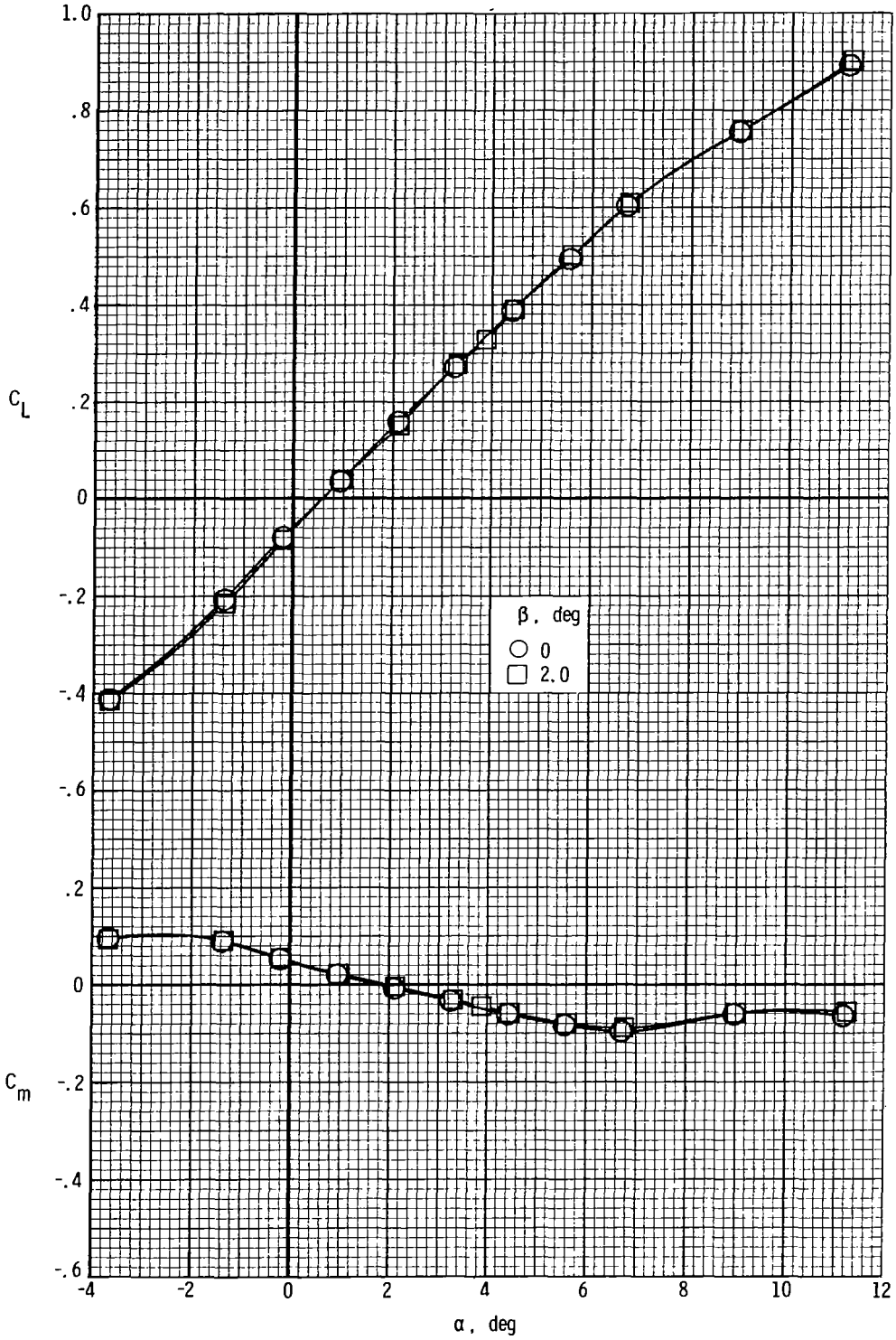

(b) M = 0.800.

Figure 9.- Continued.

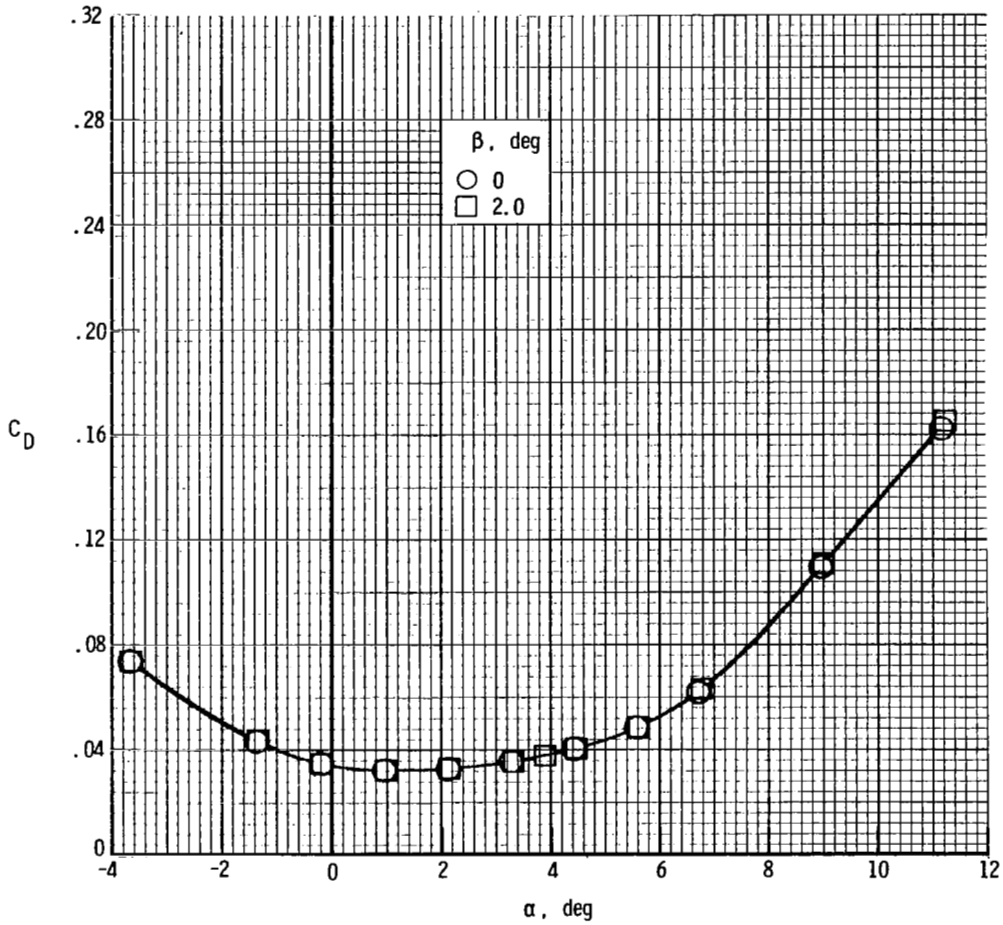

(b) M = 0.800. Concluded.

Figure 9.- Continued.

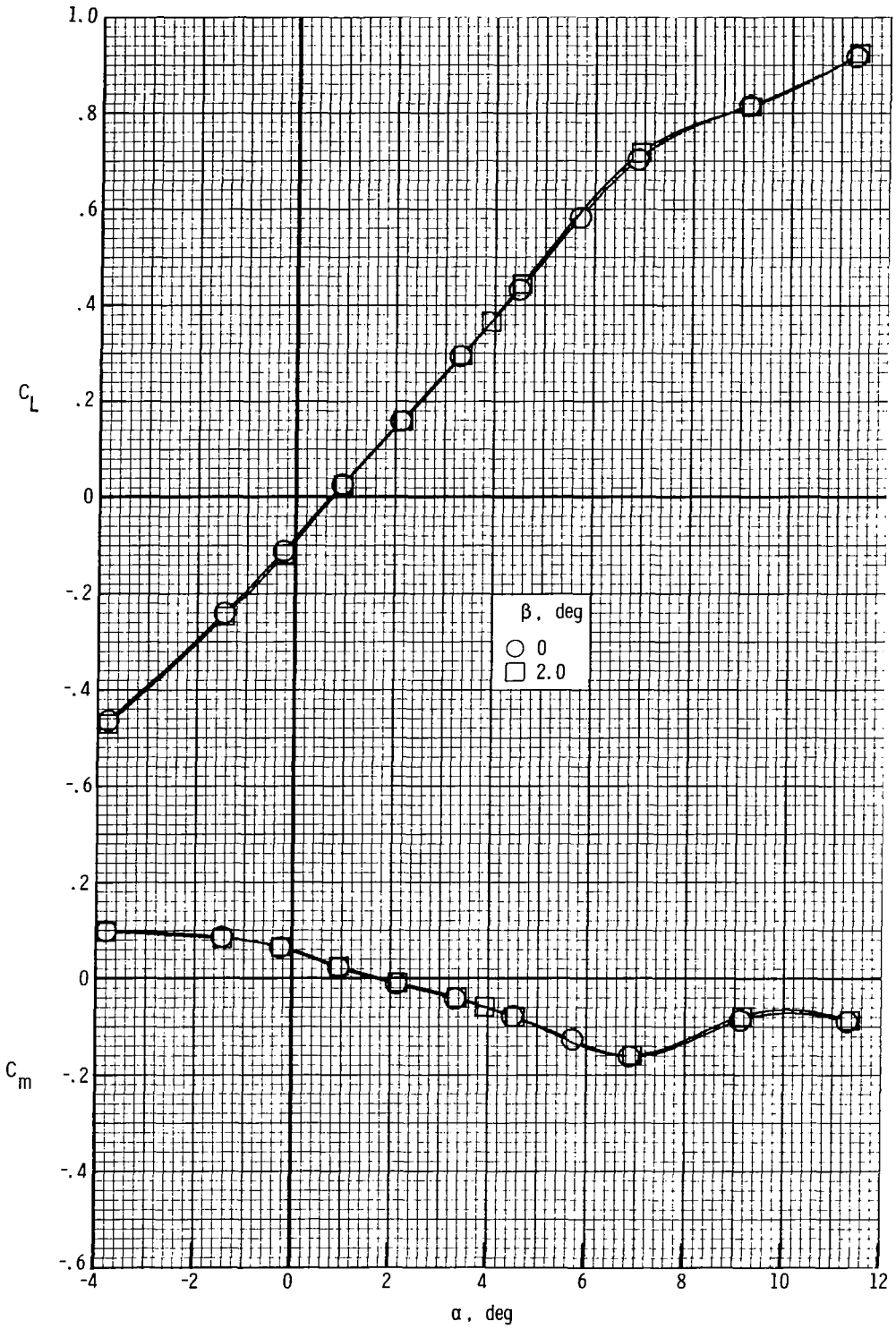

(c) M = 0.900.

Figure 9.- Continued.

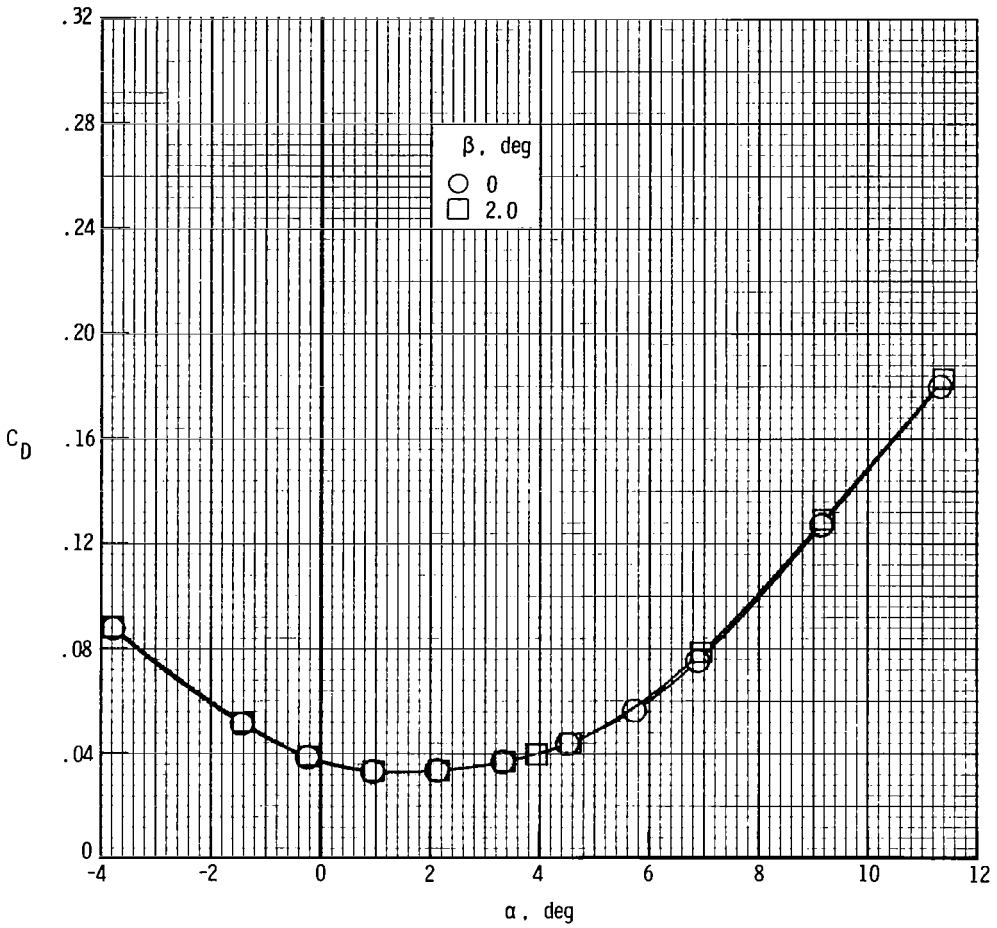

(c) M = 0.900. Concluded.

Figure 9.- Continued.

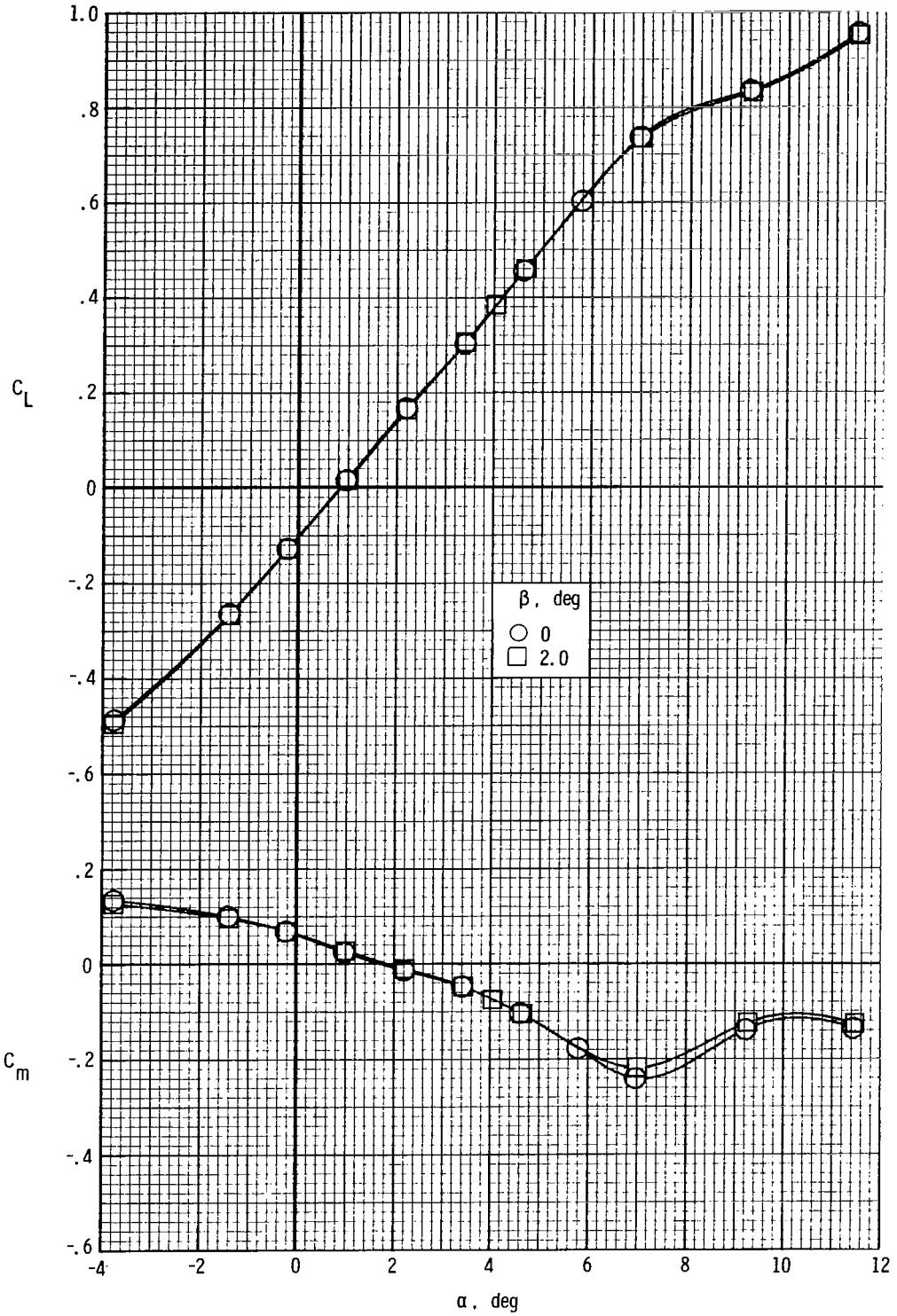

(d) M = 0.925.

Figure 9.- Continued.

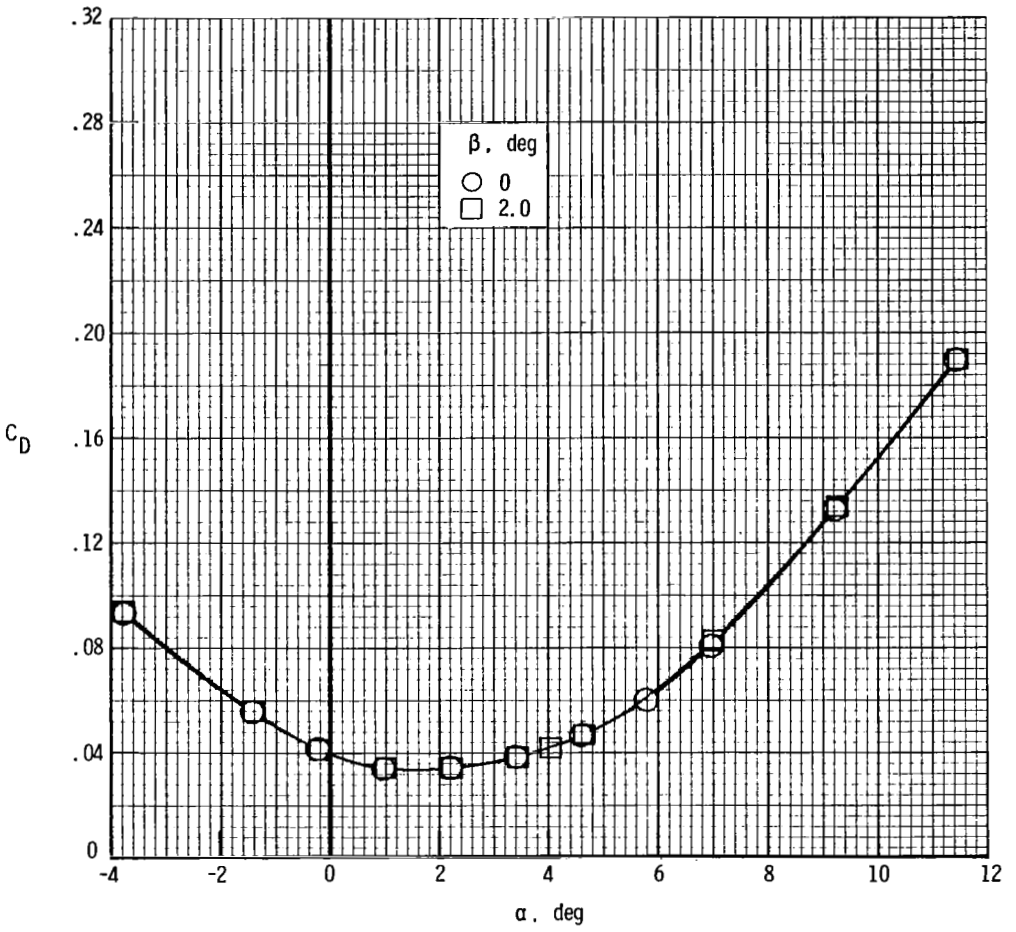

(d) M = 0.925. Concluded.

Figure 9.- Continued.

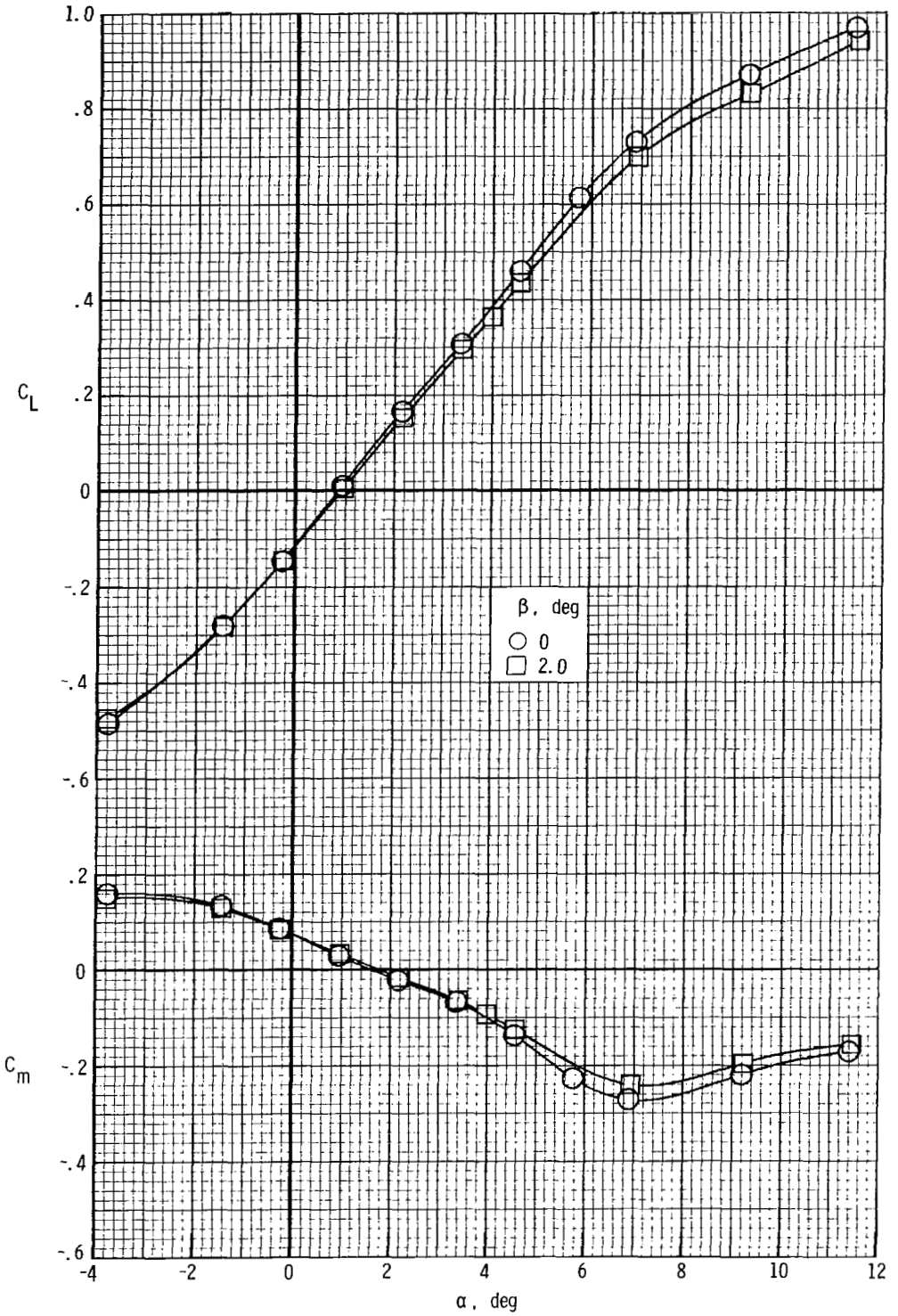

(e) M = 0.950.

Figure 9.- Continued.

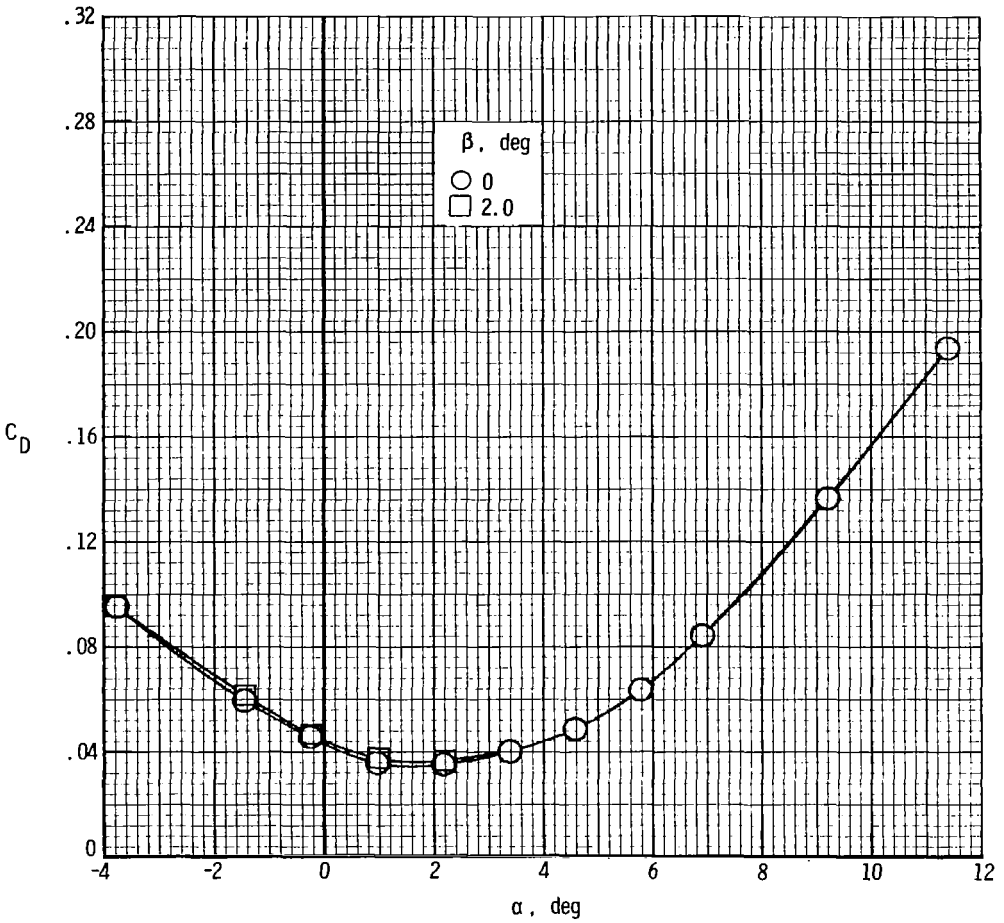

(e) M = 0.950. Concluded.

Figure 9.- Continued.

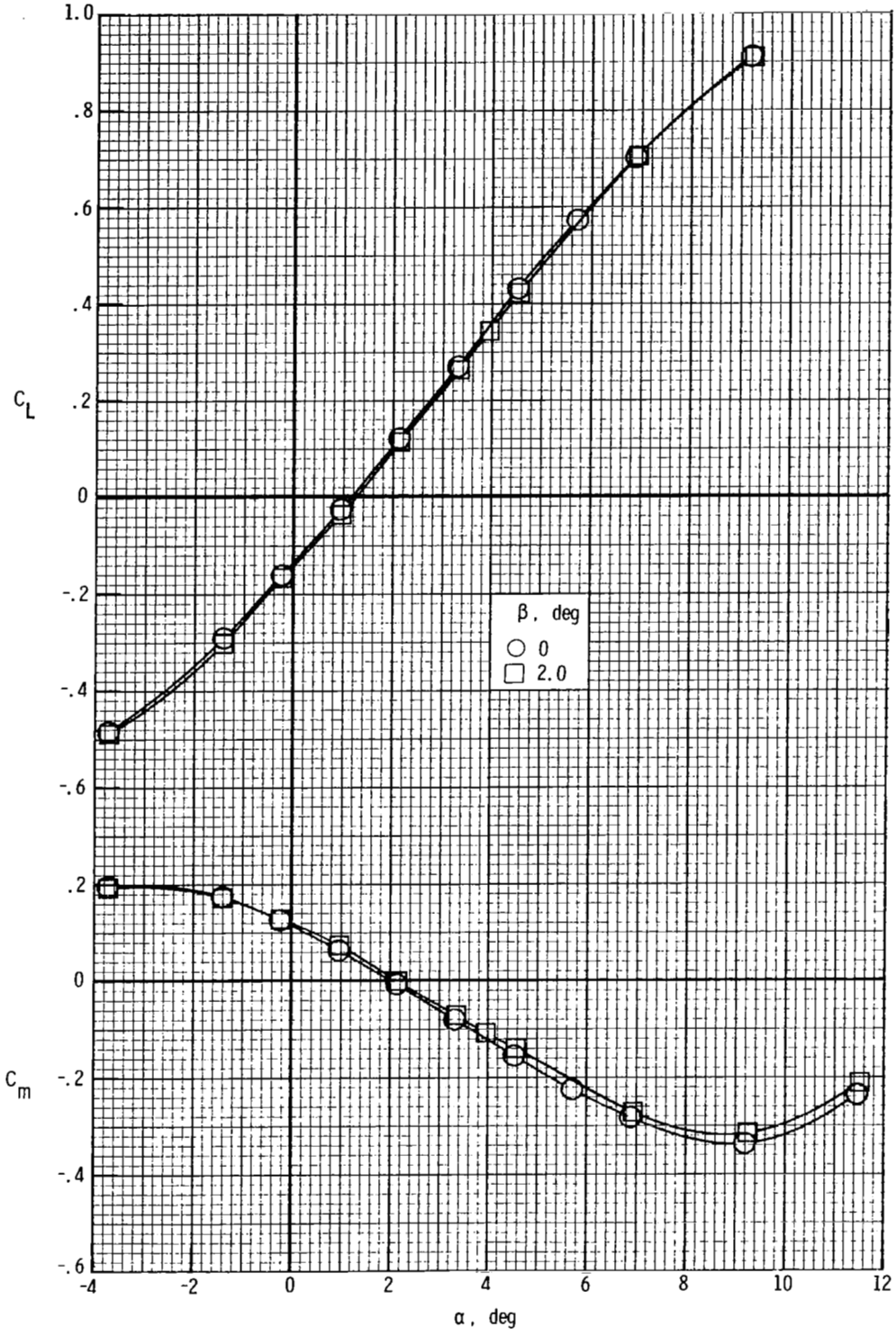

(f) M = 0.980.

Figure 9.- Continued.

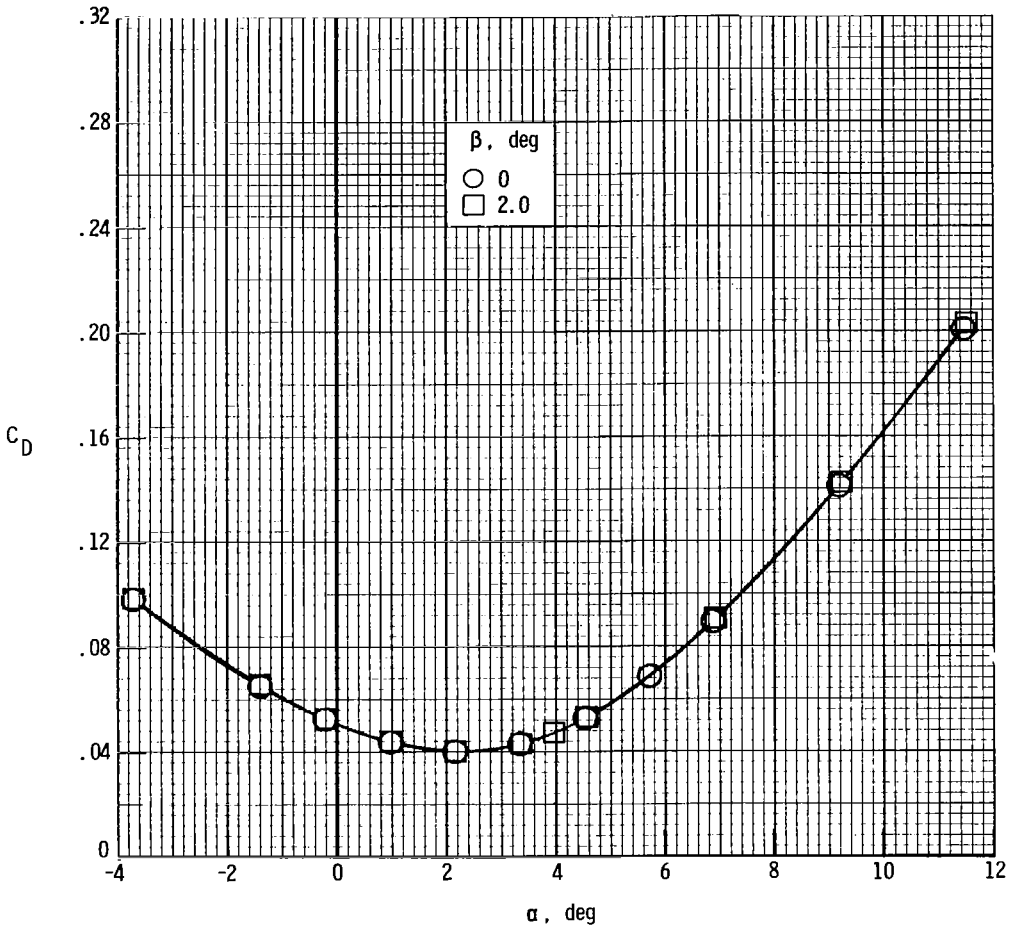

(f) M = 0.980. Concluded.

Figure 9.- Concluded.

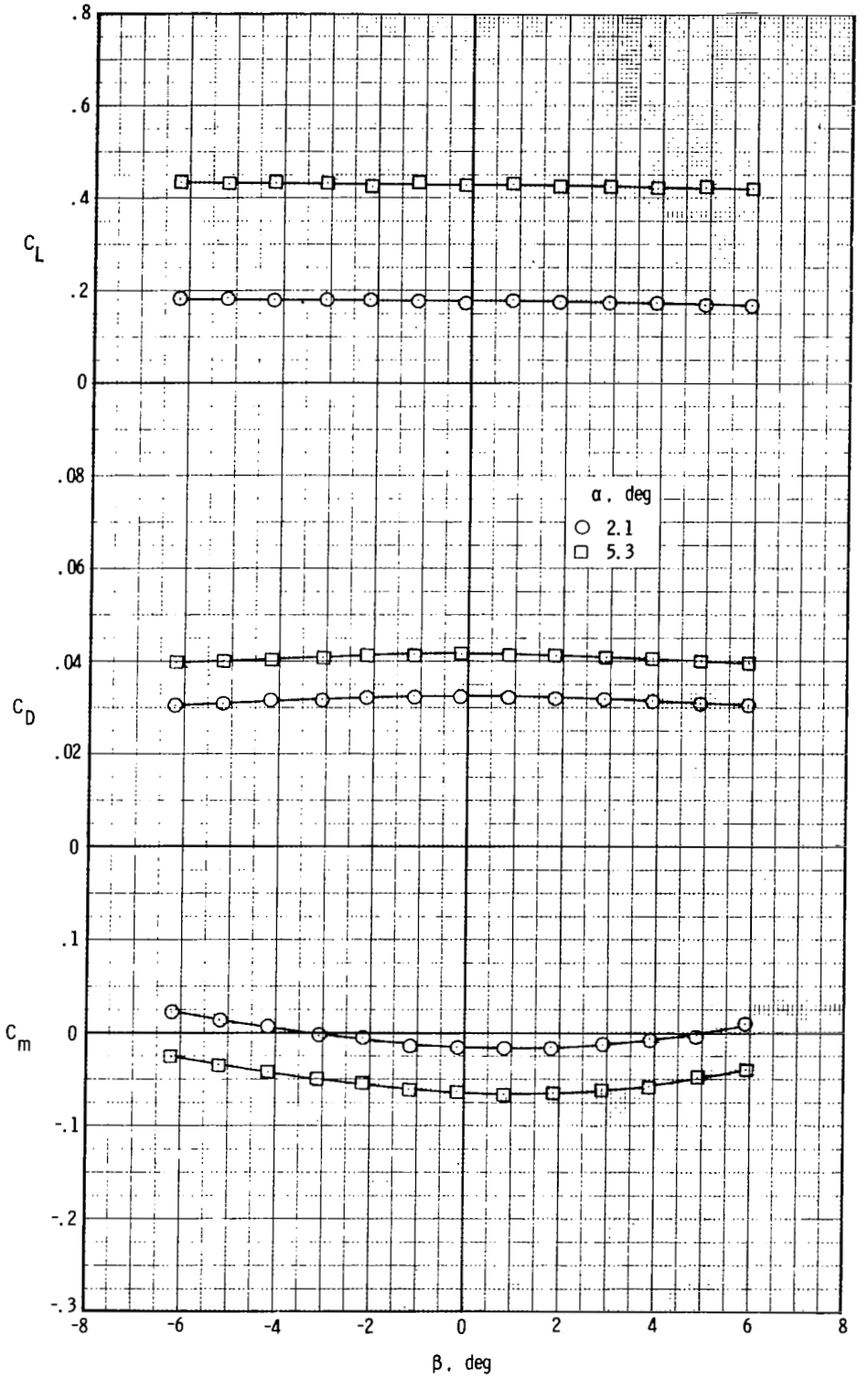

(a) M = 0.400.

Figure 10.- Variation of longitudinal aerodynamic characteristics with angle of sideslip at two angles of attack. $\delta_e = 0^{\circ}$.

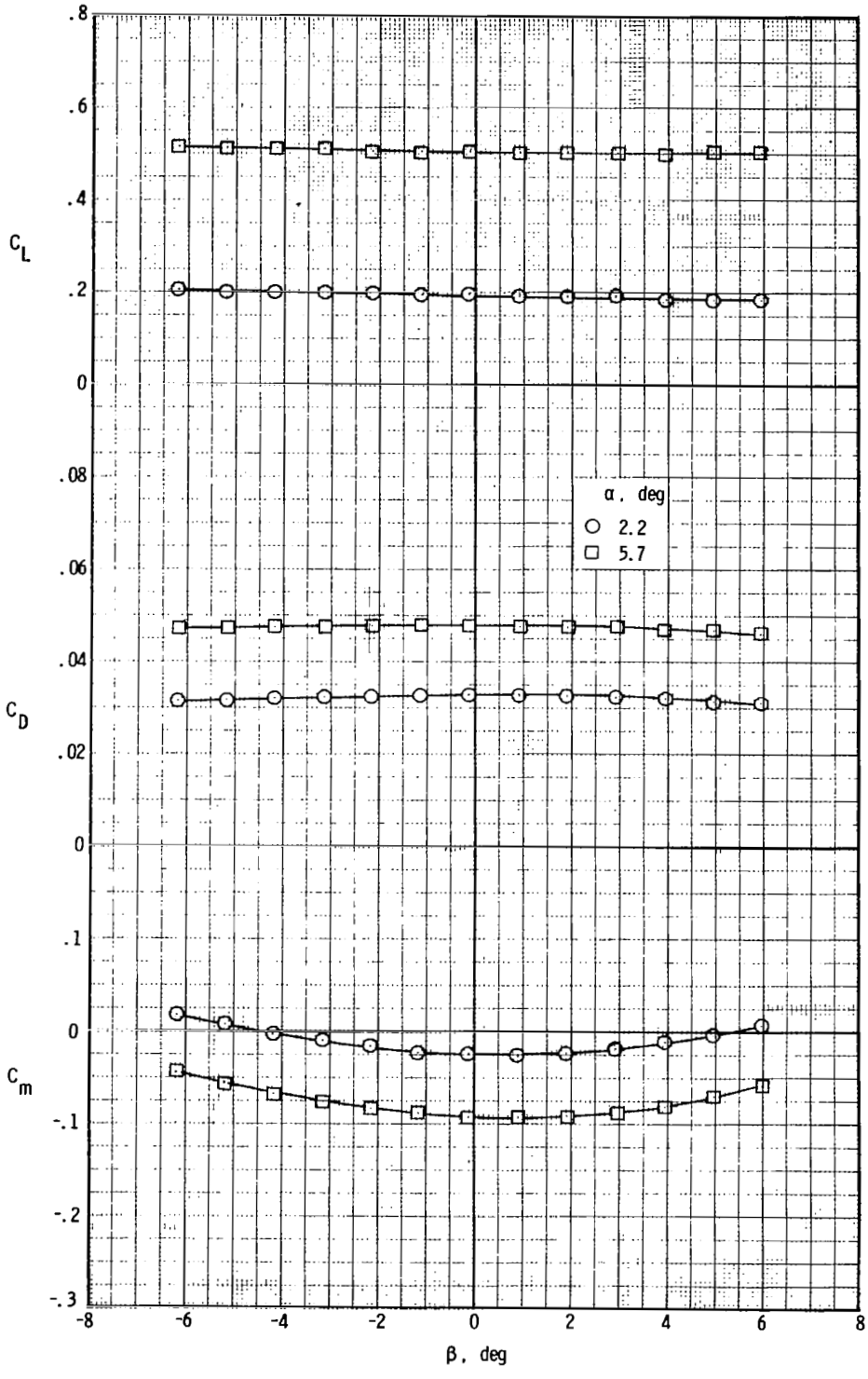

(b) M = 0.800.

Figure 10.- Continued.

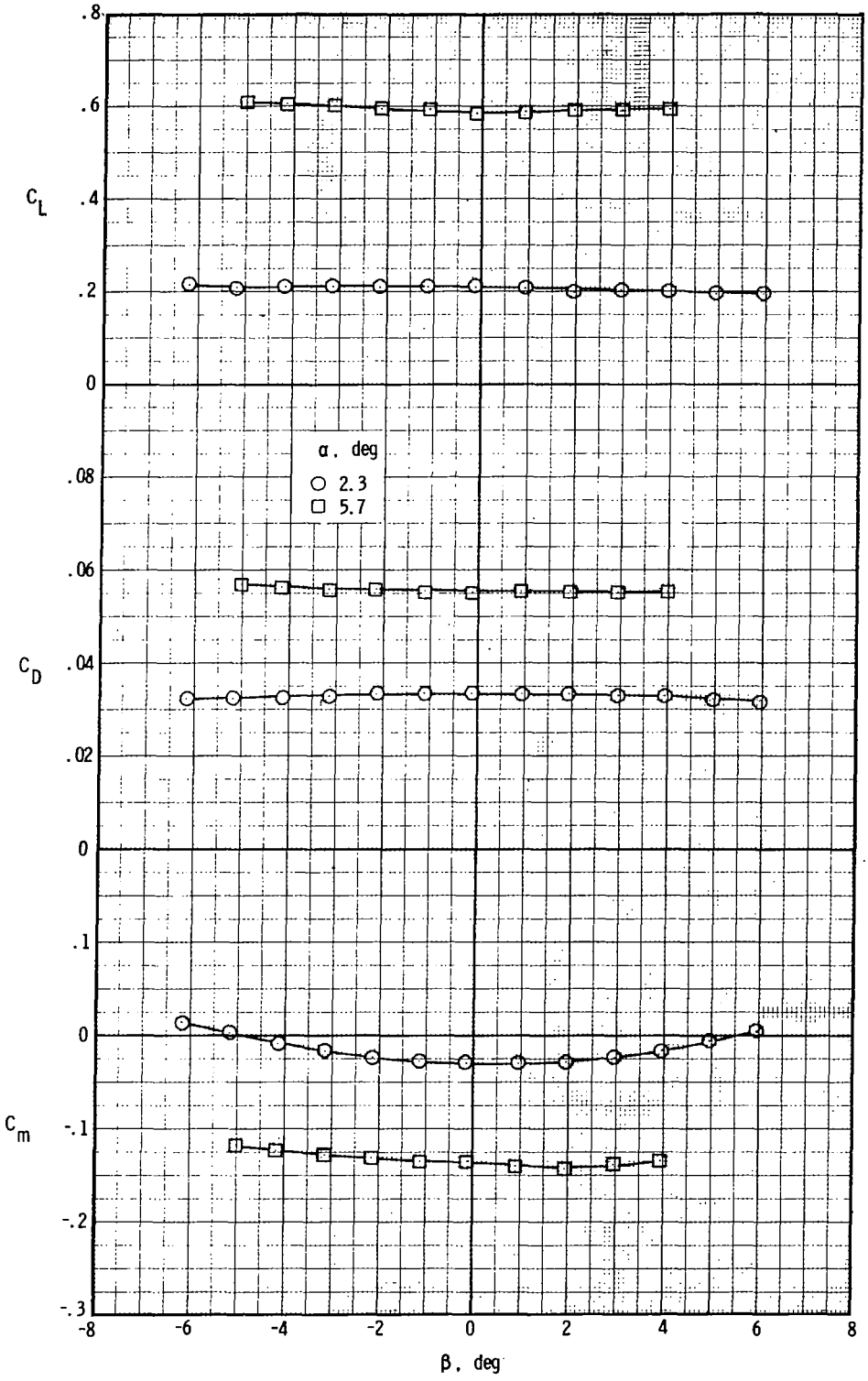

(c) M = 0.900.

Figure 10.- Continued.

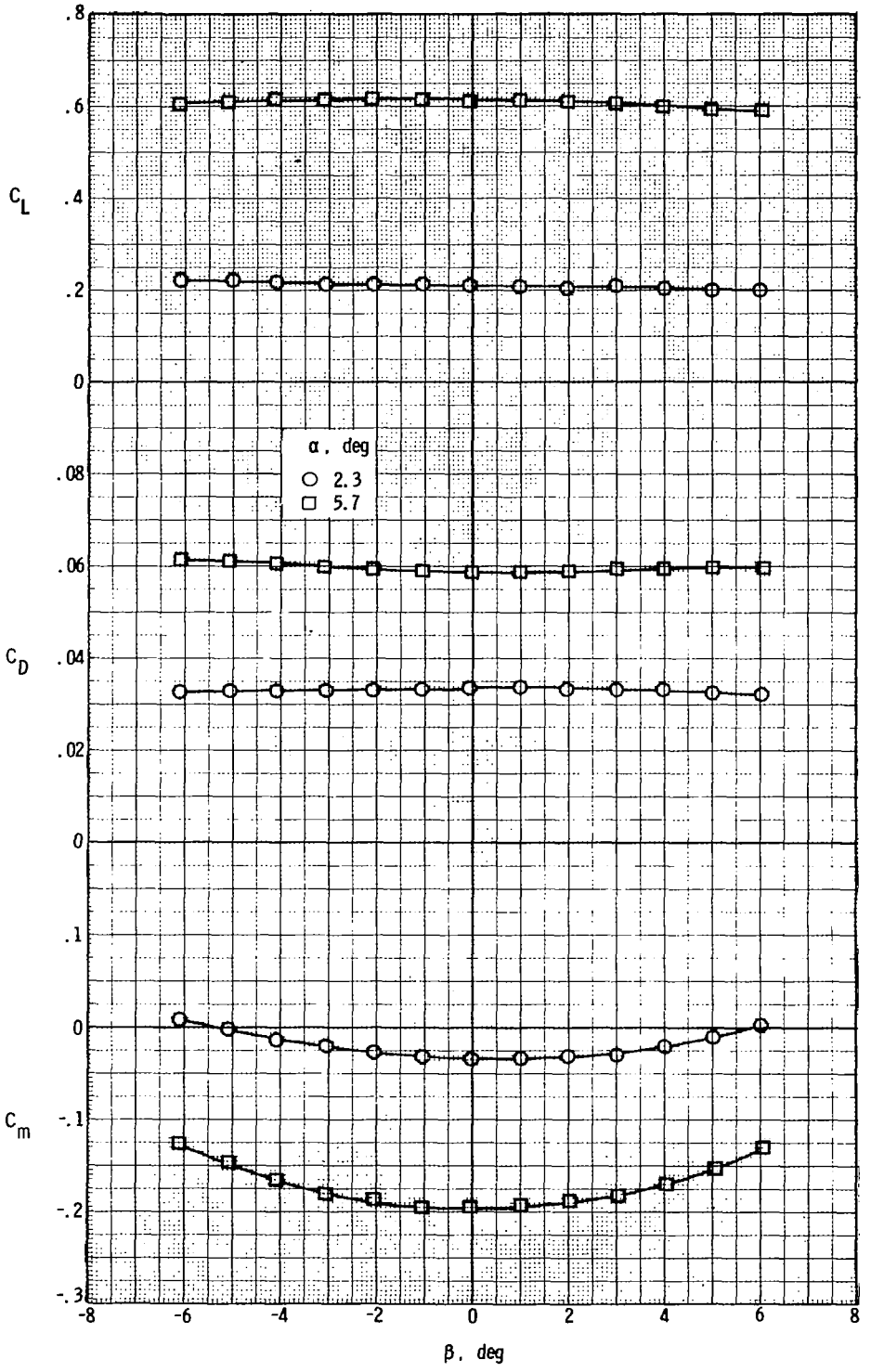

(d) M = 0.925.

Figure 10.- Continued.

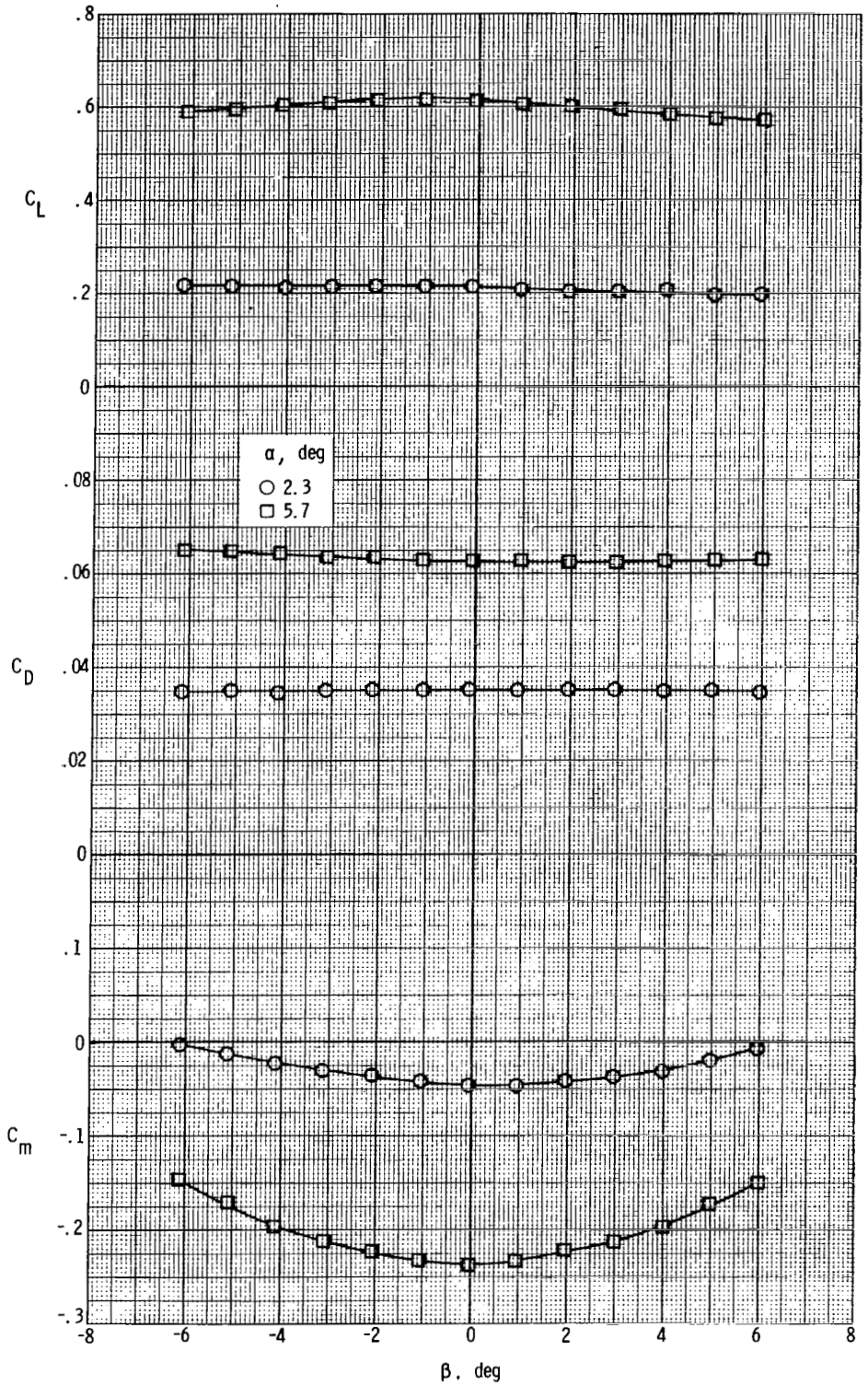

(e) M = 0.950.

Figure 10.- Continued.

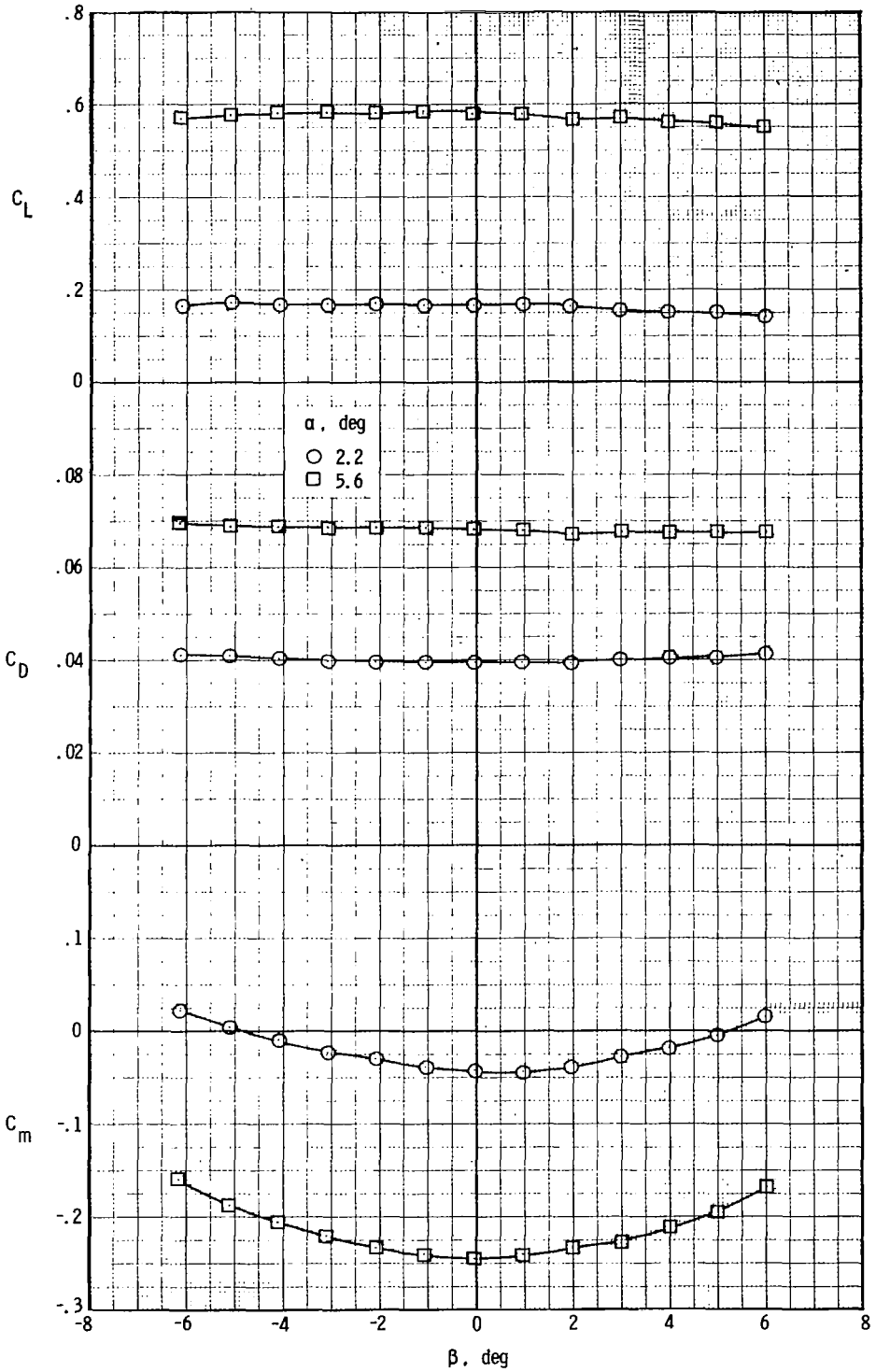

(f) M = 0.980.

Figure 10.- Concluded.

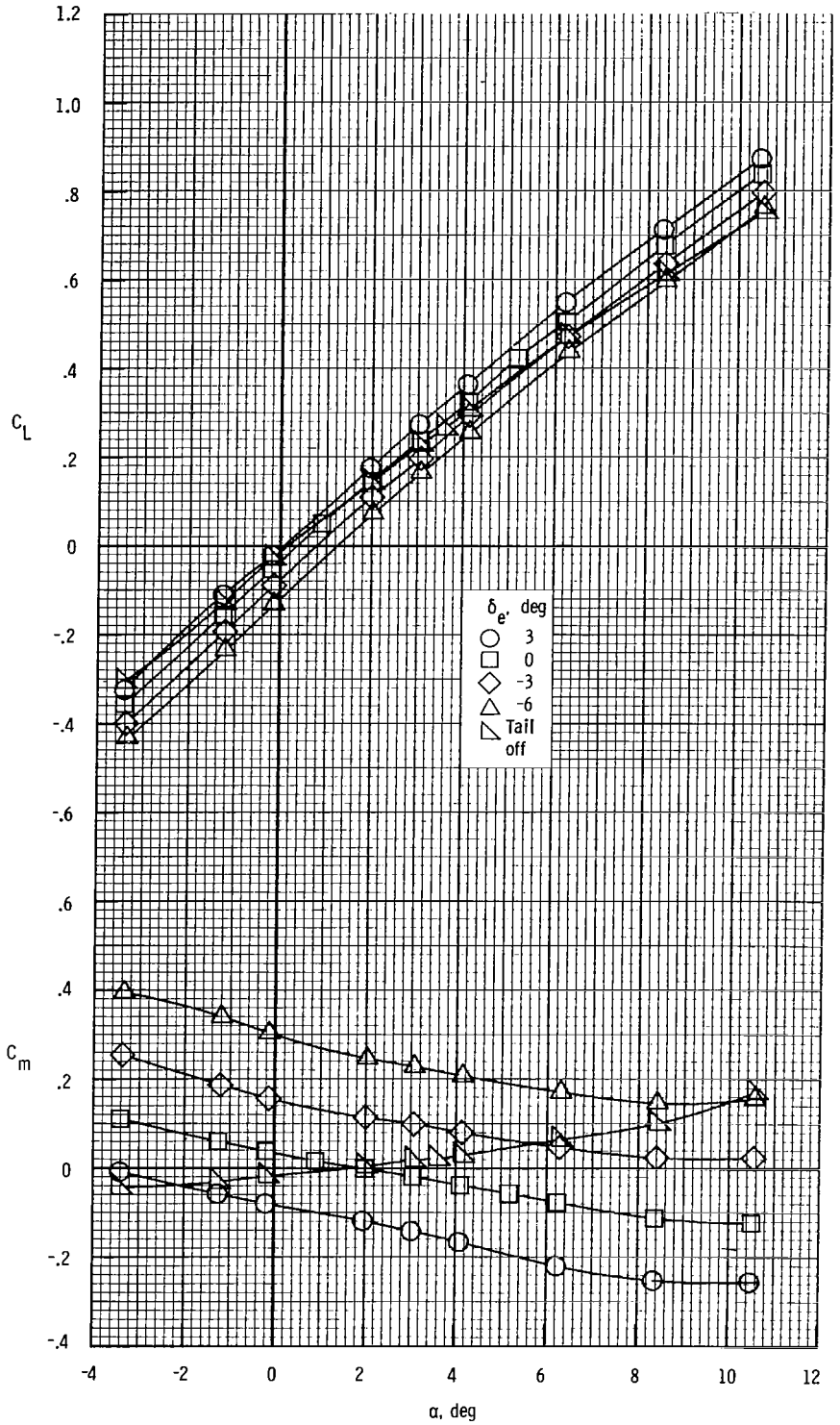

(a) M = 0.400.

Figure 11.- Effect of symmetric elevon deflection on longitudinal aerodynamic characteristics.

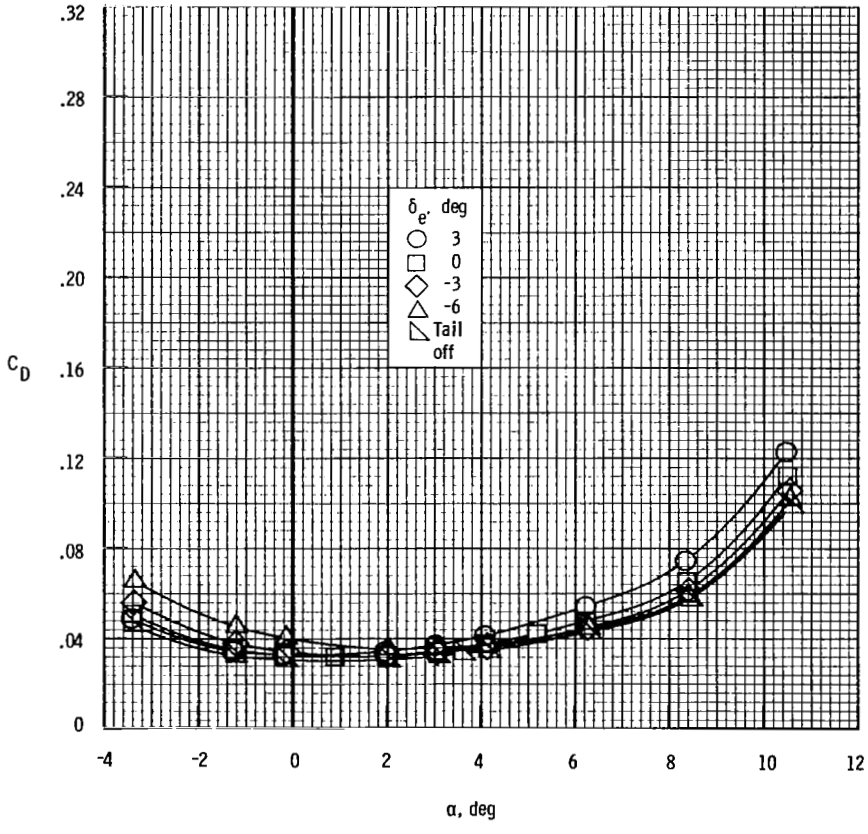

(a) M = 0.400. Concluded.

Figure 11.- Continued.

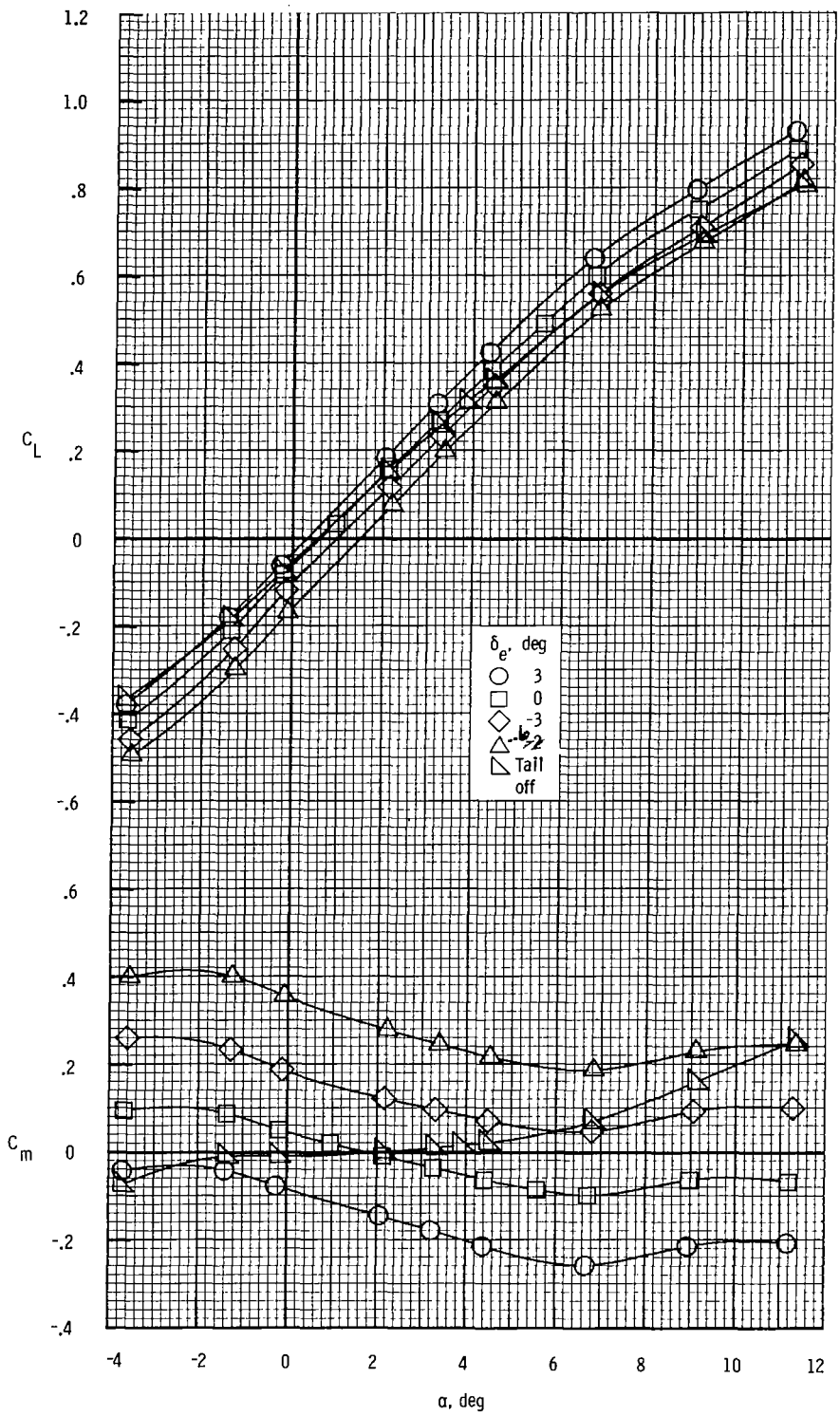

(b) M = 0.800.

Figure 11.- Continued.

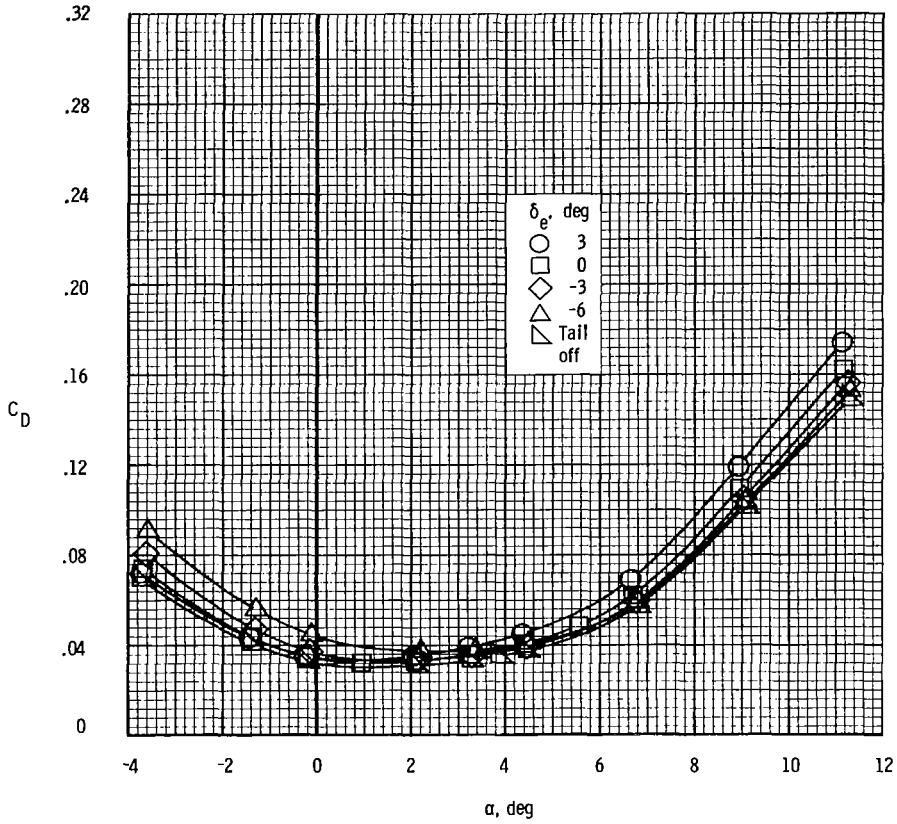

(b) M = 0.800. Concluded.

Figure 11.- Continued.

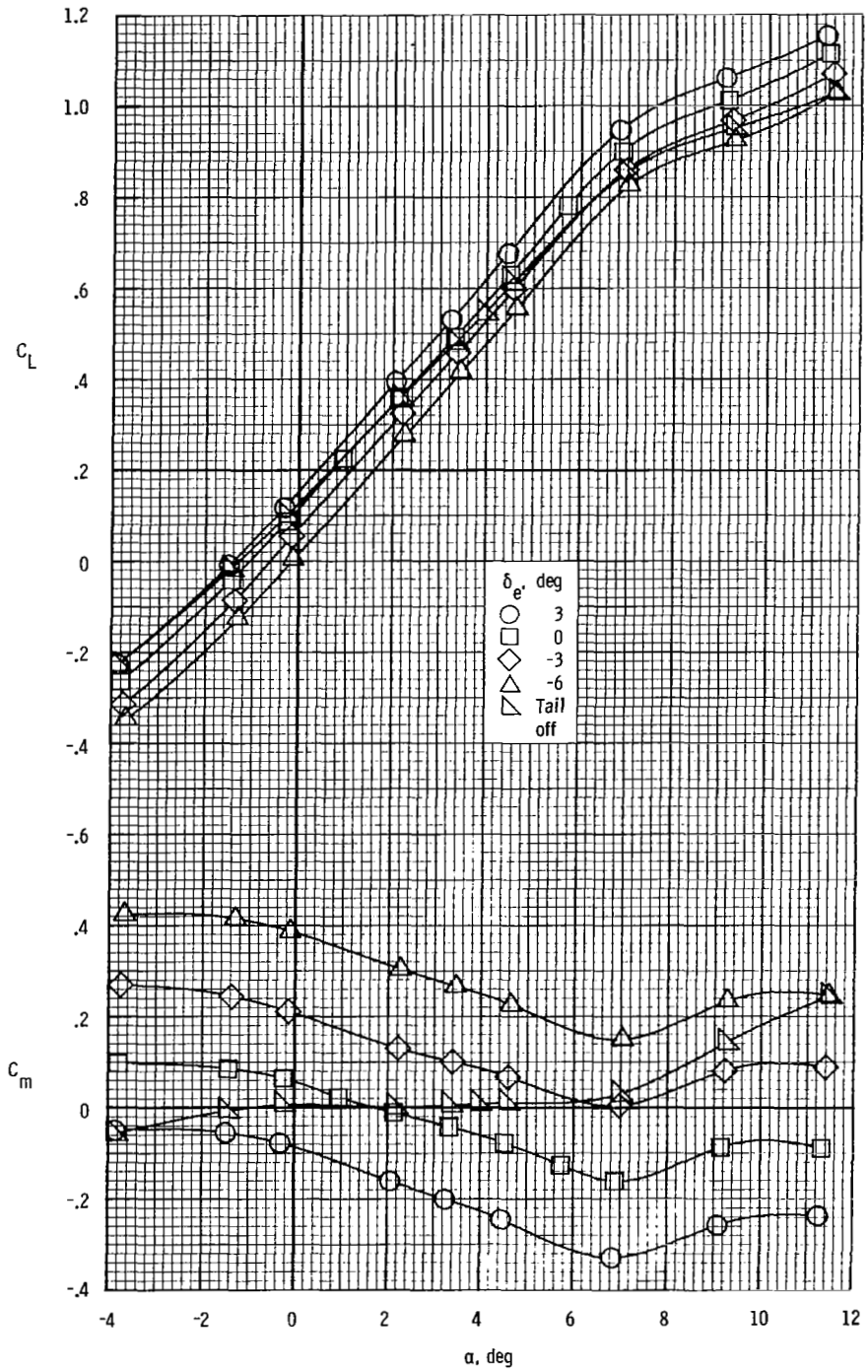

(c) M = 0.900.

Figure 11.- Continued.

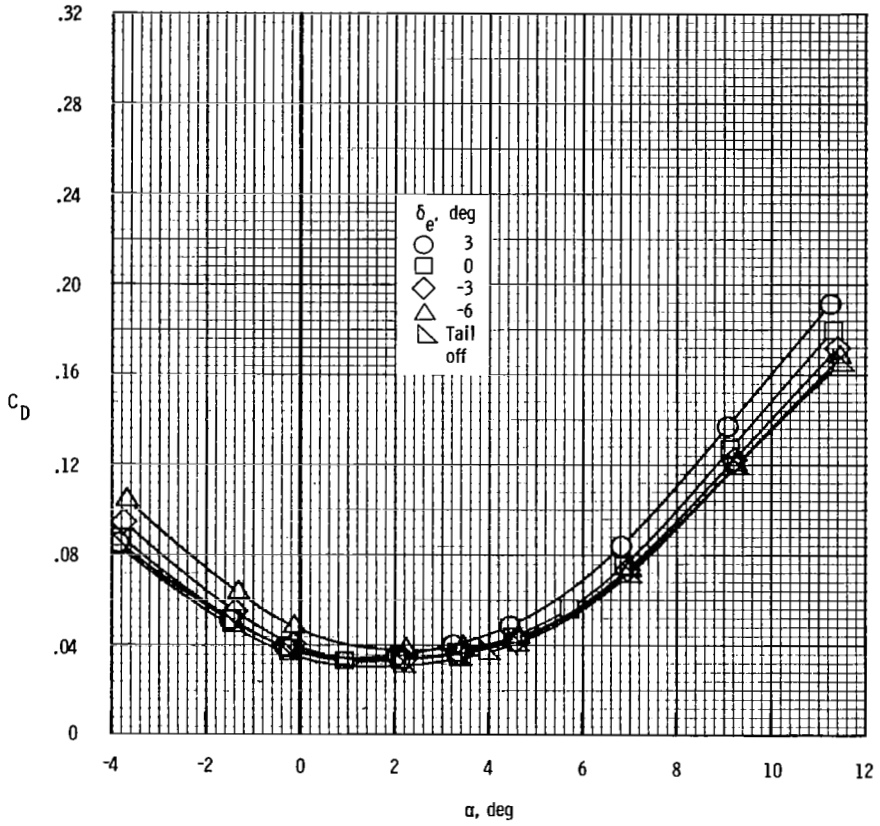

(c) M = 0.900. Concluded.

Figure 11.- Continued.

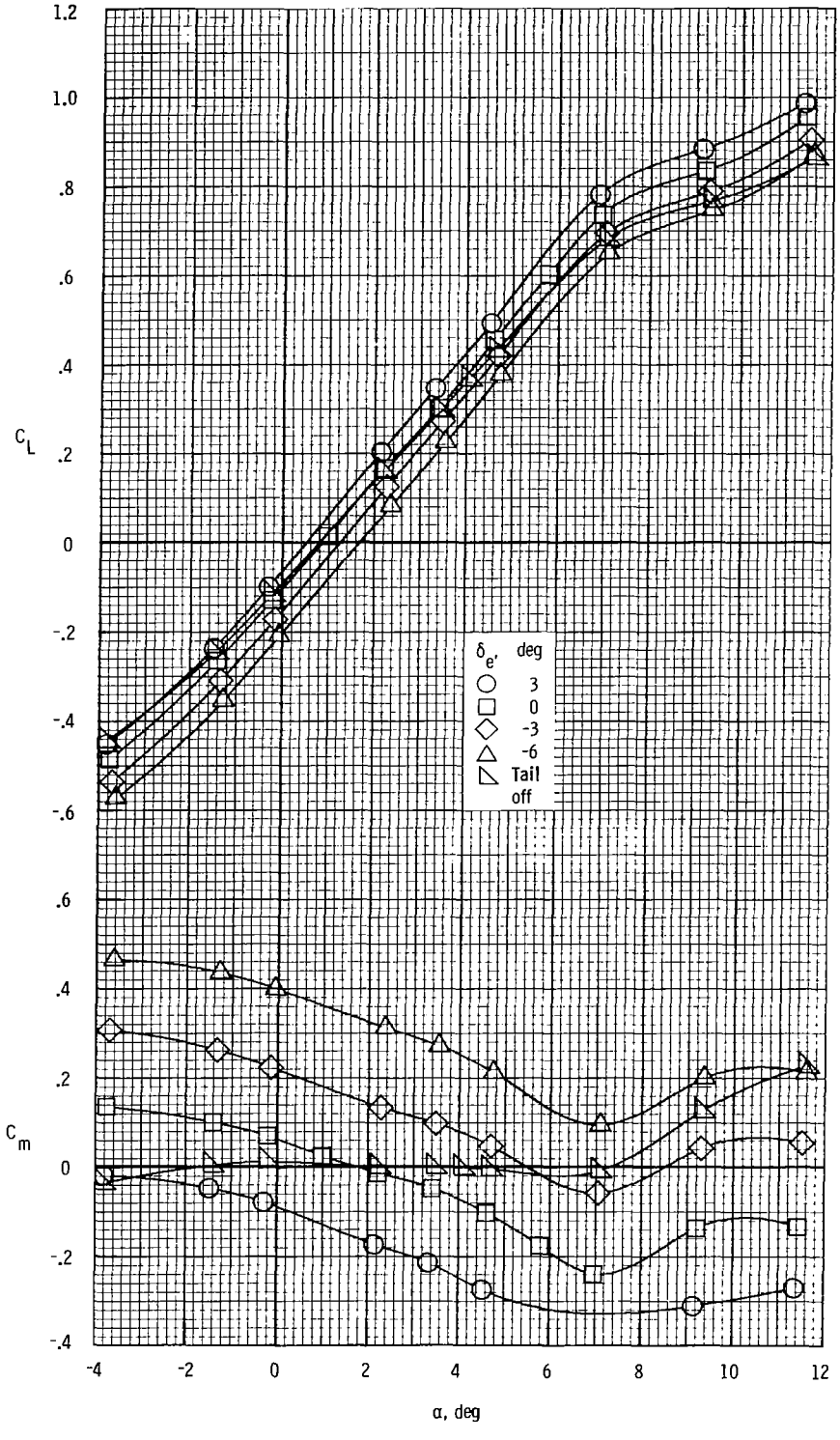

(d) M = 0.925.

Figure 11.- Continued.

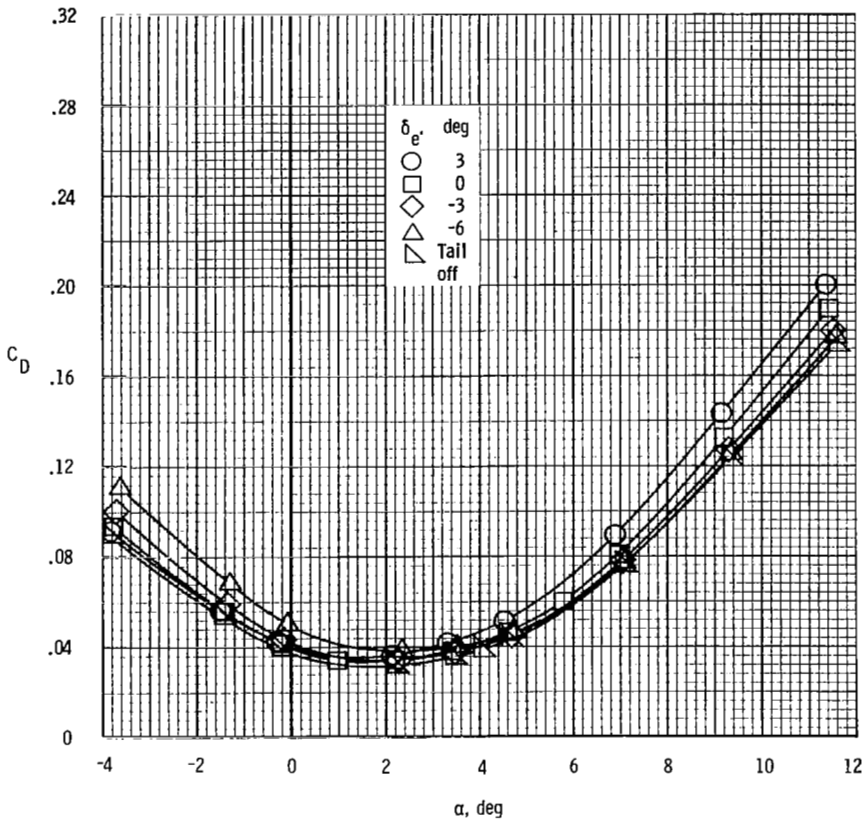

(d) M = 0.925. Concluded.

Figure 11.- Continued.

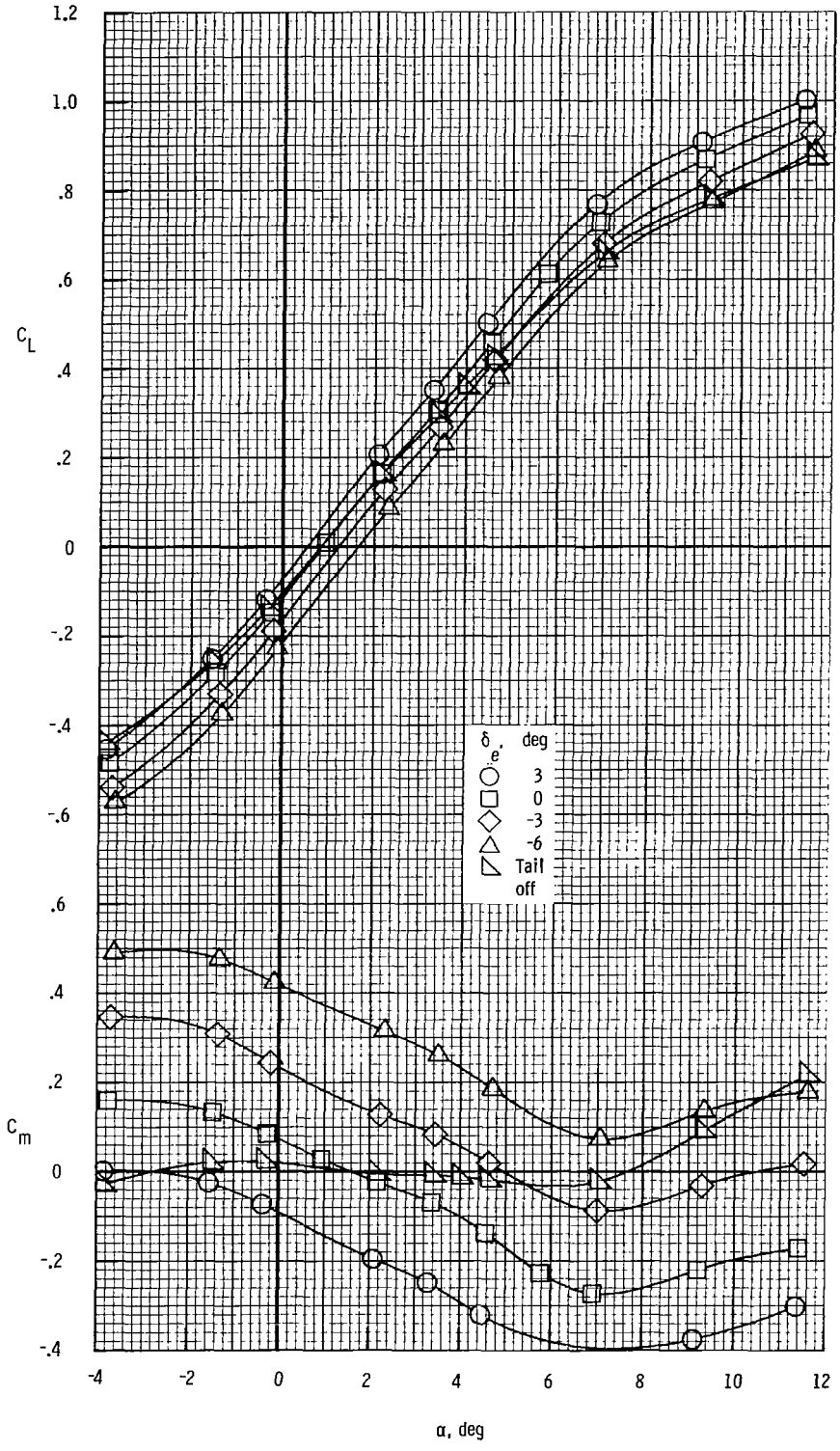

(e) M = 0.950.

Figure 11.- Continued.

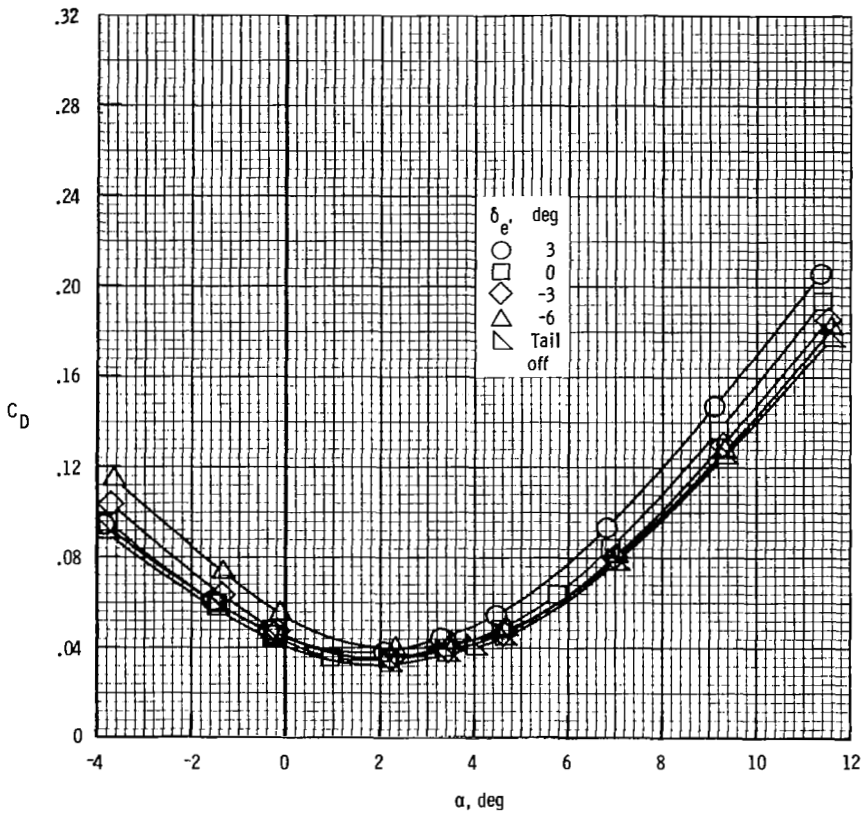

(e) M = 0.950. Concluded.

Figure 11.- Continued.

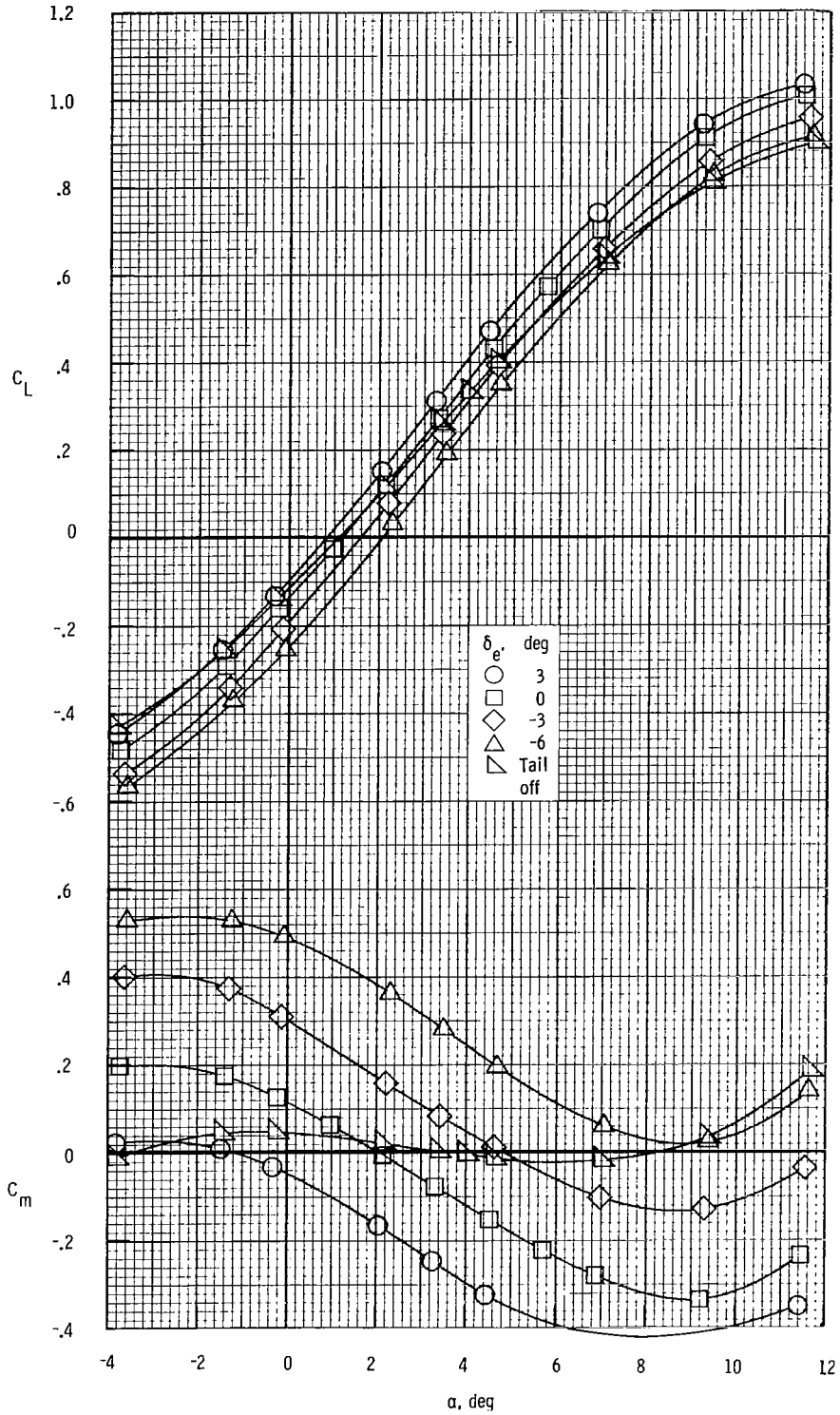

(f) M = 0.980.

Figure 11.- Continued.

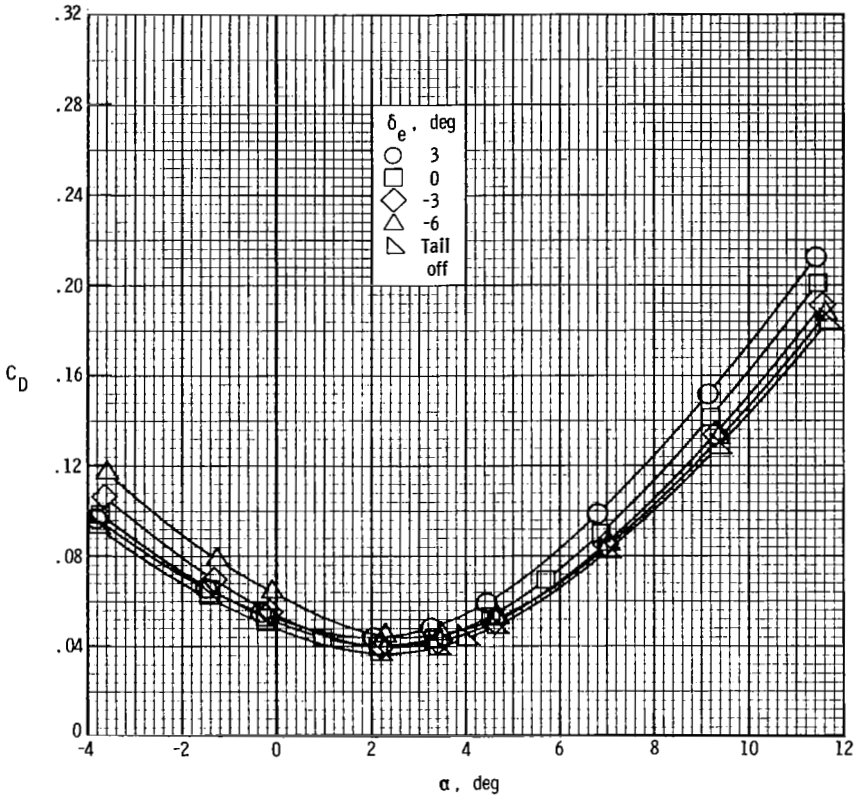

(f) M = 0.980. Concluded.

Figure 11.- Concluded.

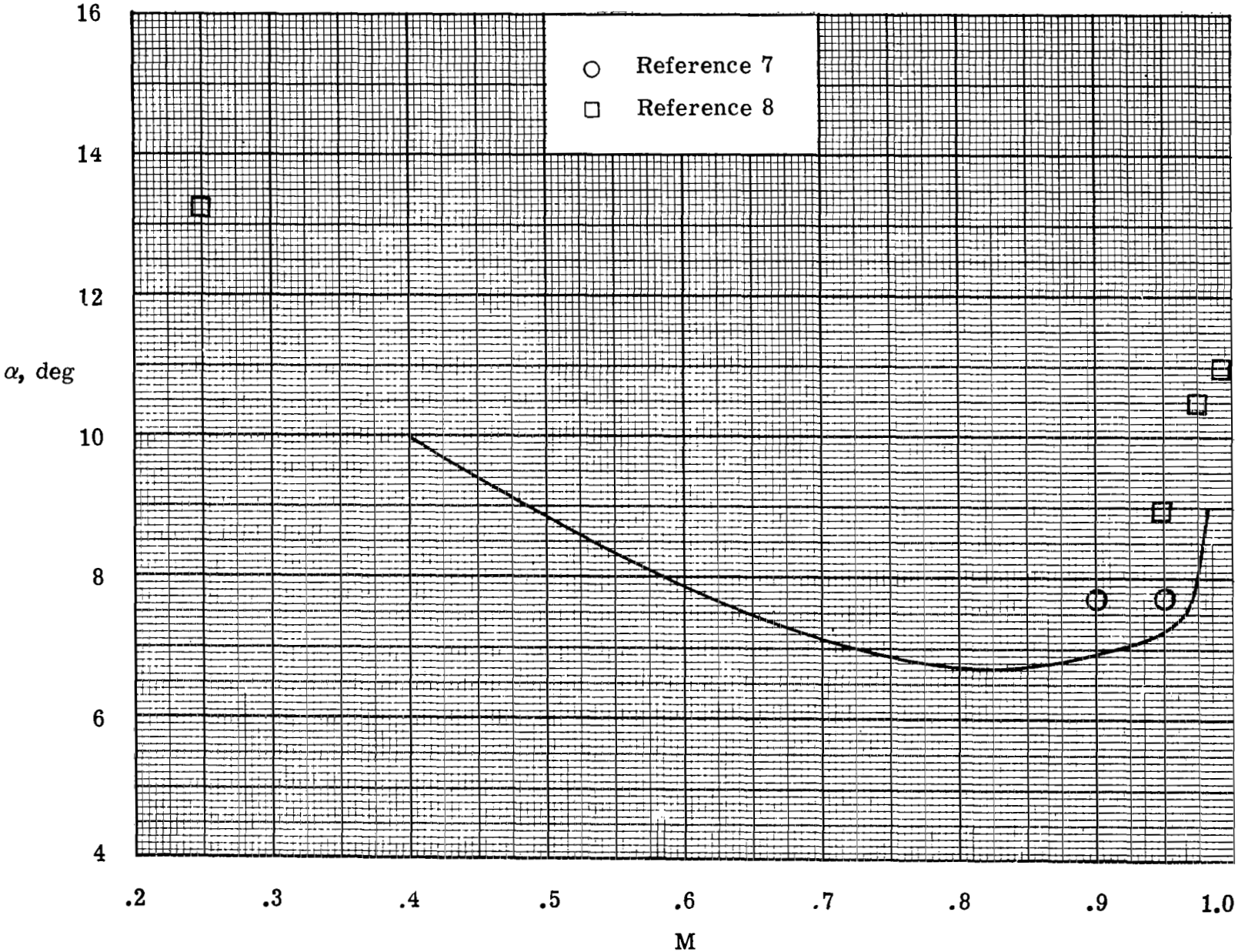

Figure 12.- Variation of pitch-up angle of attack $\left(C_{m_\alpha} = 0\right)$ with Mach number. $\delta_e = 0^\circ$.

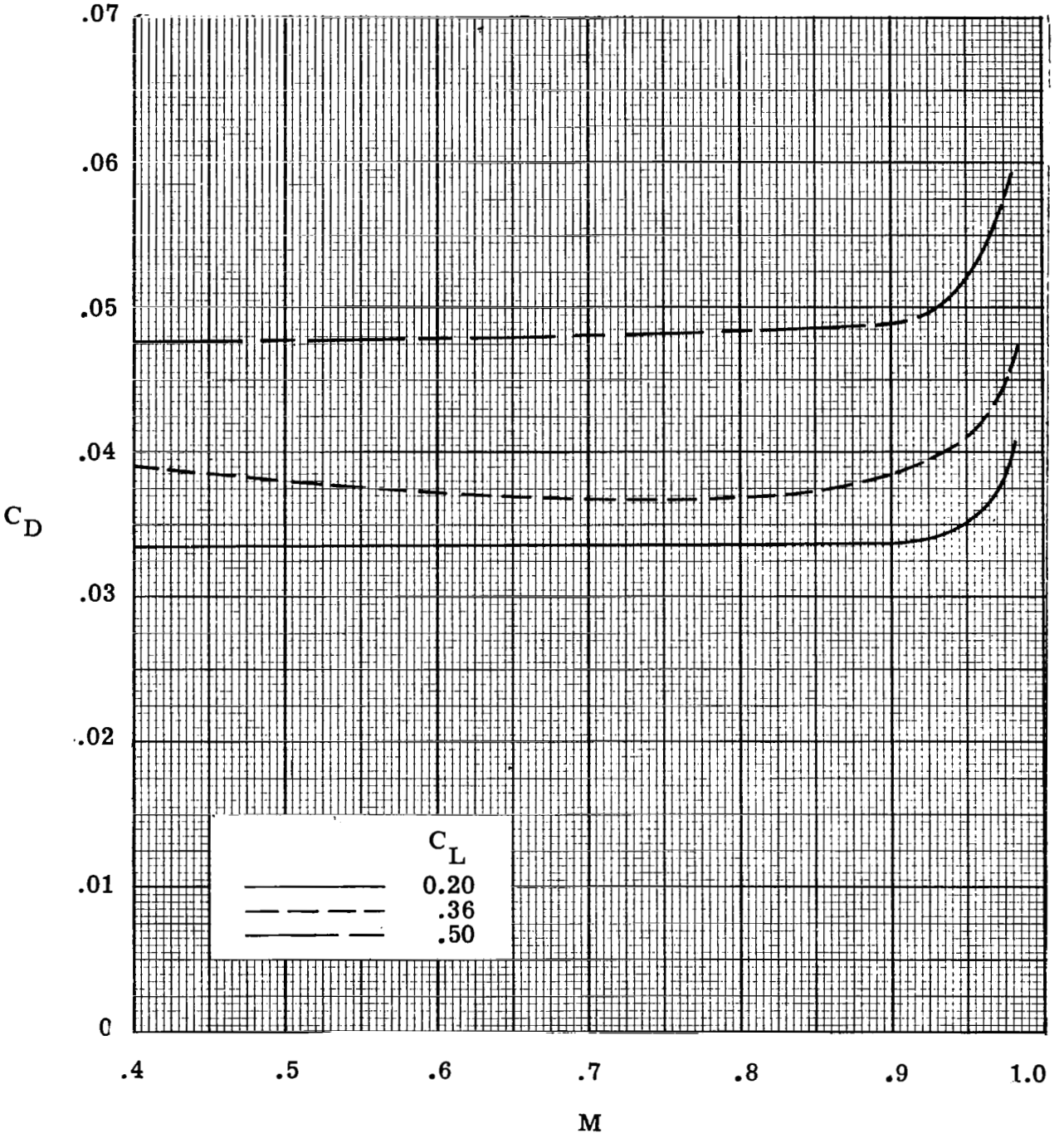

Figure 13.- Variation of drag coefficient with Mach number for three values of lift coefficient. $R = 6.6 \times 10^6$ per meter. $\delta_e = 0^\circ$.

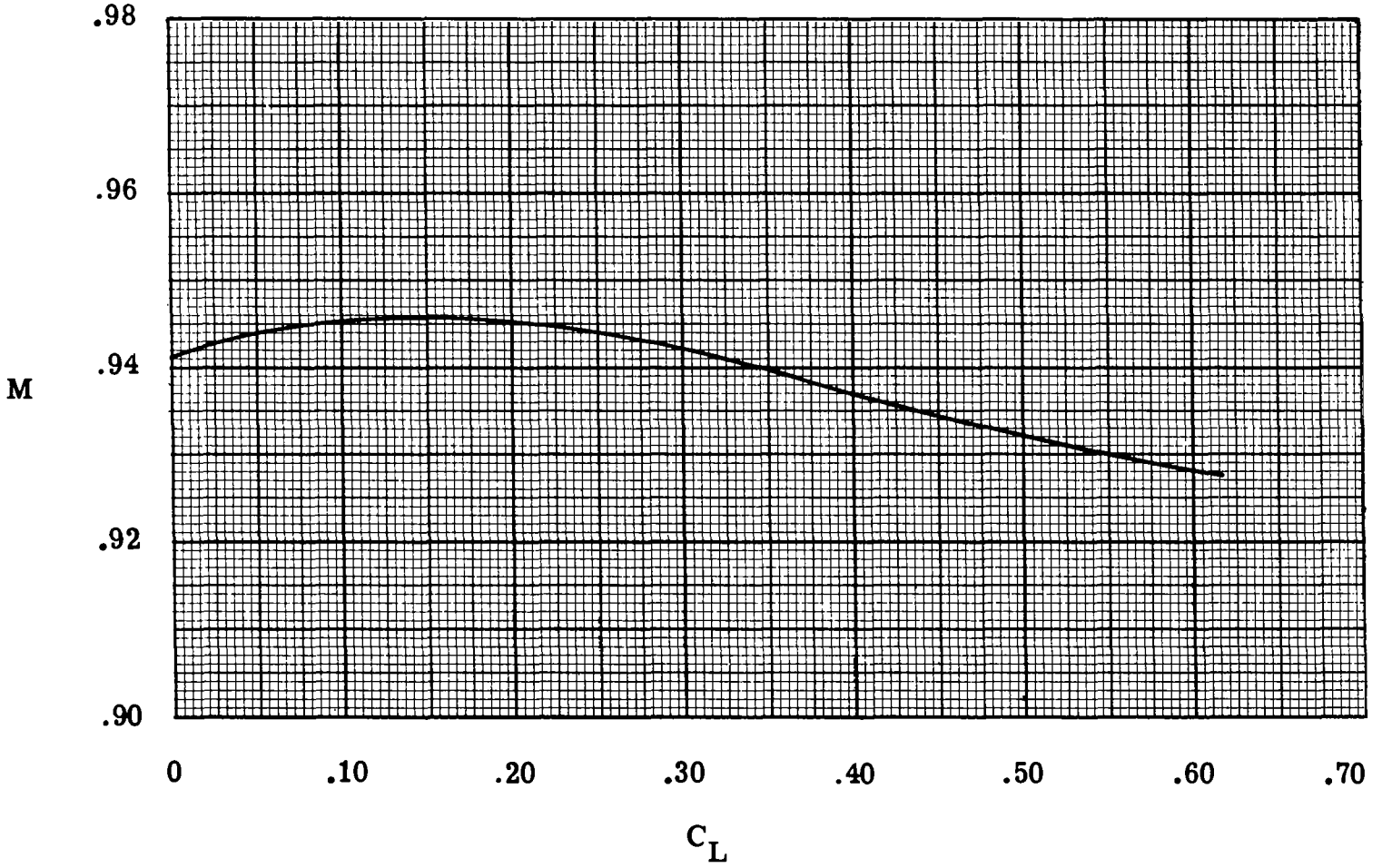

Figure 14.- Variation of drag-divergence Mach number with lift coefficient. $R = 6.6 \times 10^6$ per meter.

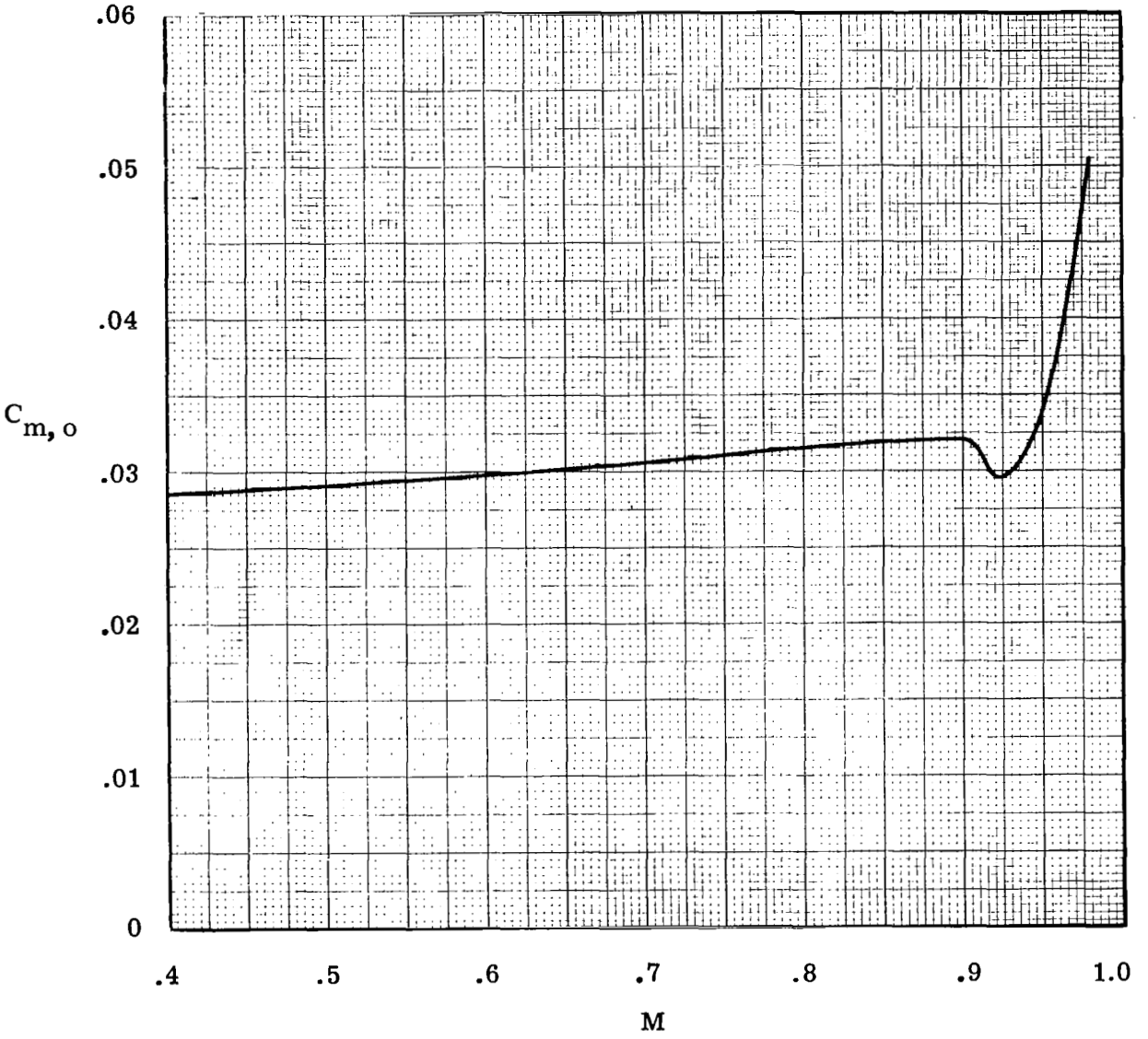

Figure 15.- Variation of zero-lift pitching-moment coefficient with Mach number. $\delta_e = 0^o$.

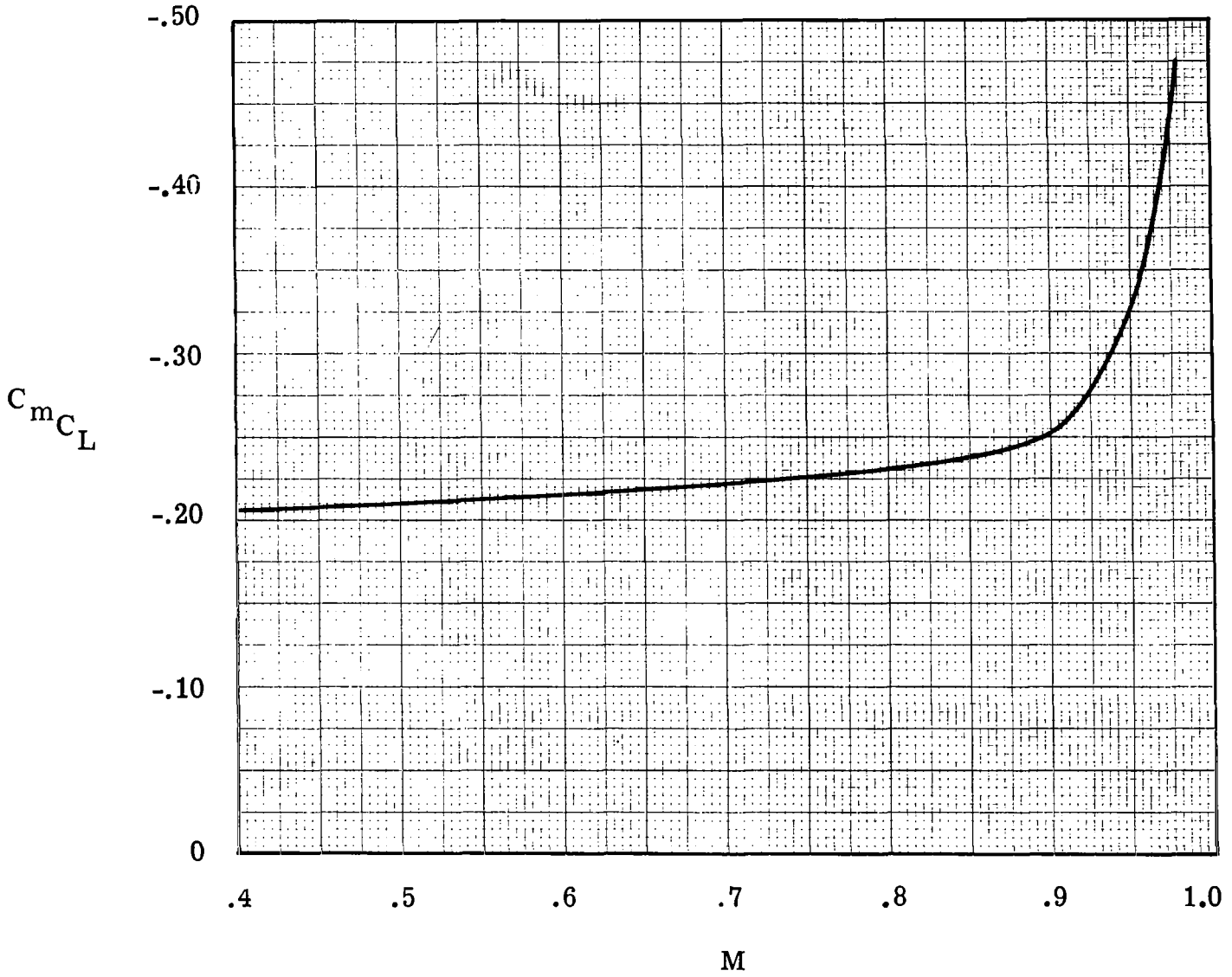

Figure 16.- Variation of $C_{m_{C_L}}$ with Mach number. Applicable range, $0 \leqq C_L \leqq 0.50$. $\delta_e = 0^o$.

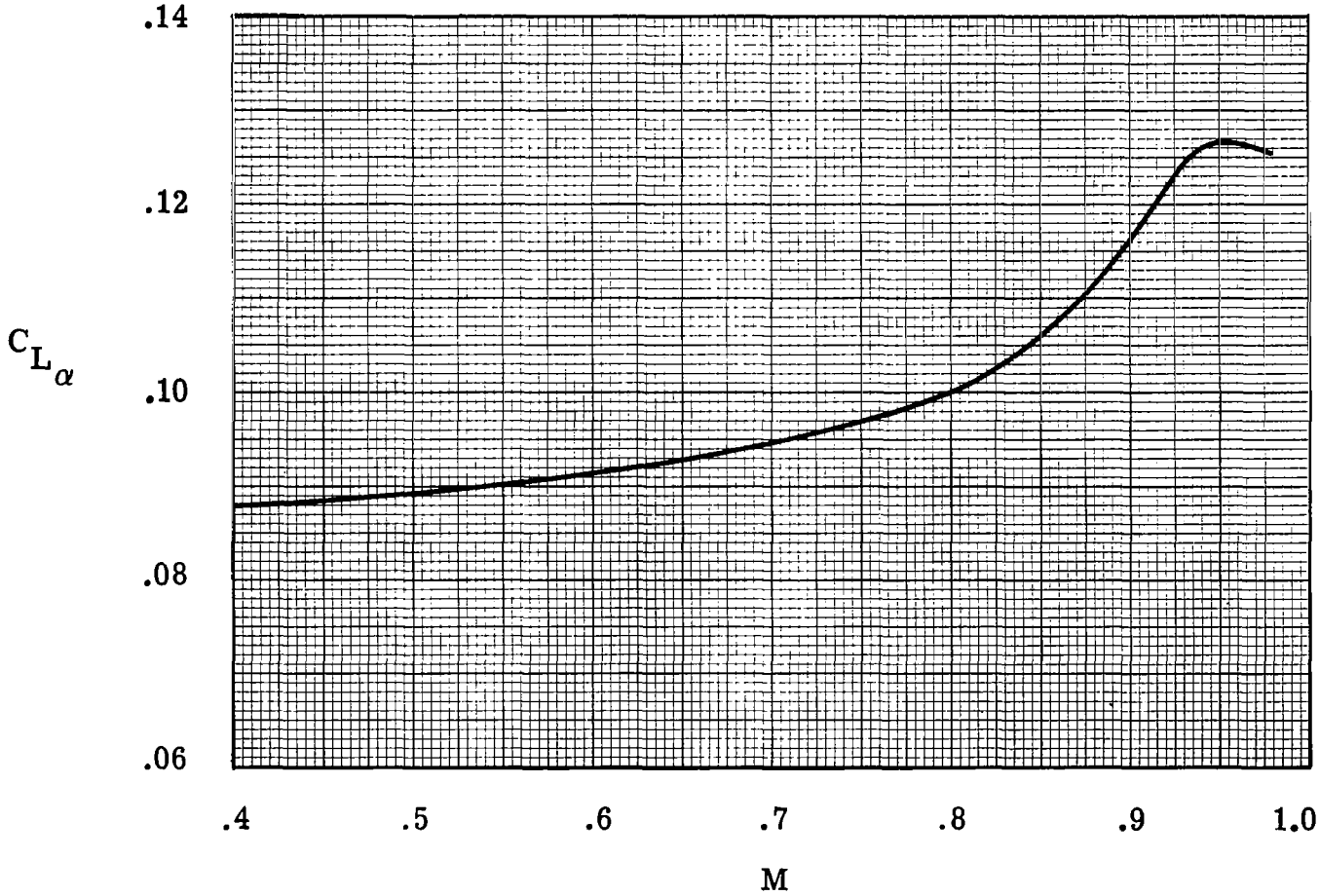

Figure 17.- Variation of untrimmed lift-curve slope with Mach number. Applicable range, $1^\circ \leqq \alpha \leqq 5^\circ$. $\delta_e = 0^\circ$.

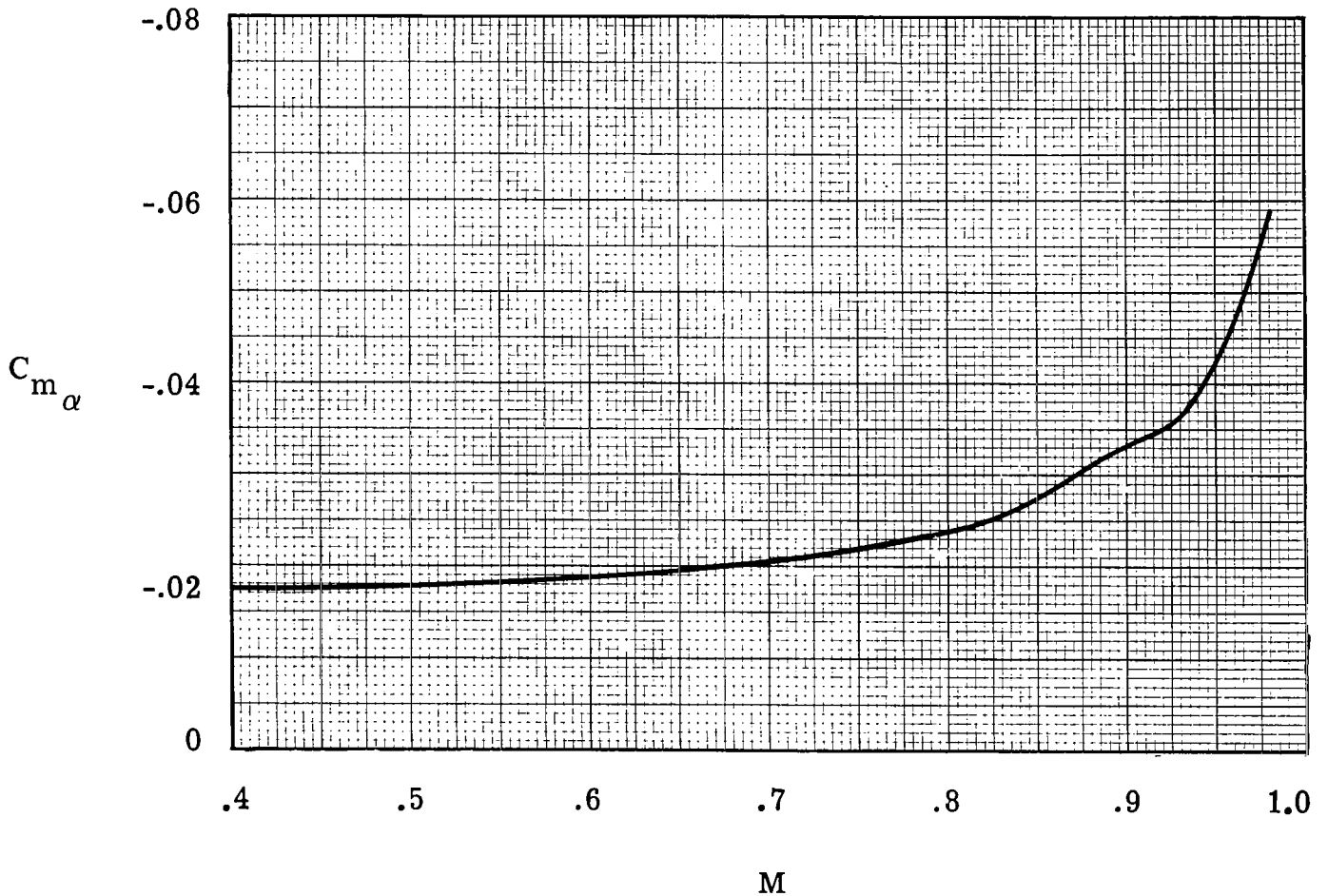

Figure 18.- Variation of pitching-moment-curve slope with Mach number. Applicable range, $1^\circ \leqq \alpha \leqq 5^\circ$. $\delta_e = 0^\circ$.

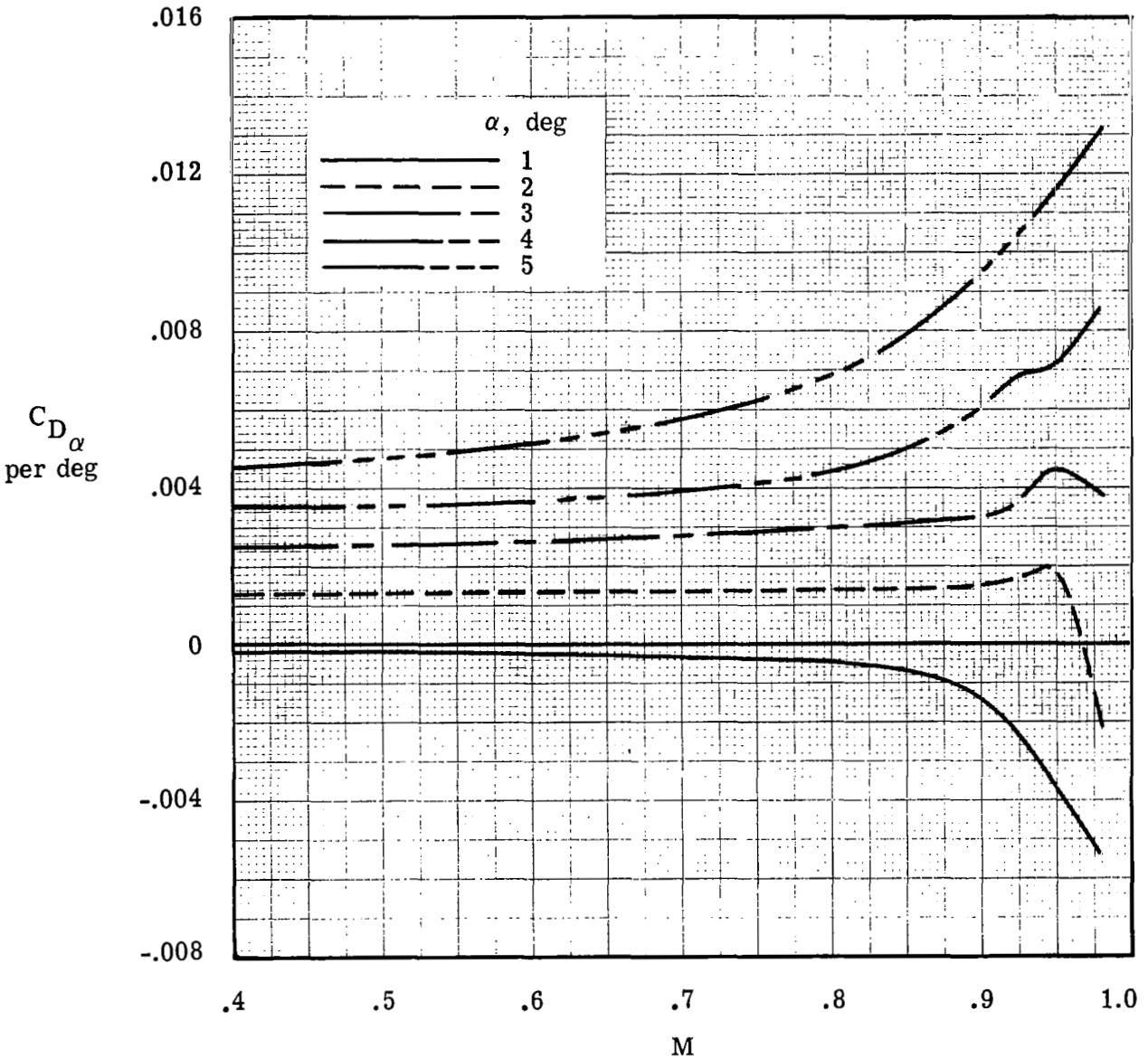

Figure 19.- Variation of drag-curve slope with Mach number for five angles of attack. $\delta_e = 0^{\circ}$.

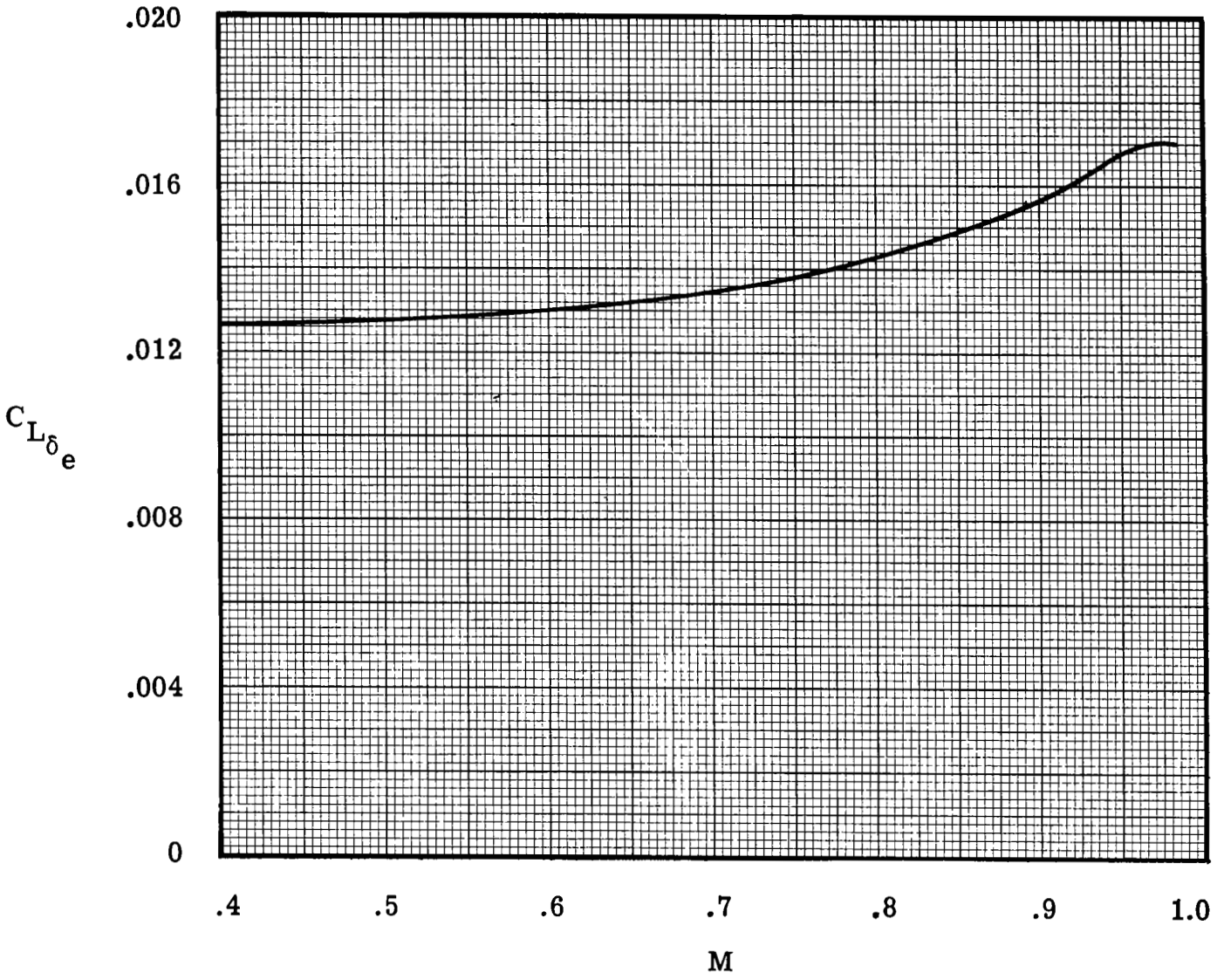

Figure 20.- Variation with Mach number of rate of change of lift coefficient with symmetric elevon deflection. Applicable ranges, $-6^{\circ} \leqq \delta_e \leqq 3^{\circ}$ and $2^{\circ} \leqq \alpha \leqq 6^{\circ}$.

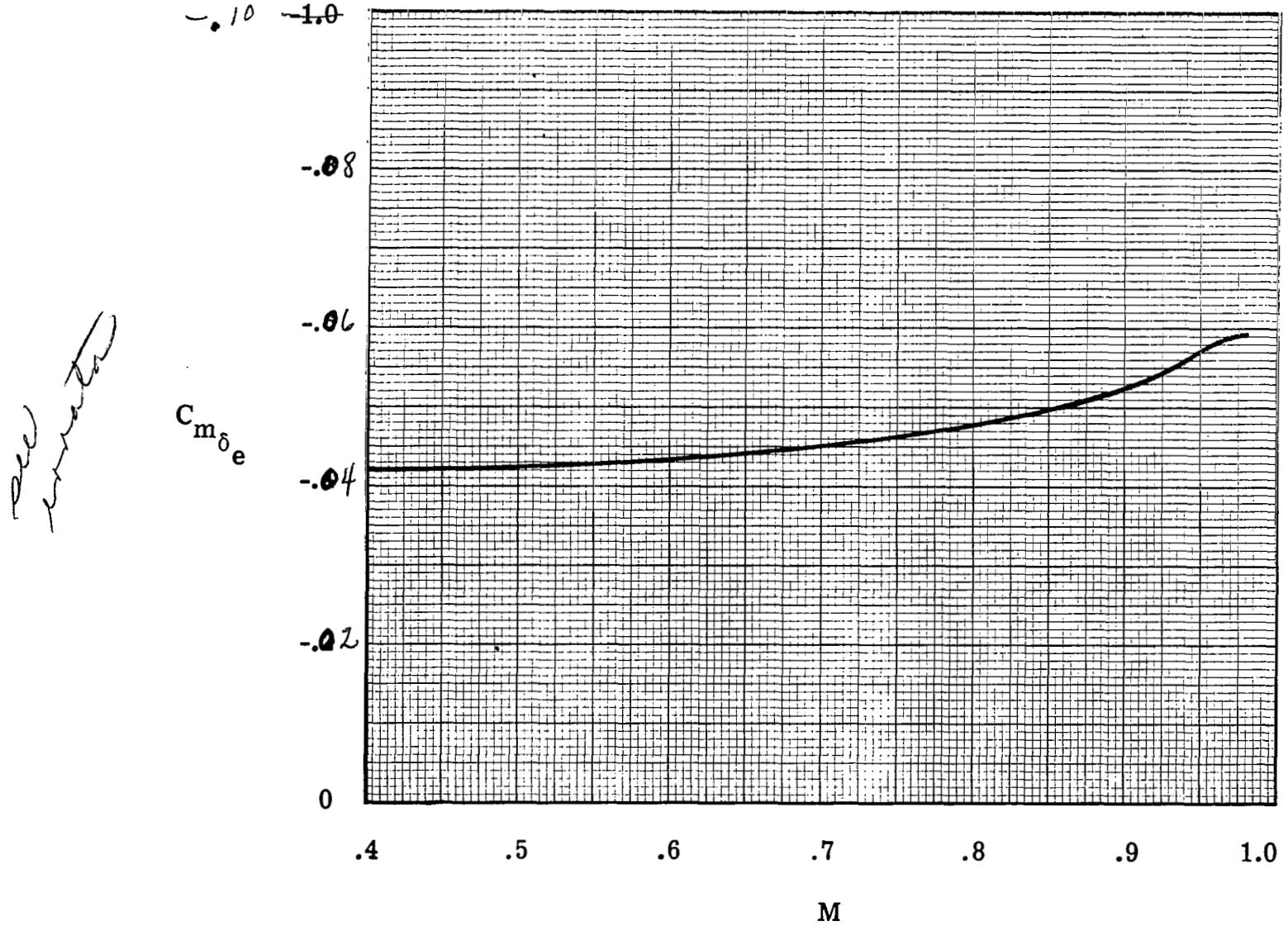

Figure 21.- Variation with Mach number of rate of change of pitching-moment coefficient with symmetric elevon deflection. Applicable ranges, $-6^{\circ} \leqq \delta_e \leqq 3^{\circ}$ and $2^{\circ} \leqq \alpha \leqq 6^{\circ}$.

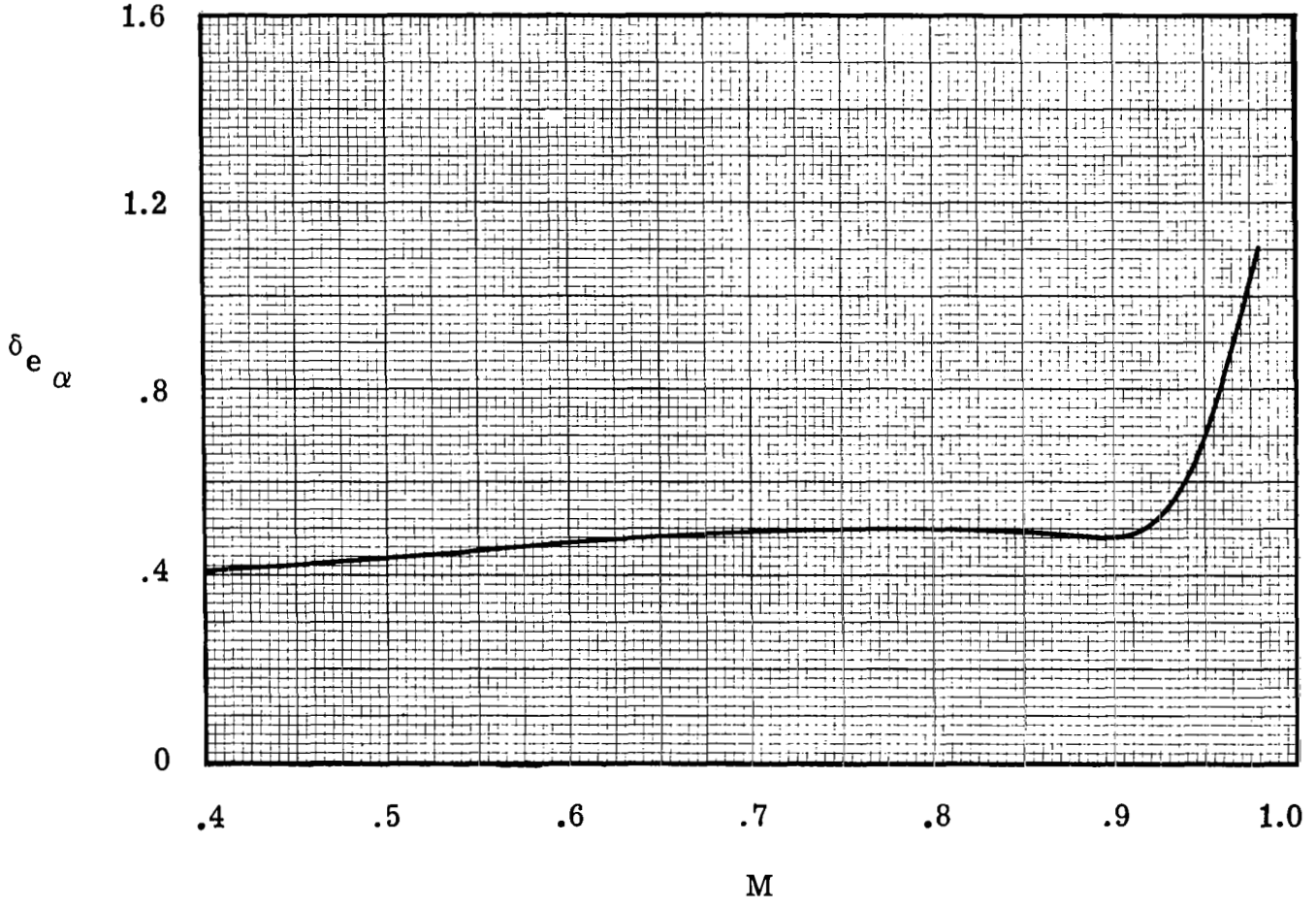

Figure 22.- Variation of pitch-control sensitivity (symmetric elevon) with Mach number. Applicable ranges, $-6^{\circ} \leqq \delta_e \leqq 3^{\circ}$ and $2^{\circ} \leqq \alpha \leqq 6^{\circ}$.

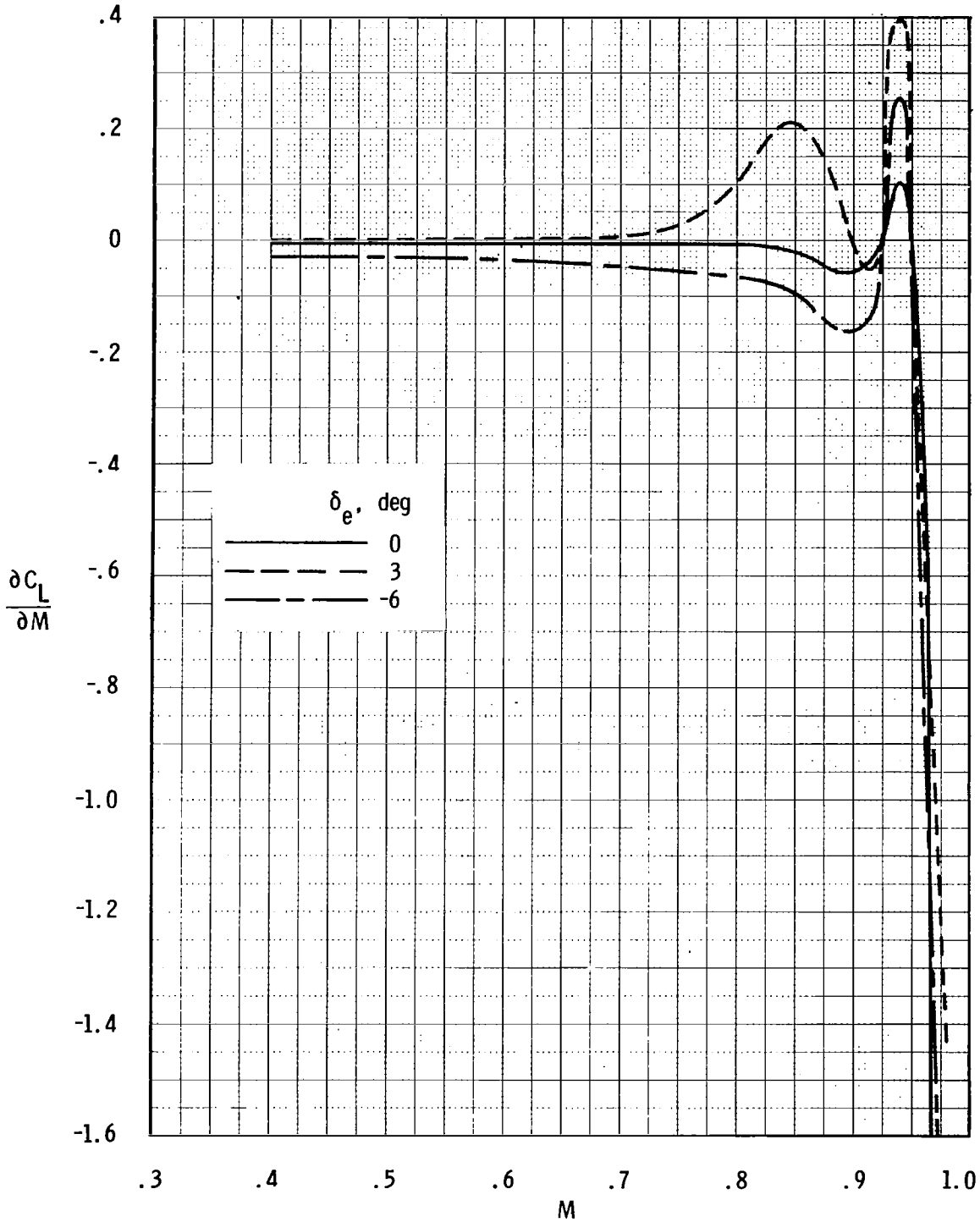

(a) $\alpha = 2^{\circ}$.

Figure 23.- Variations of $\partial C_L/\partial M$ with Mach number for three symmetric elevon deflections.

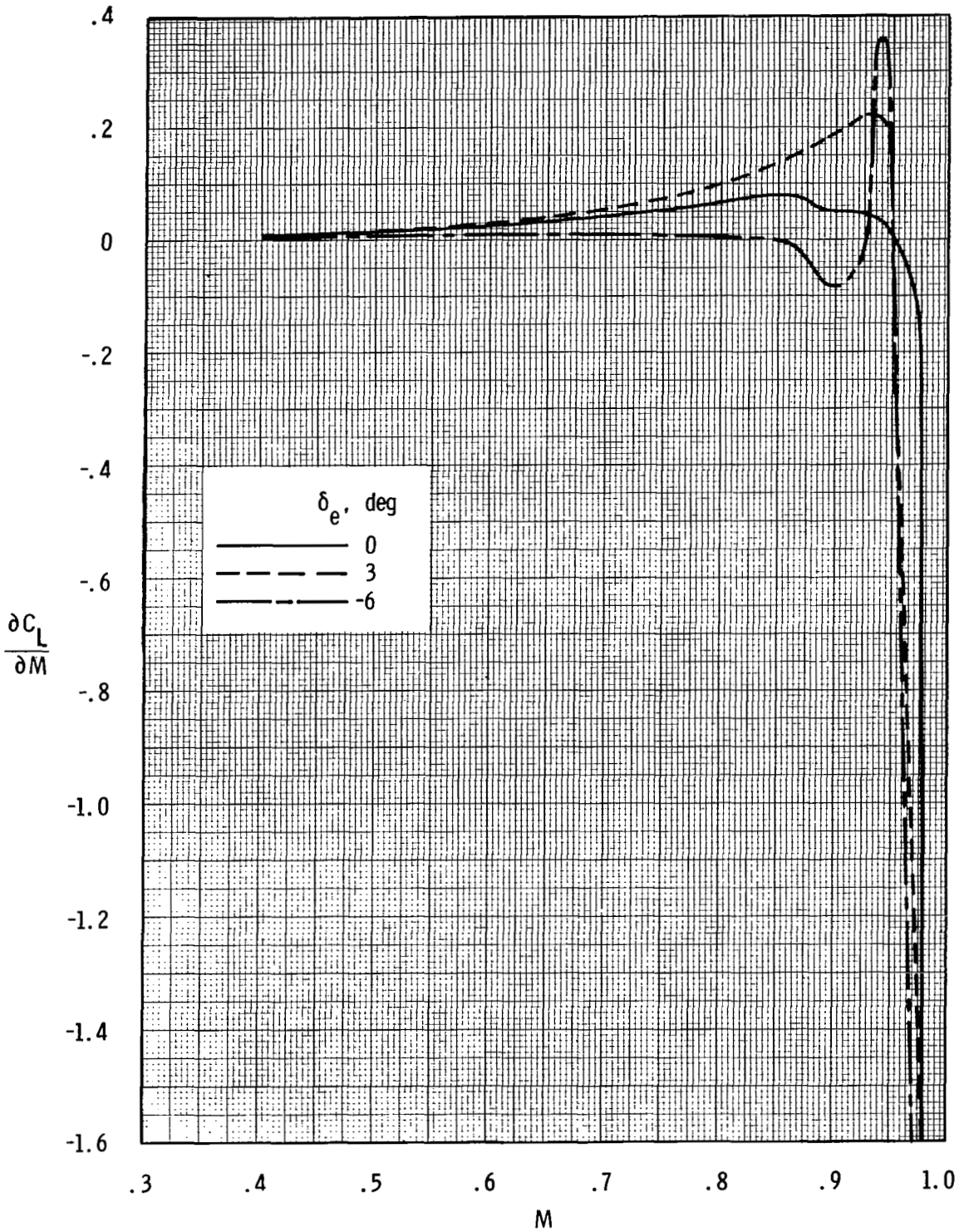

(b) $\alpha = 3^{\circ}$.

Figure 23.- Continued.

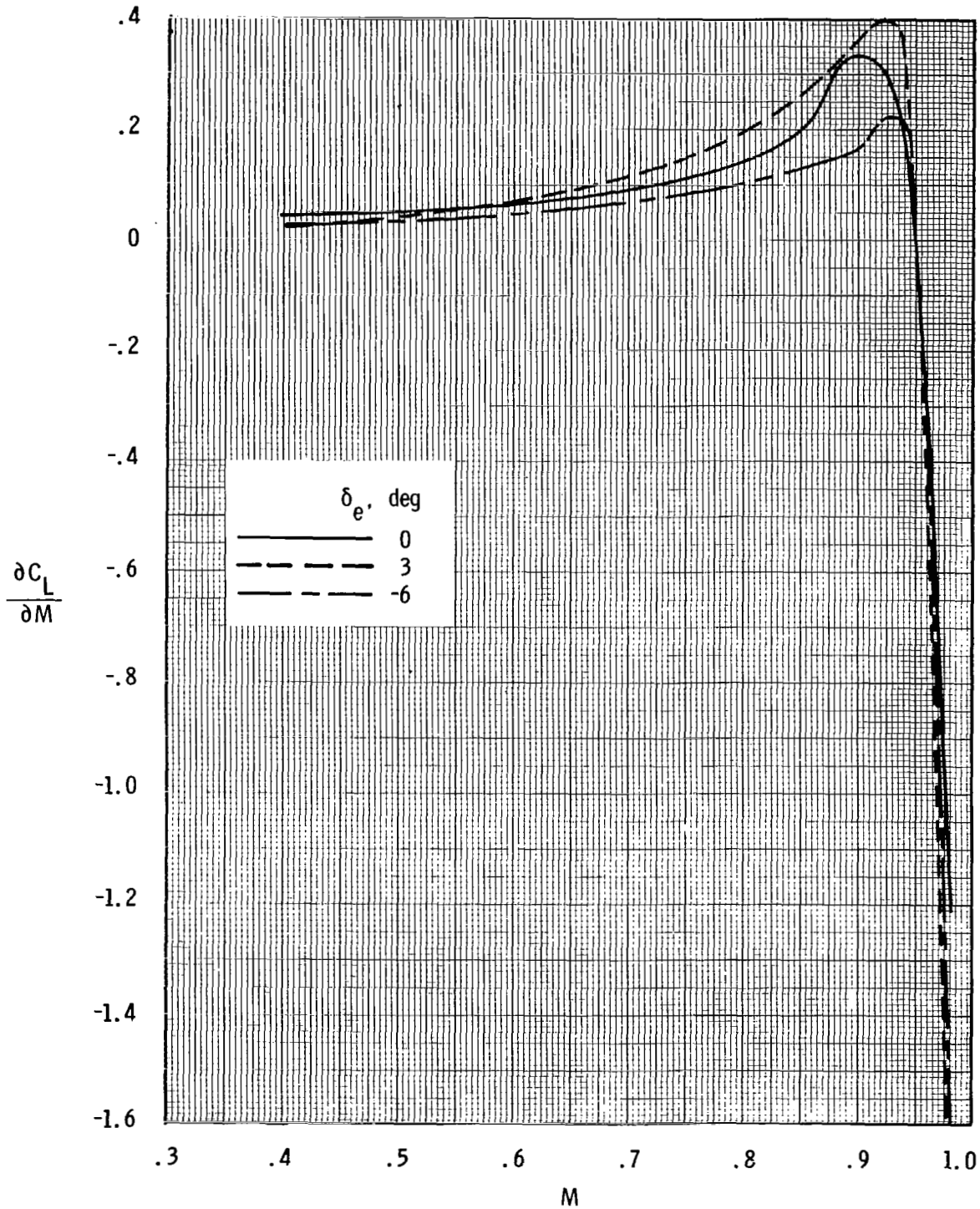

(c) $\alpha = 4^{\circ}$.

Figure 23.- Concluded.

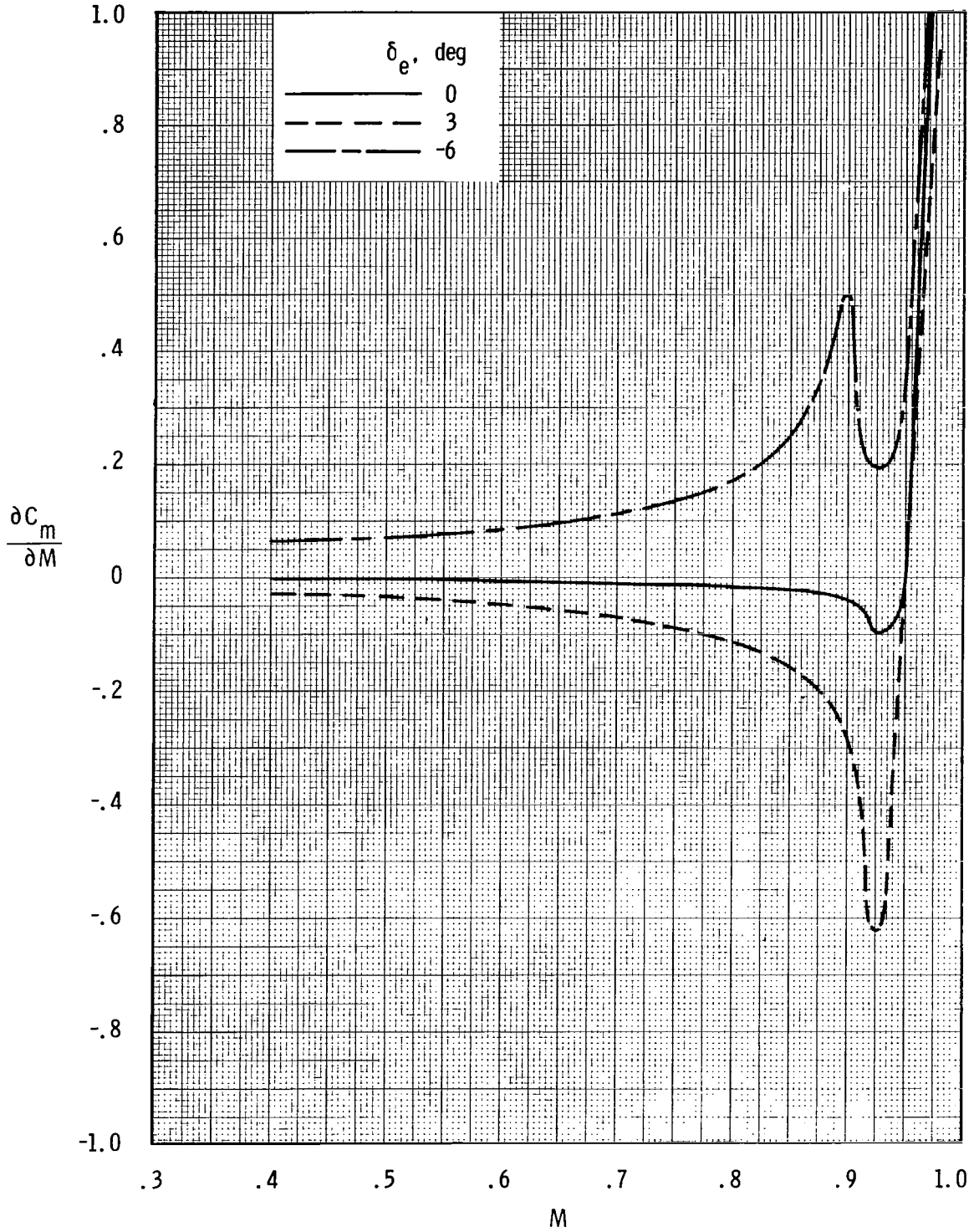

(a) $\alpha = 2^{\circ}$.

Figure 24.- Variations of $\partial C_m/\partial M$ with Mach number for three symmetric elevon deflections.

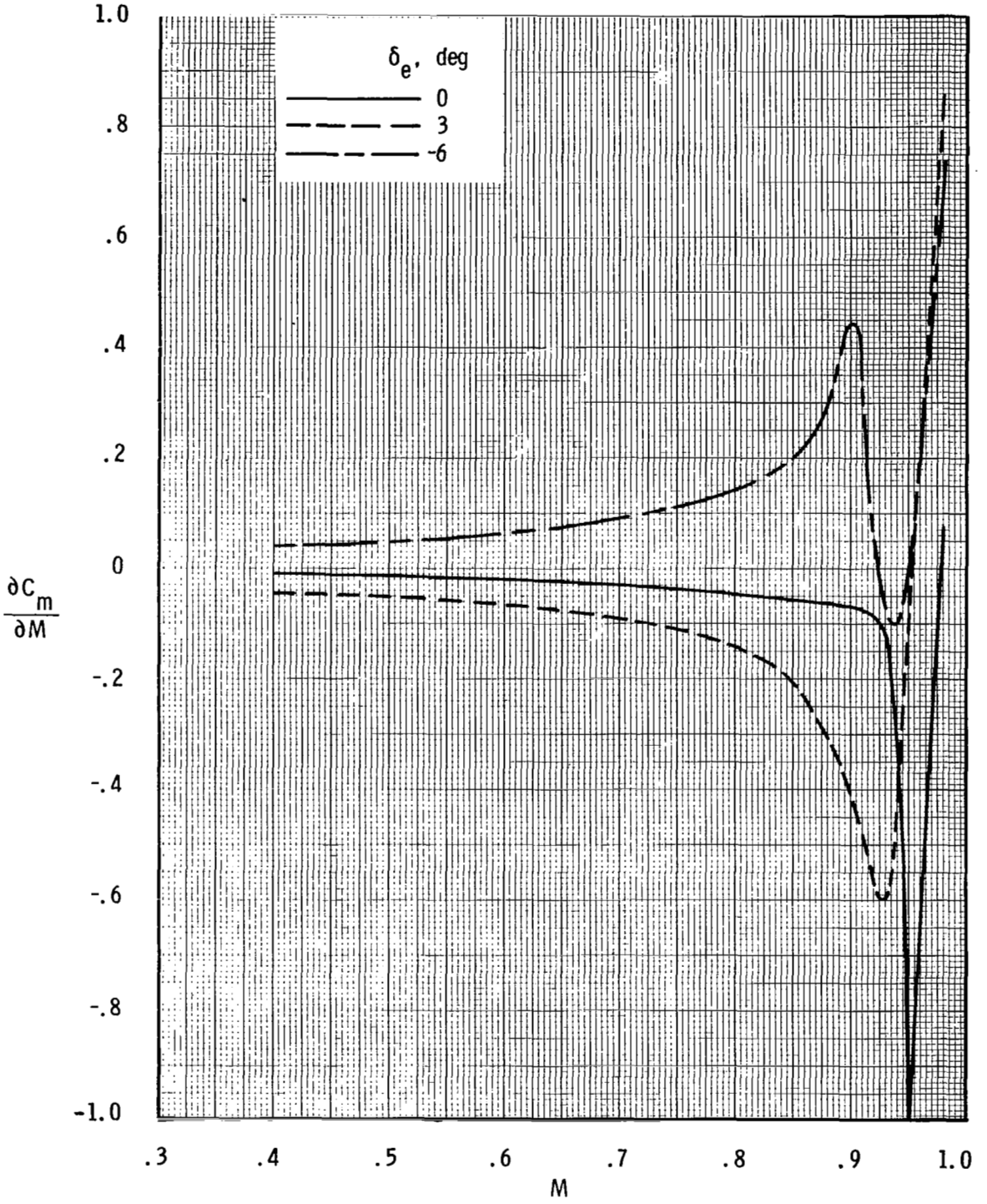

(b) $\alpha = 3^{\circ}$.

Figure 24.- Continued.

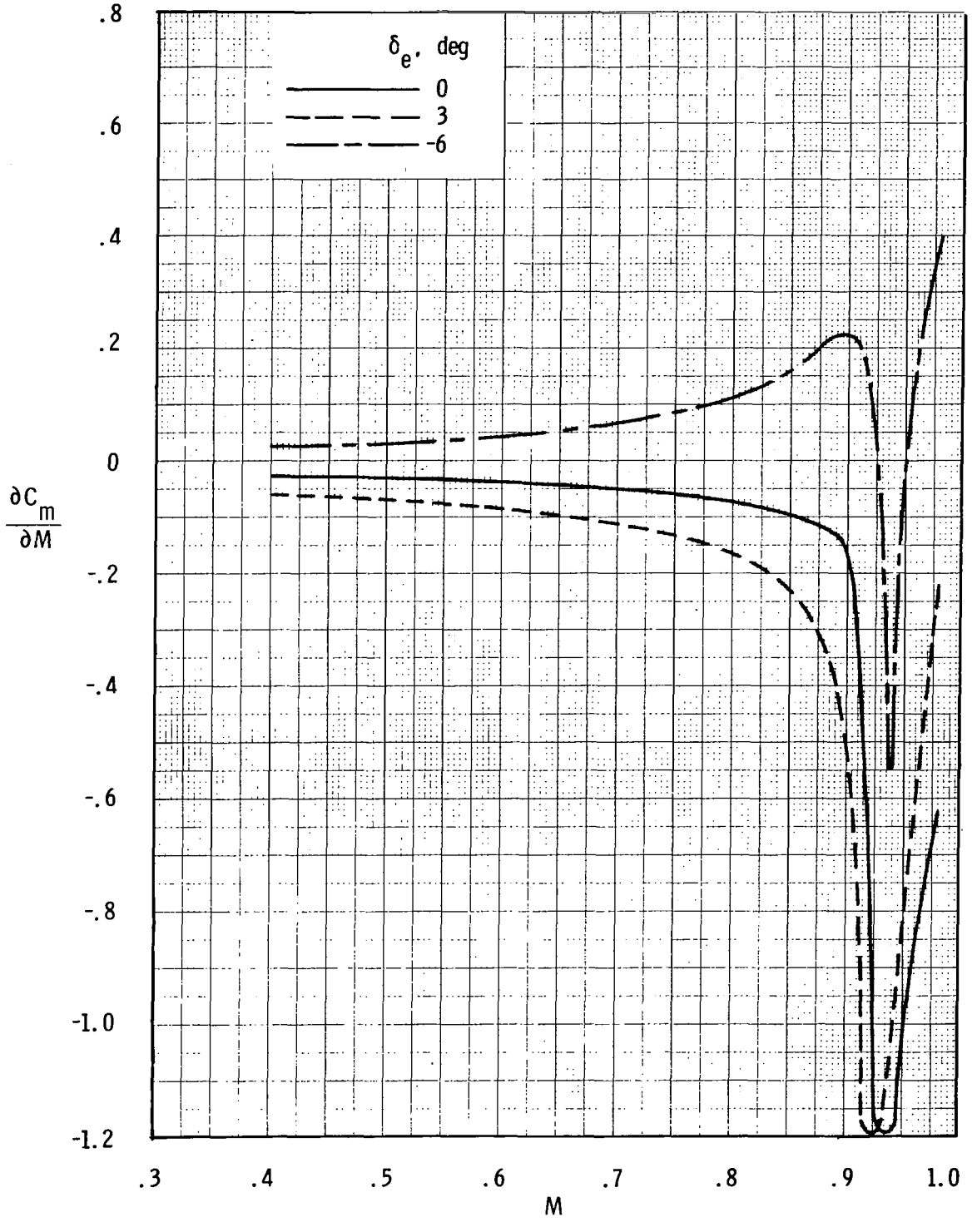

(c) $\alpha = 4^{\circ}$.

Figure 24.- Concluded.

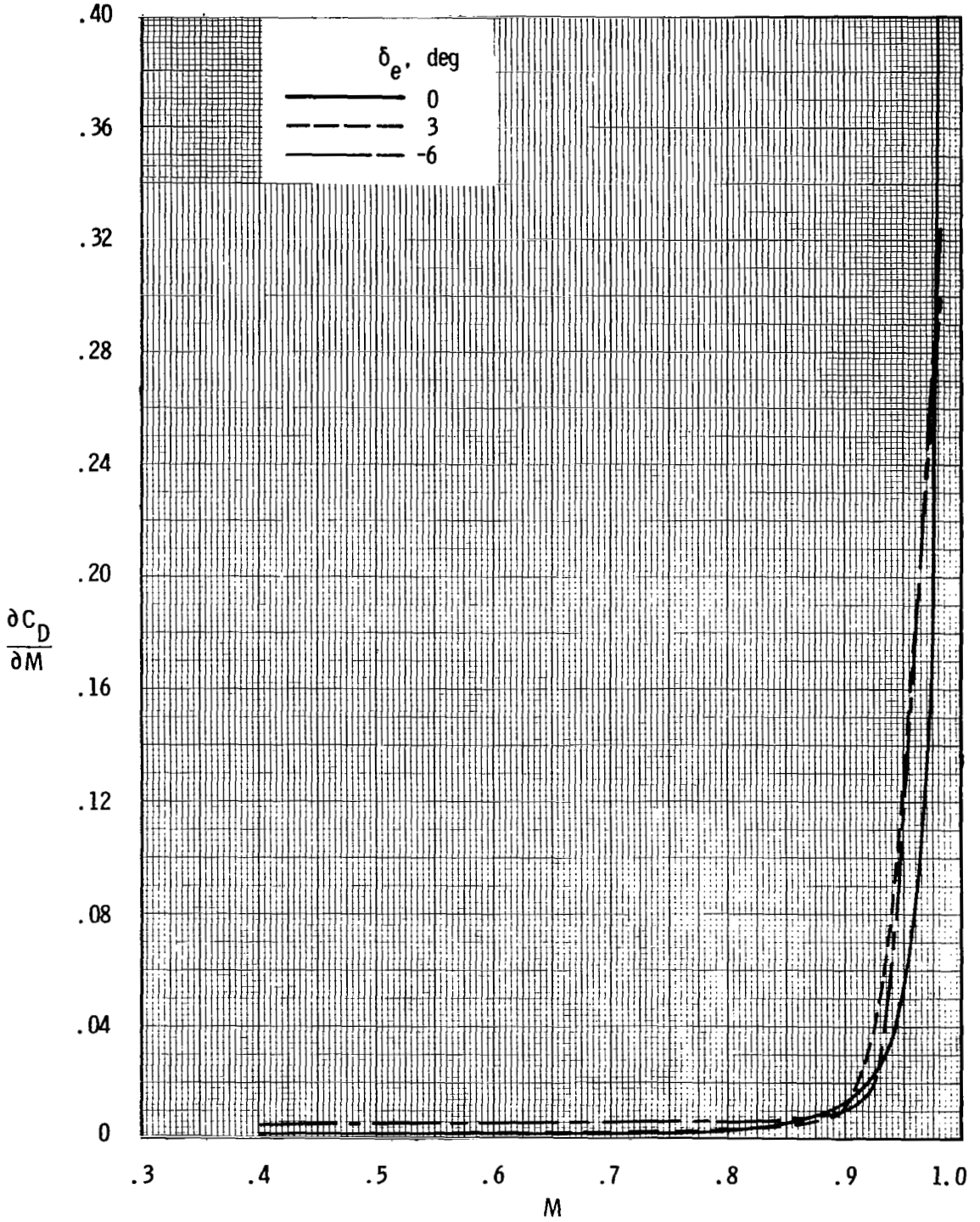

(a) $\alpha = 2^{\circ}$.

Figure 25.- Variation of $\partial C_D/\partial M$ with Mach number for three symmetric elevon deflections.

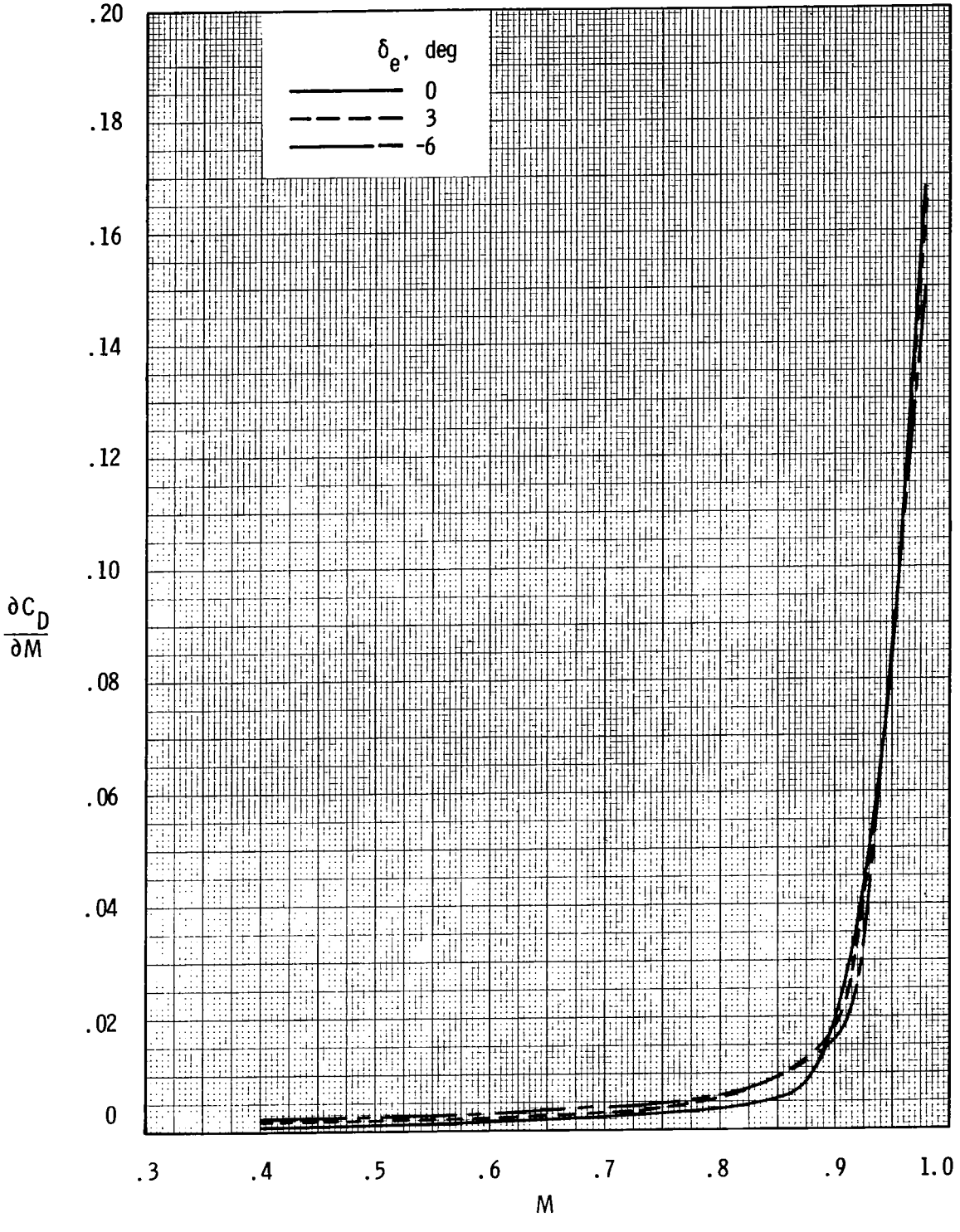

(b) $\alpha = 3^{\circ}$.

Figure 25.- Continued.

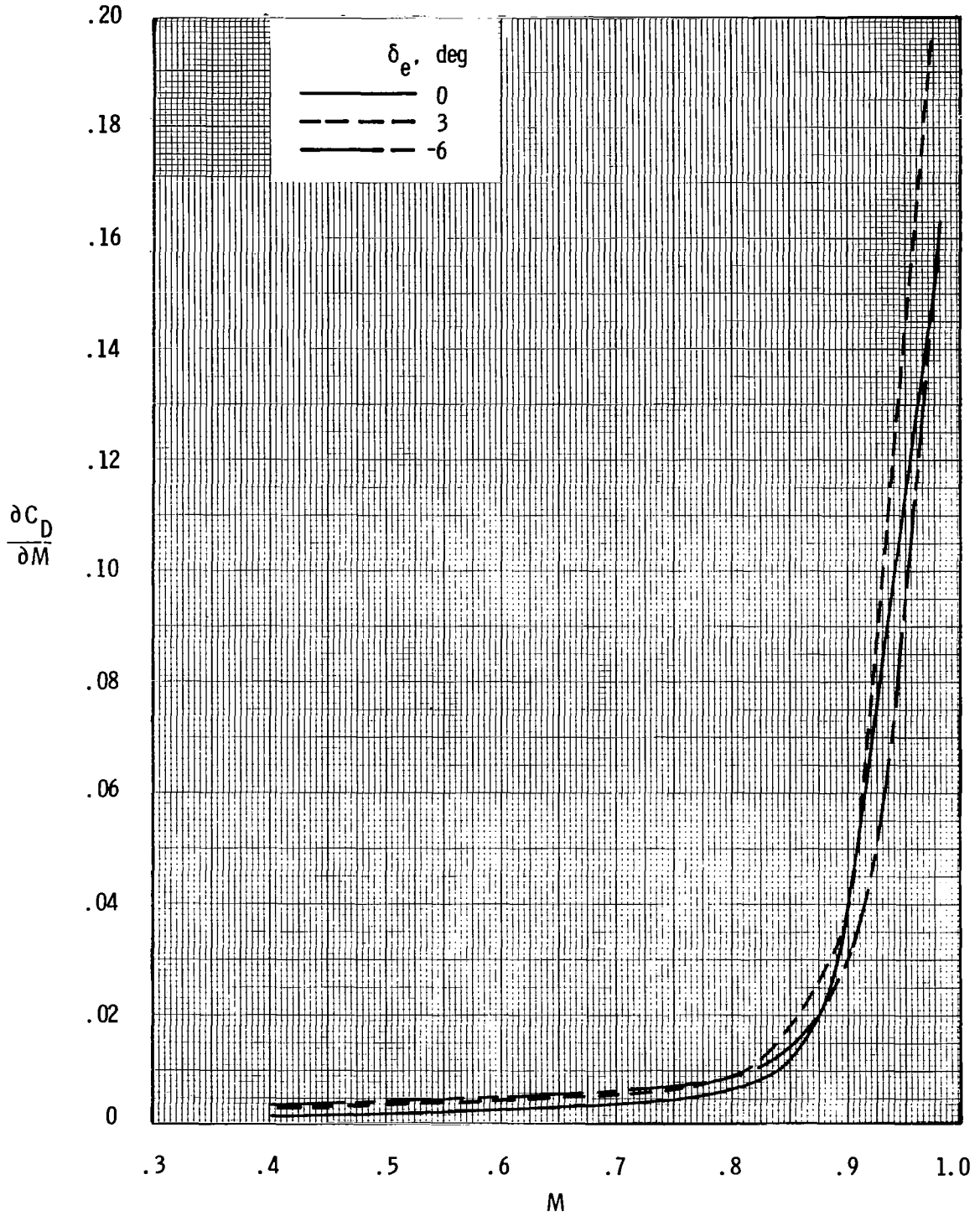

(c) $\alpha = 4^{\circ}$.

Figure 25.- Concluded.

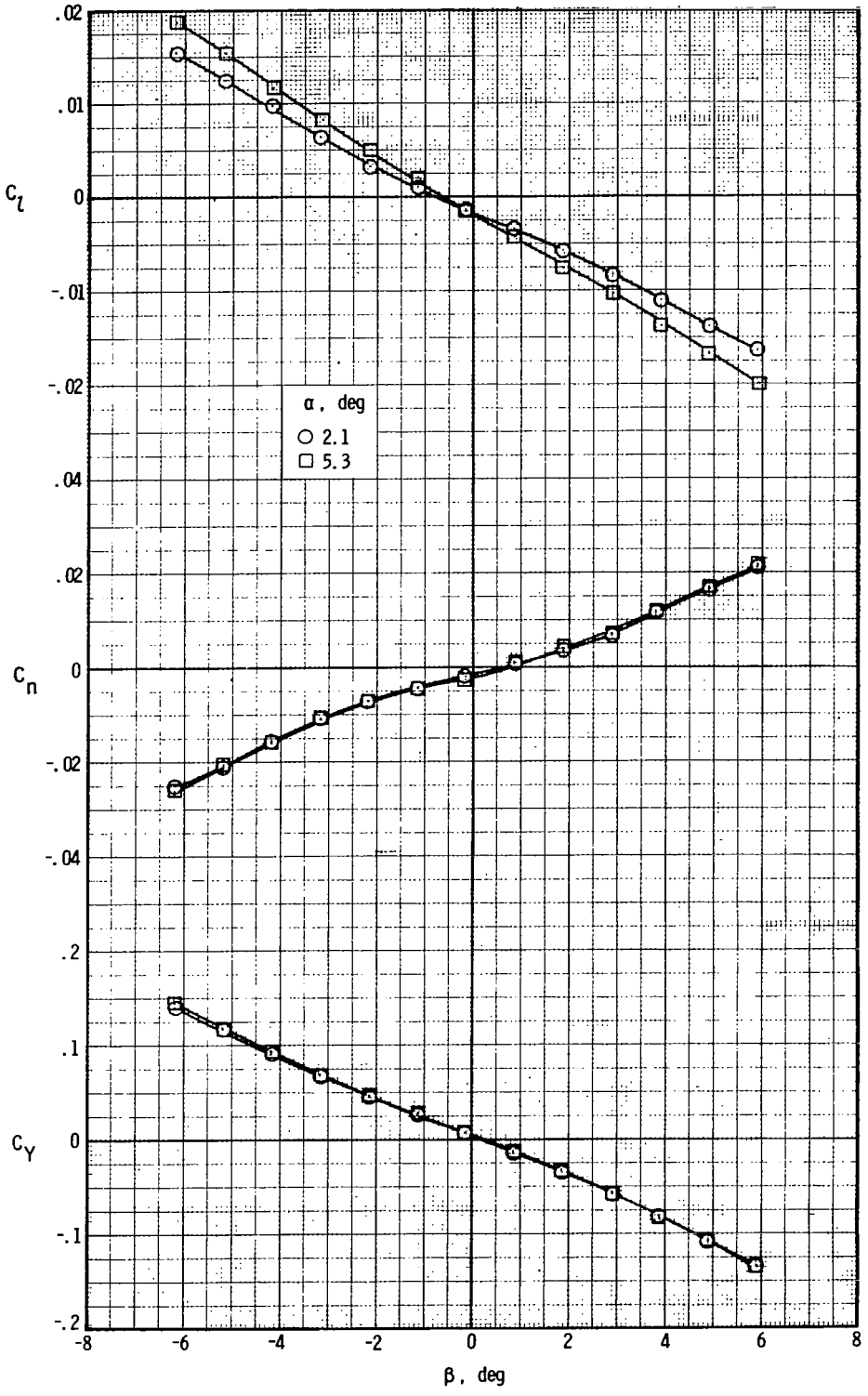

(a) M = 0.400.

Figure 26.- Variation of lateral aerodynamic characteristics with angle of sideslip for two angles of attack. $\delta_e = 0^o$.

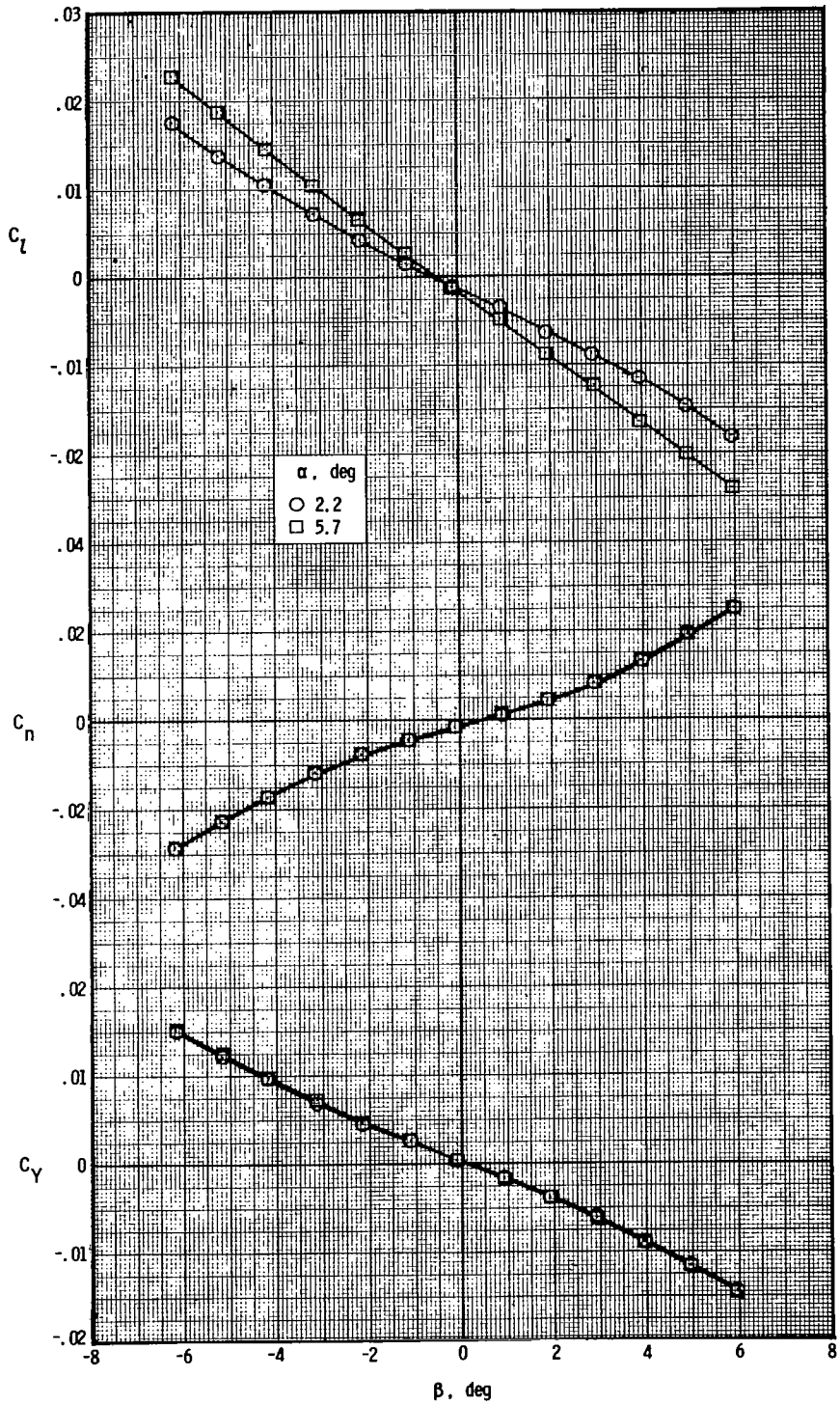

(b) M = 0.800.

Figure 26.- Continued.

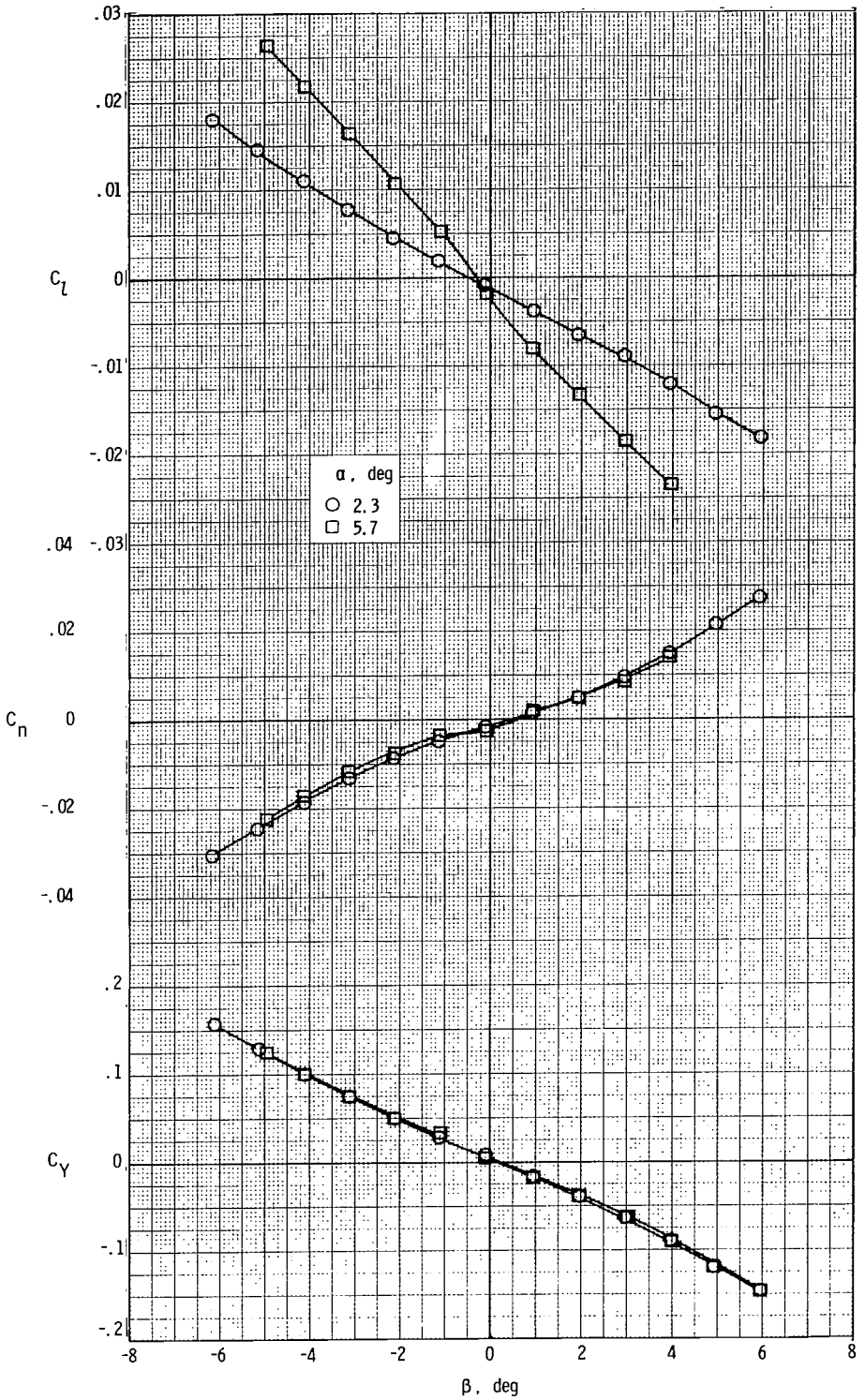

(c) M = 0.900.

Figure 26.- Continued.

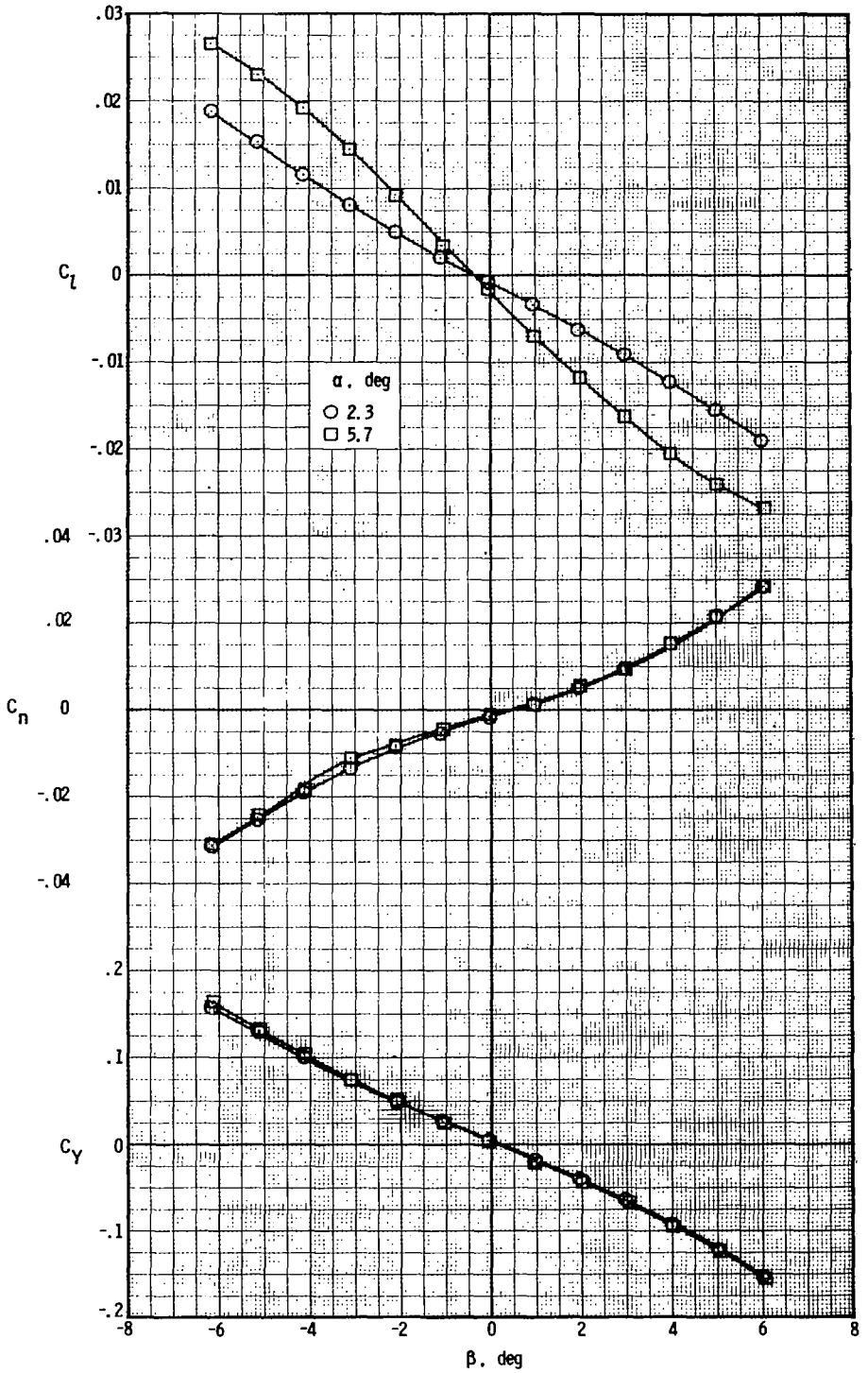

(d) M = 0.925.

Figure 26.- Continued.

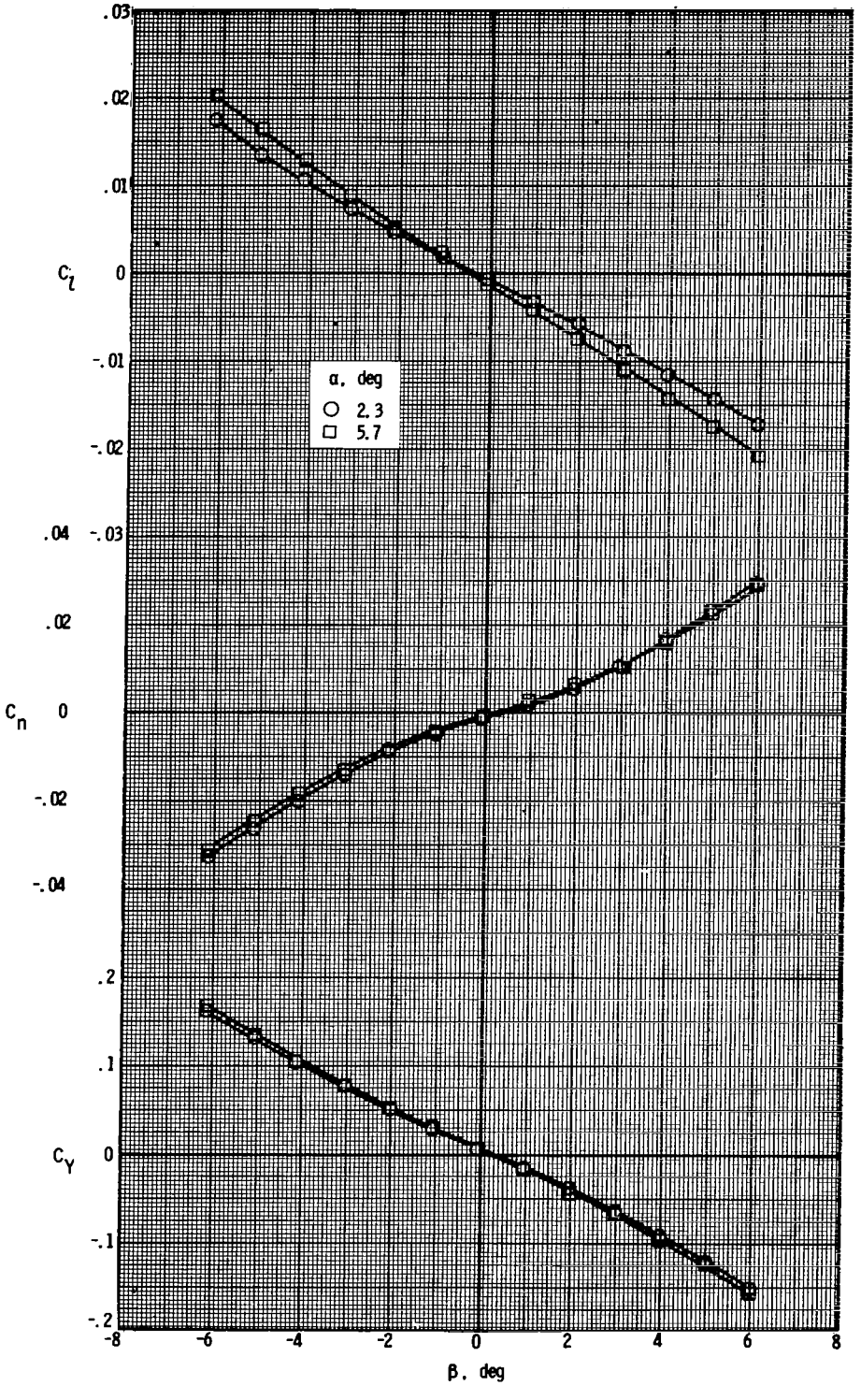

(e) M = 0.950.

Figure 26.- Continued.

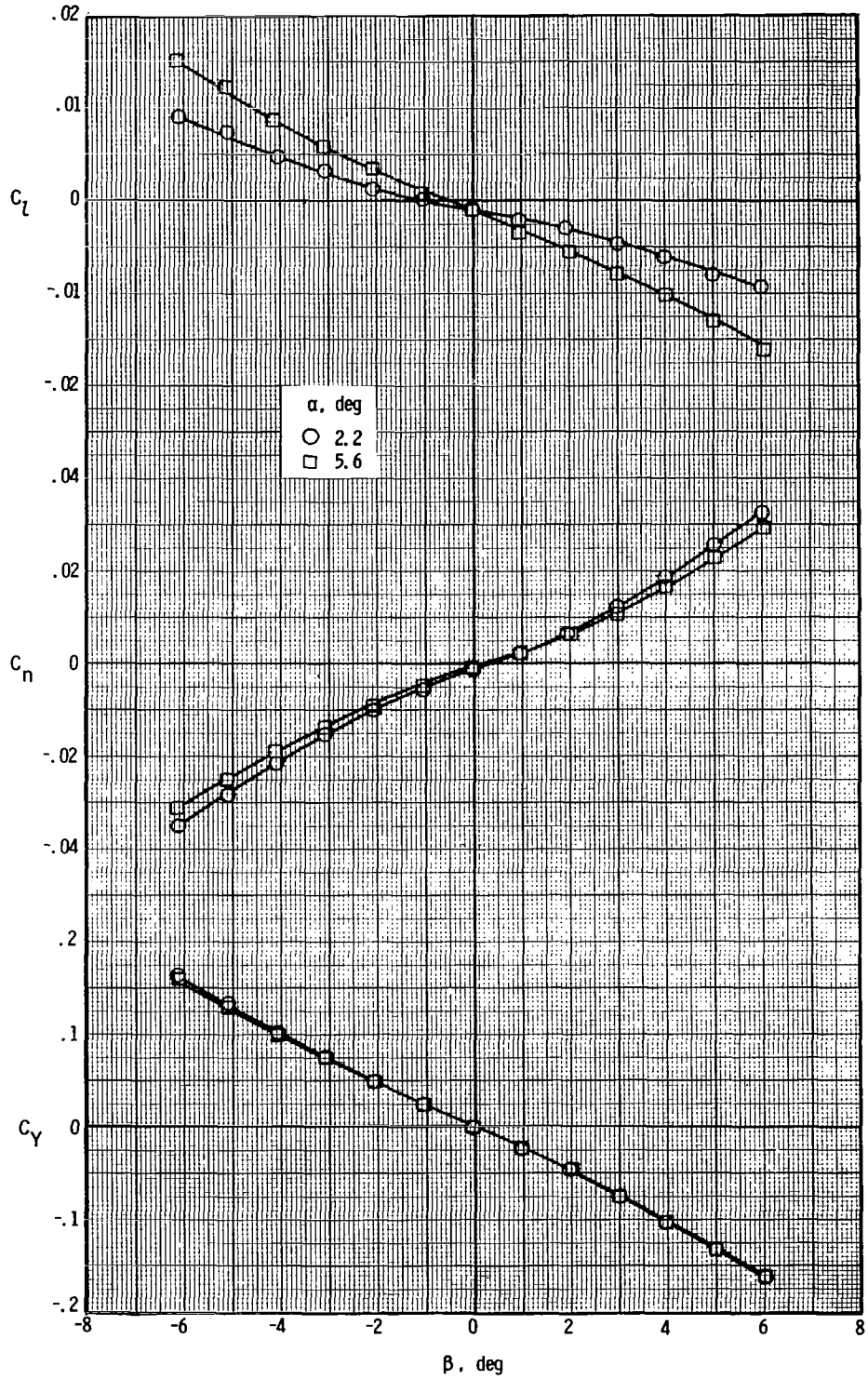

(f) M = 0.980.

Figure 26.- Concluded.

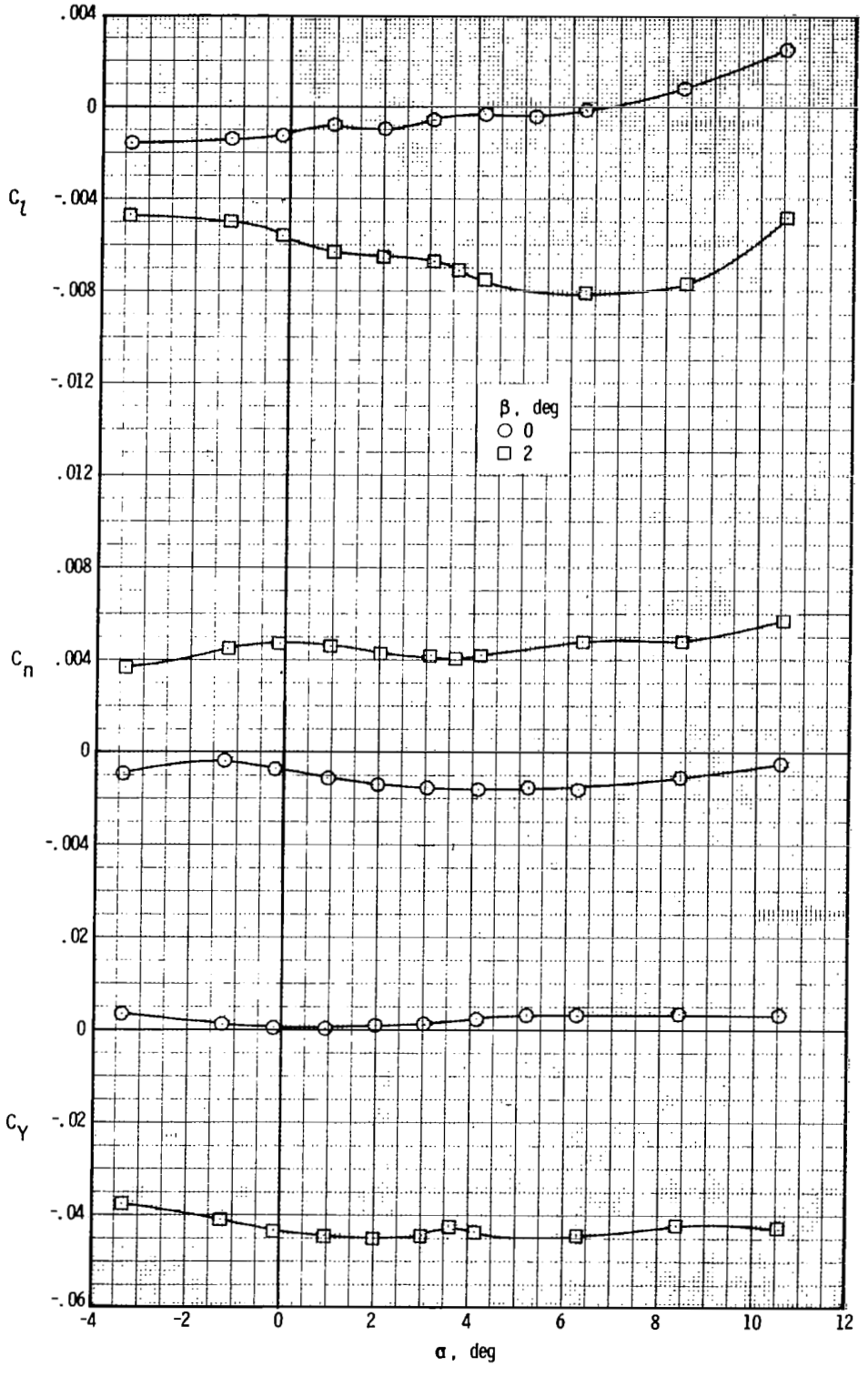

(a) M = 0.400.

Figure 27.- Variation of lateral-directional aerodynamic characteristics with angle of attack for two angles of sideslip. $\delta_e = 0^o$.

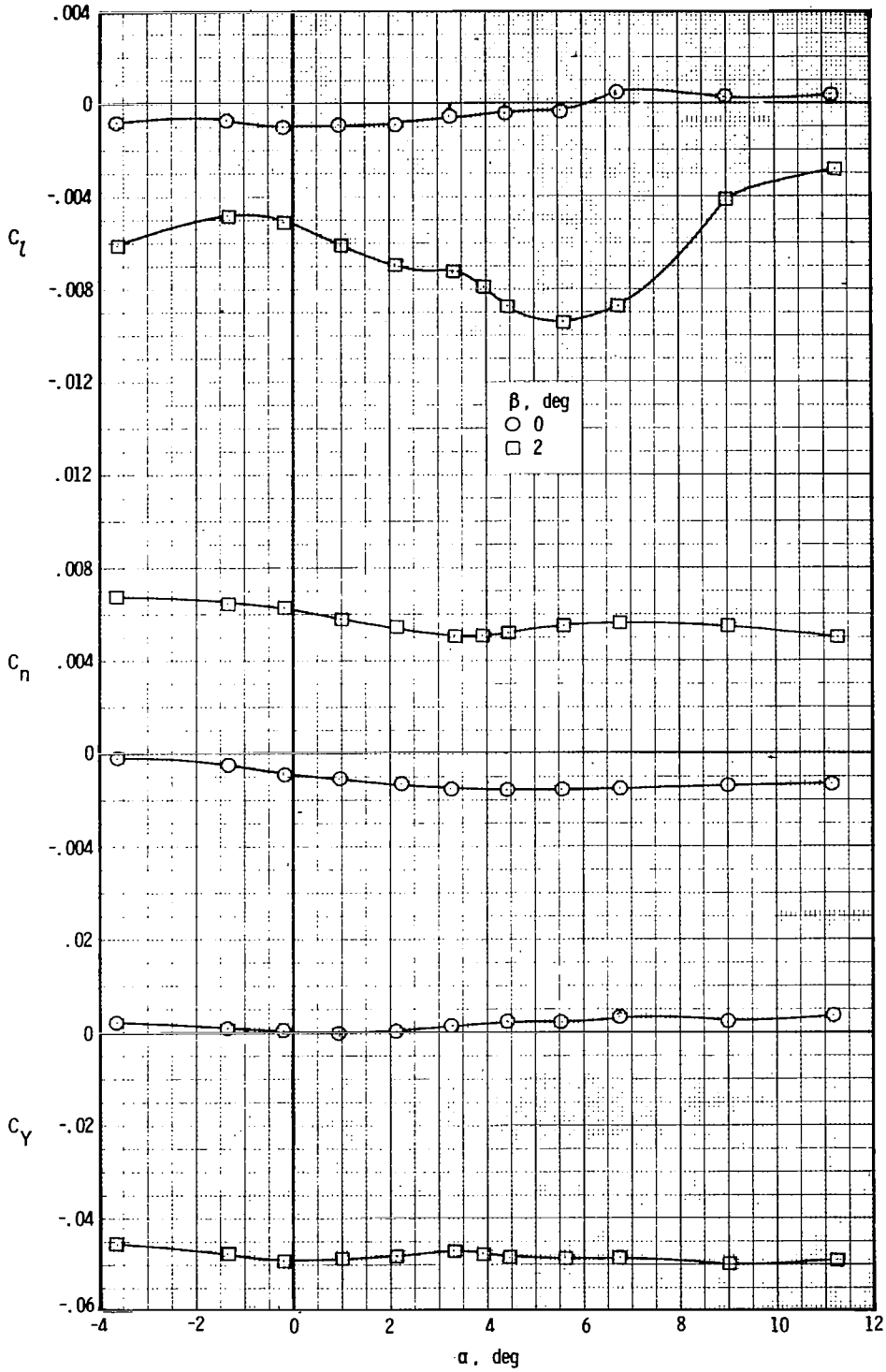

(b) M = 0.800.

Figure 27.- Continued.

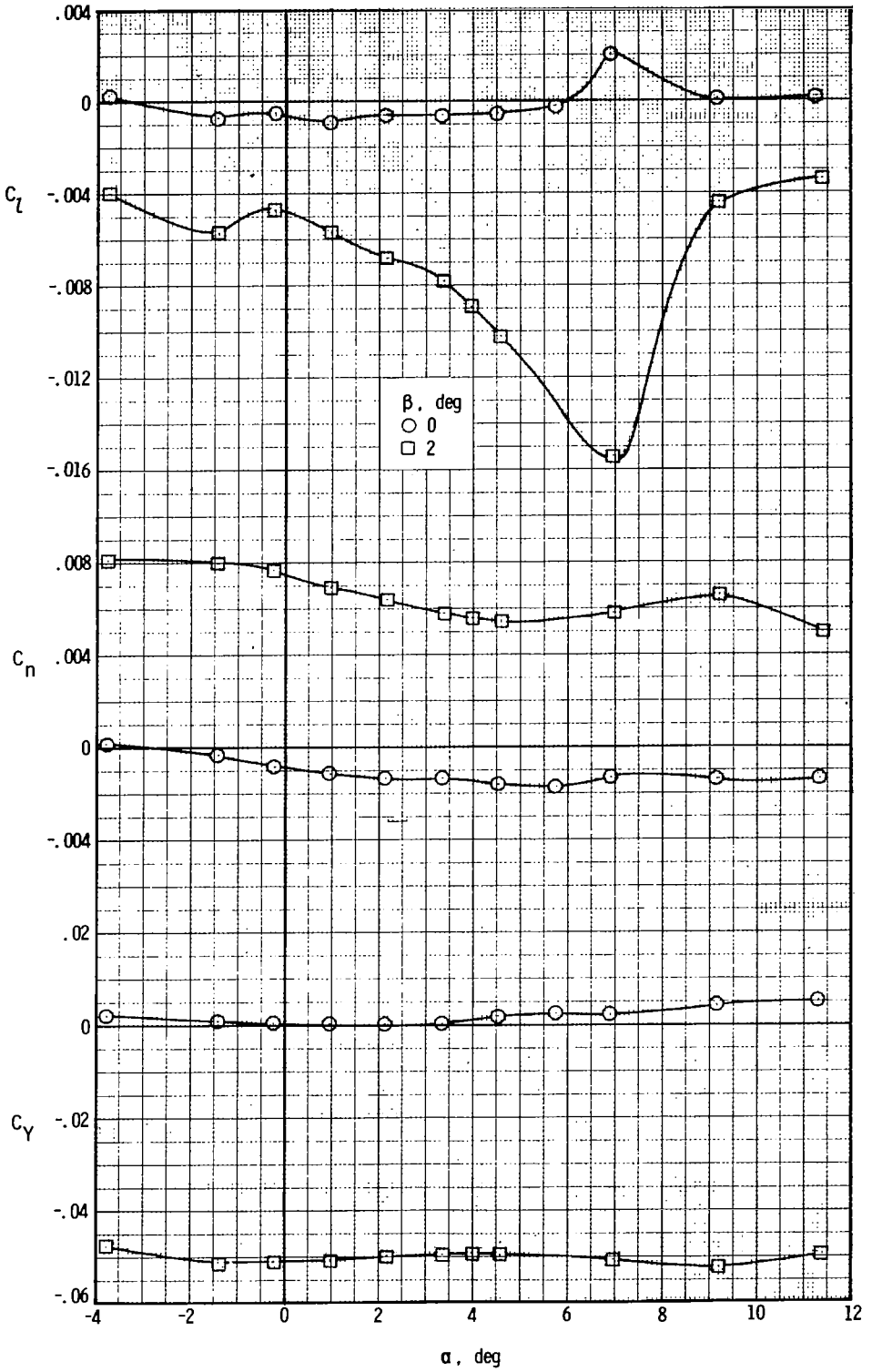

(c) M = 0.900.

Figure 27.- Continued.

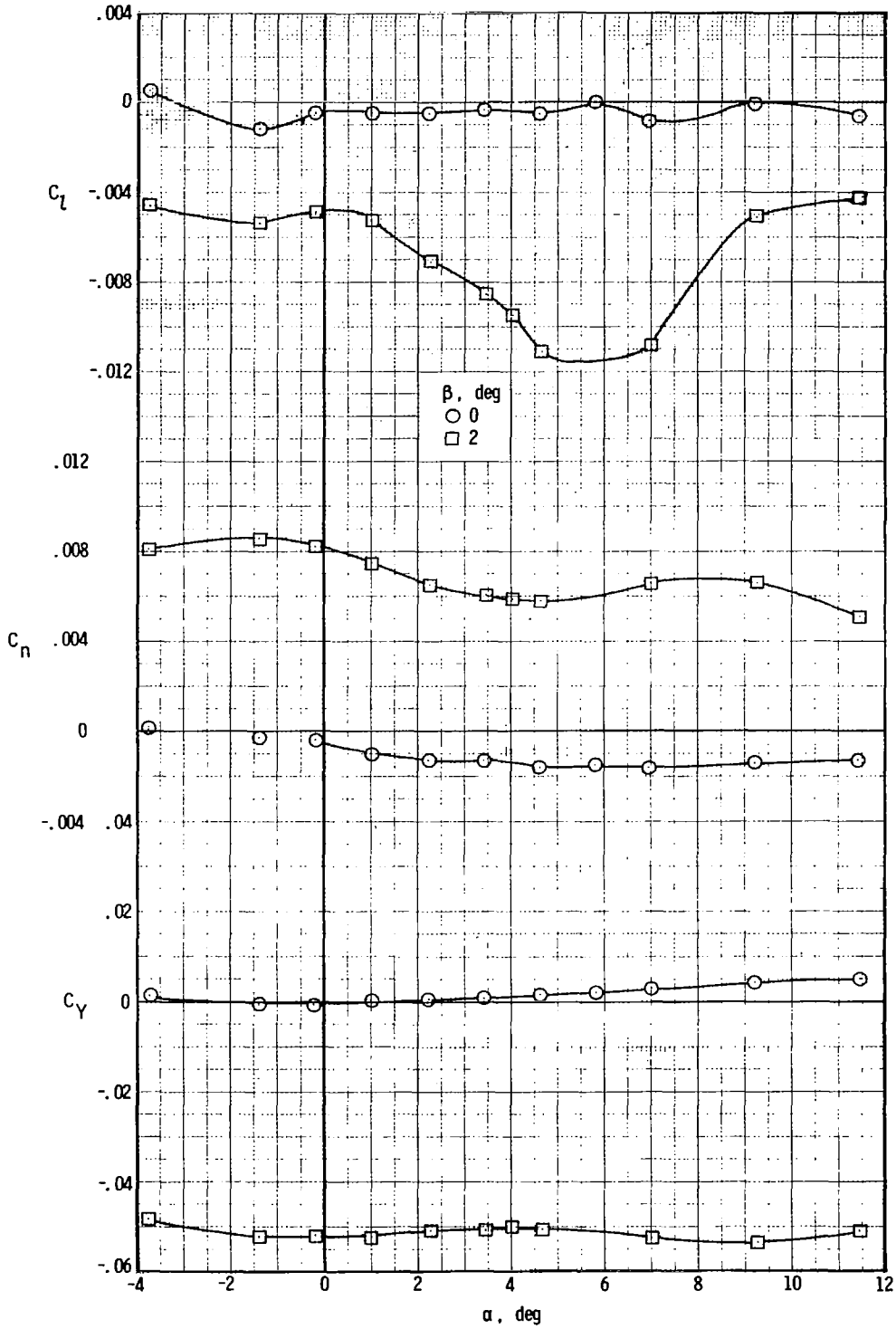

(d) M = 0.925.

Figure 27.- Continued.

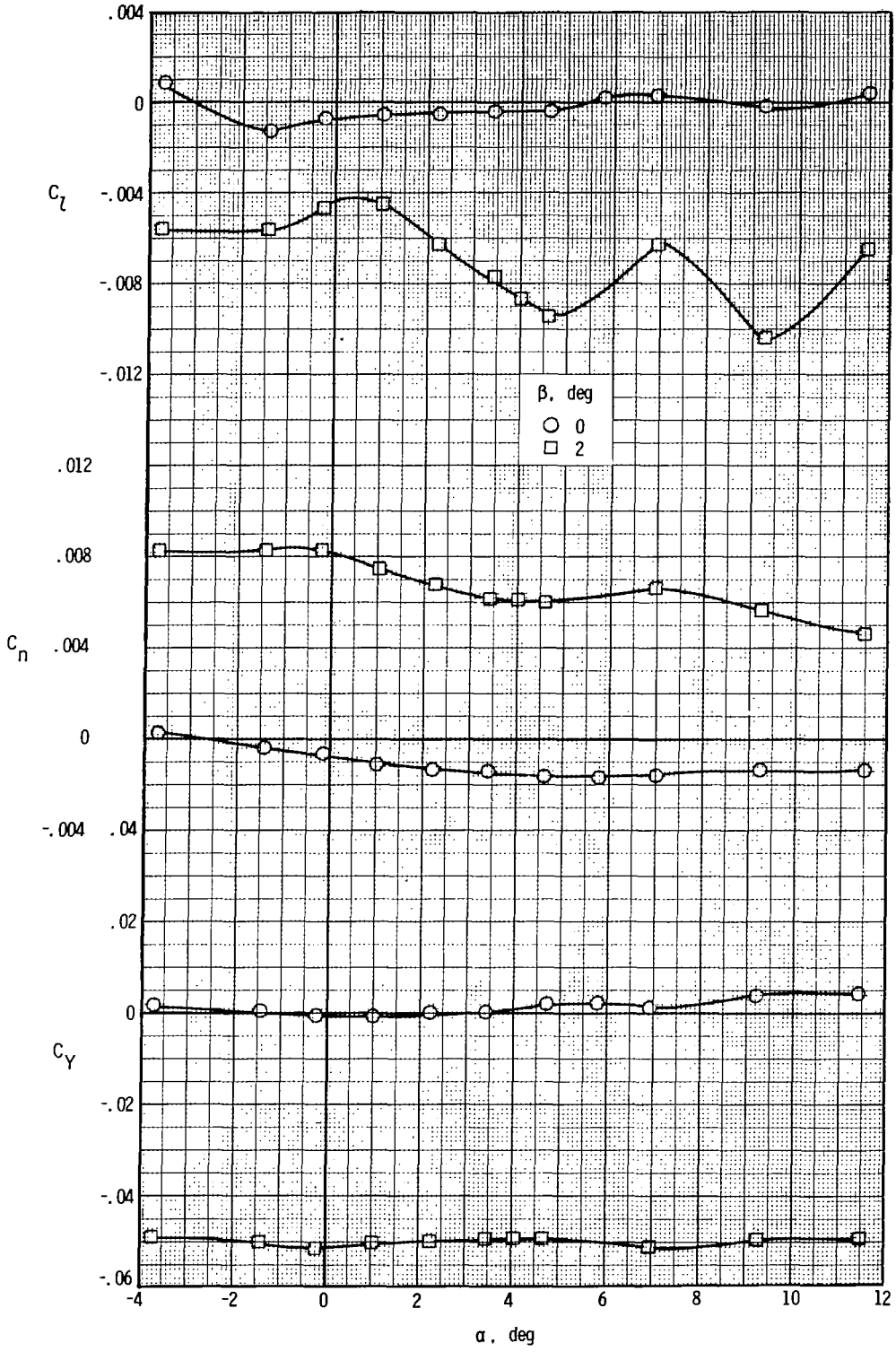

(e) M = 0.950.

Figure 27.- Continued.

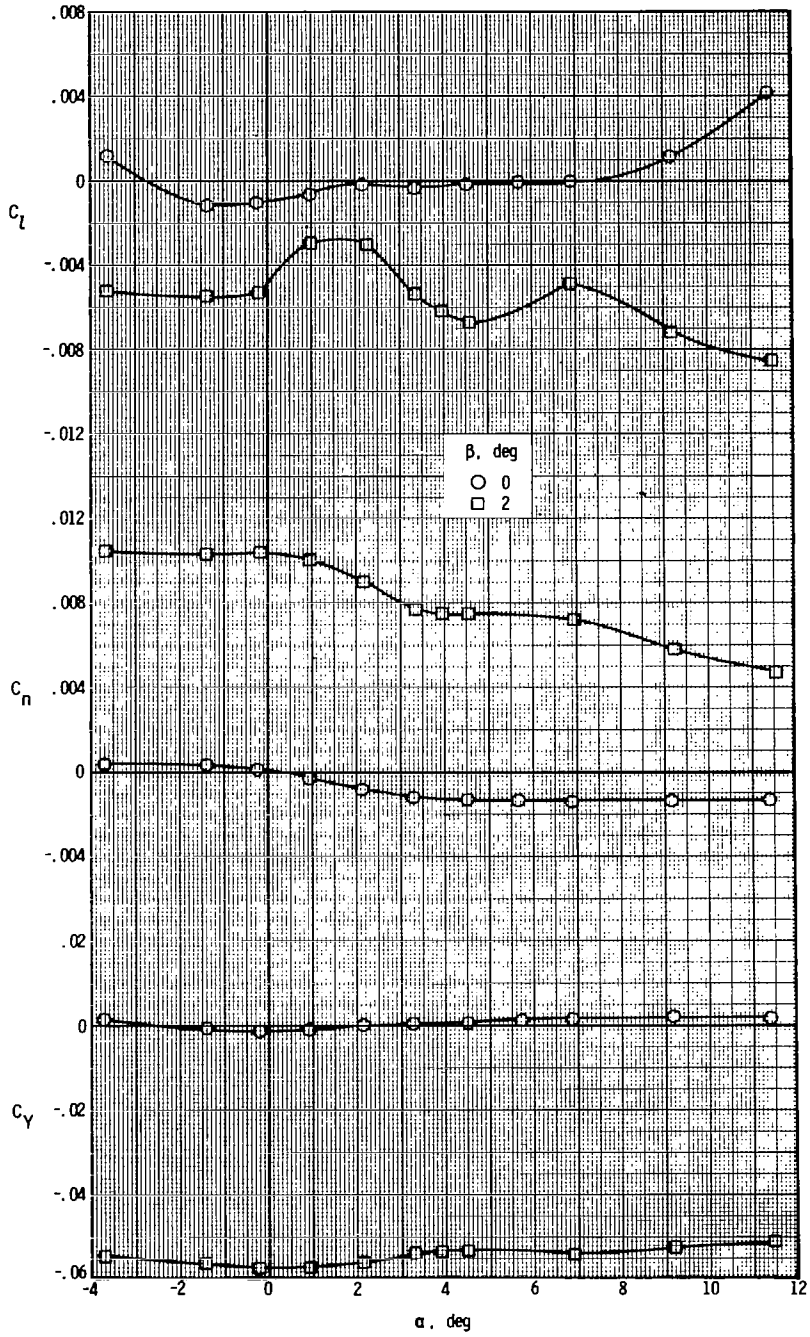

(f) M = 0.980.

Figure 27.- Concluded.

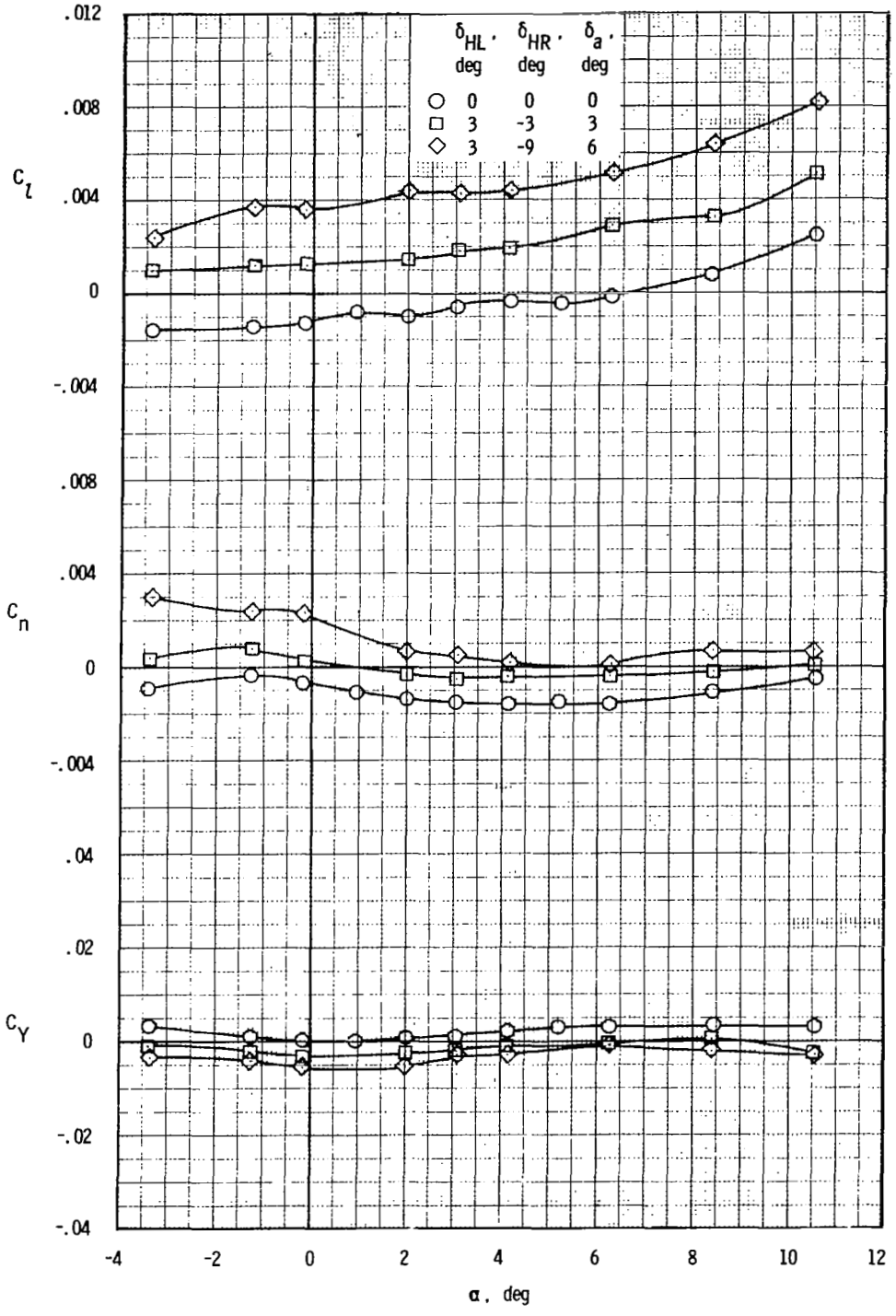

(a) M = 0.400.

Figure 28.- Effect of asymmetric elevon deflections on lateral-directional aerodynamic characteristics. $\beta = 0^{\circ}$.

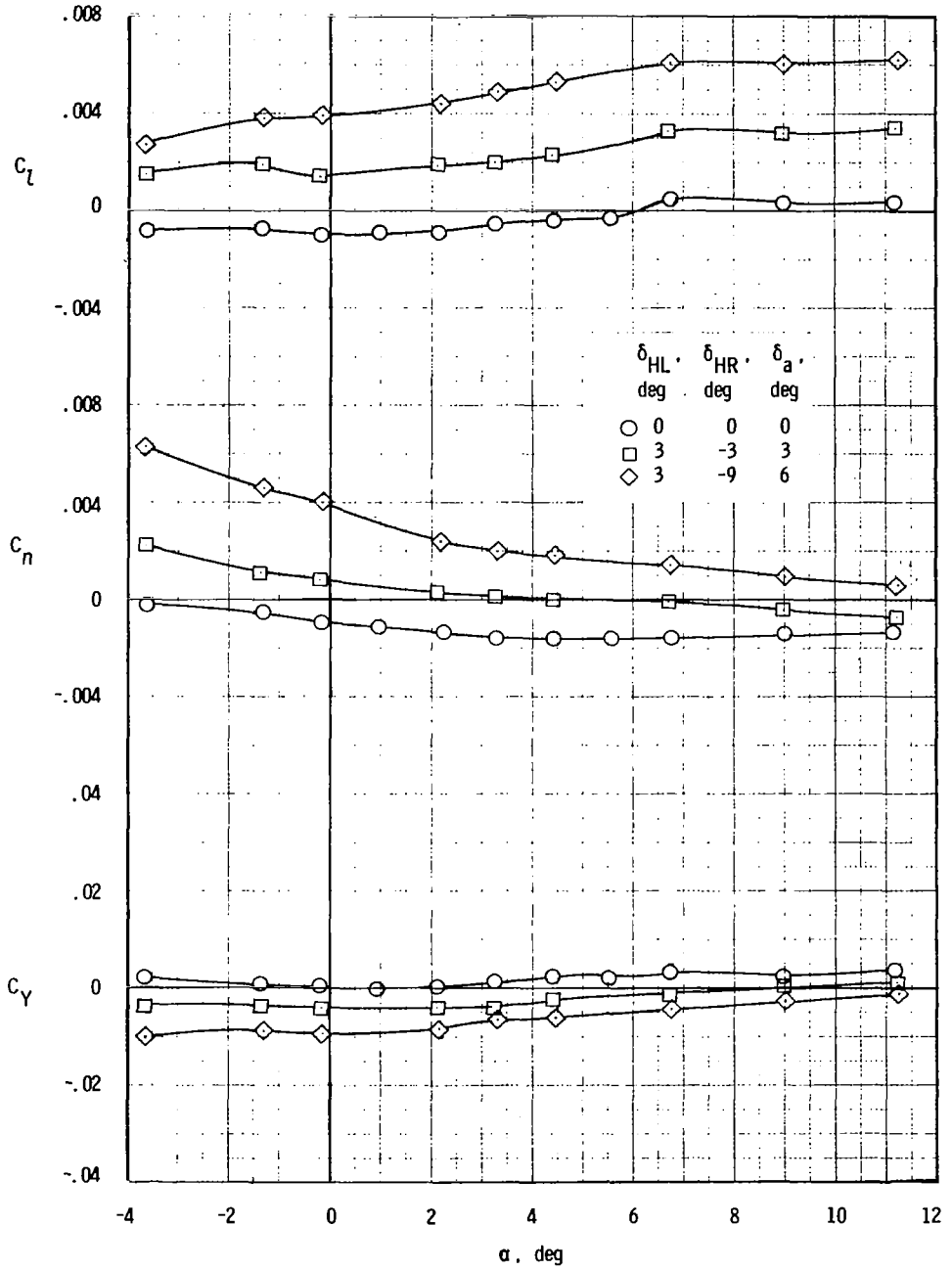

(b) M = 0.800.

Figure 28.- Continued.

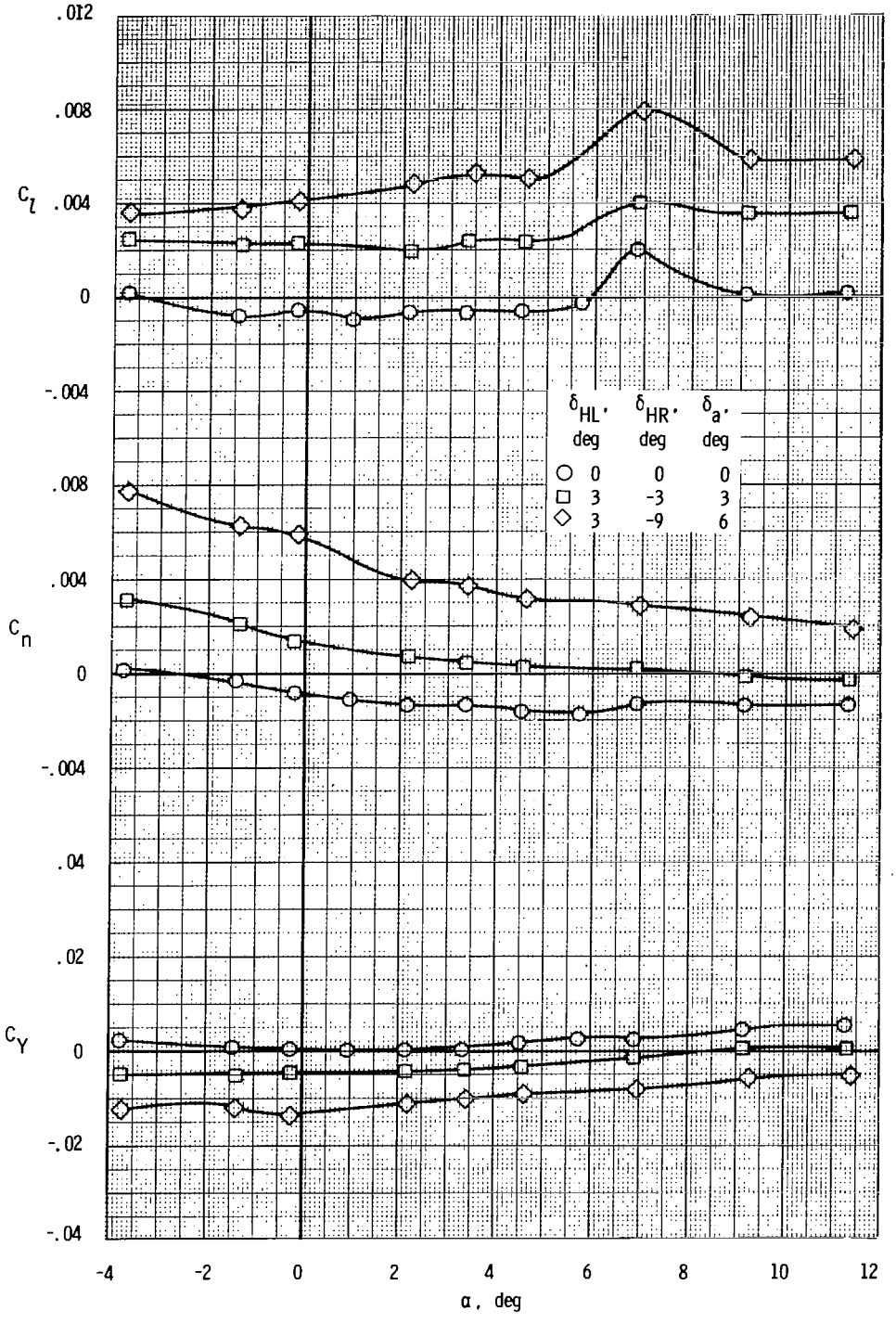

(c) M = 0.900.

Figure 28.- Continued.

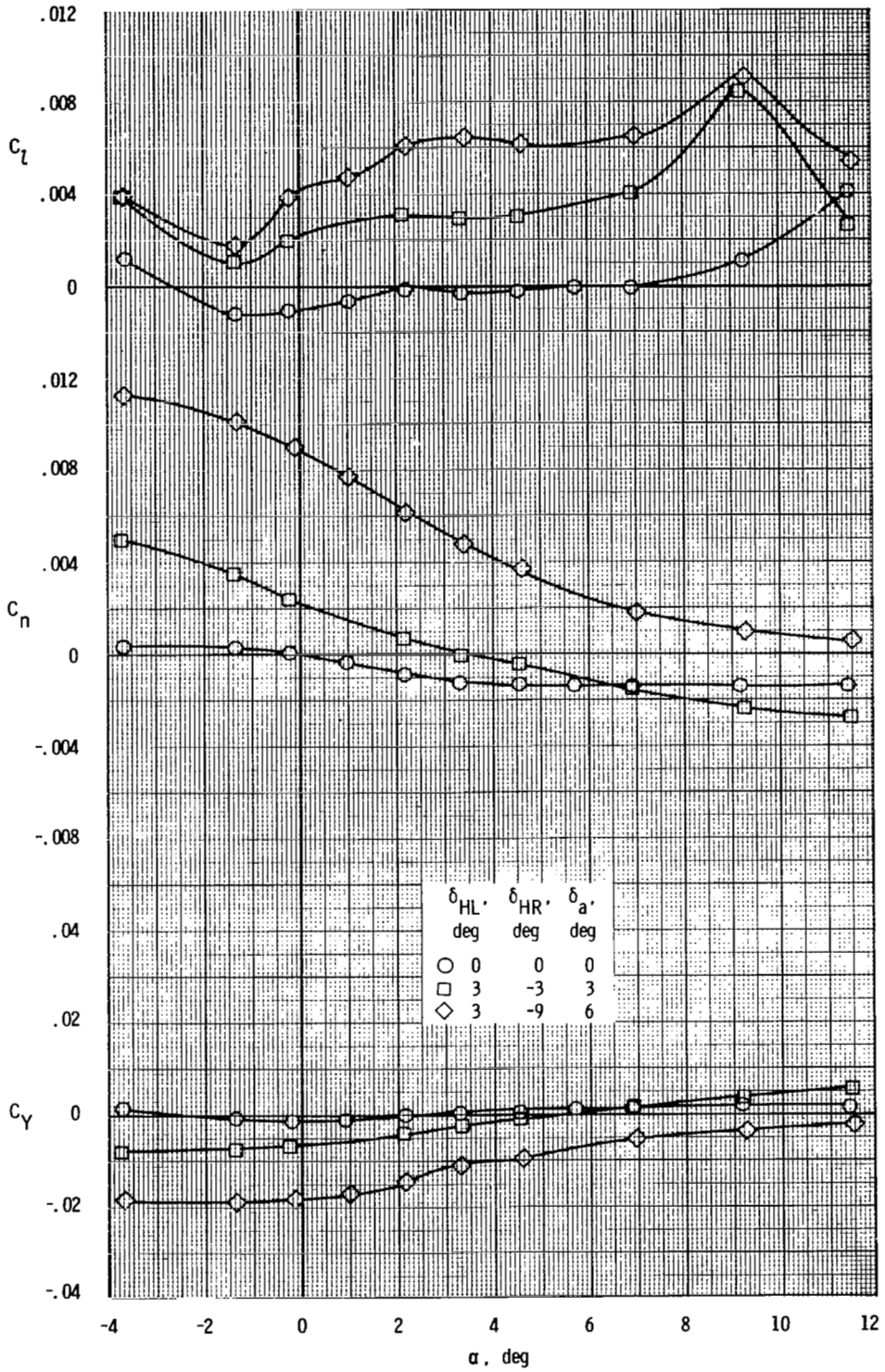

(d) M = 0.980.

Figure 28.- Concluded.

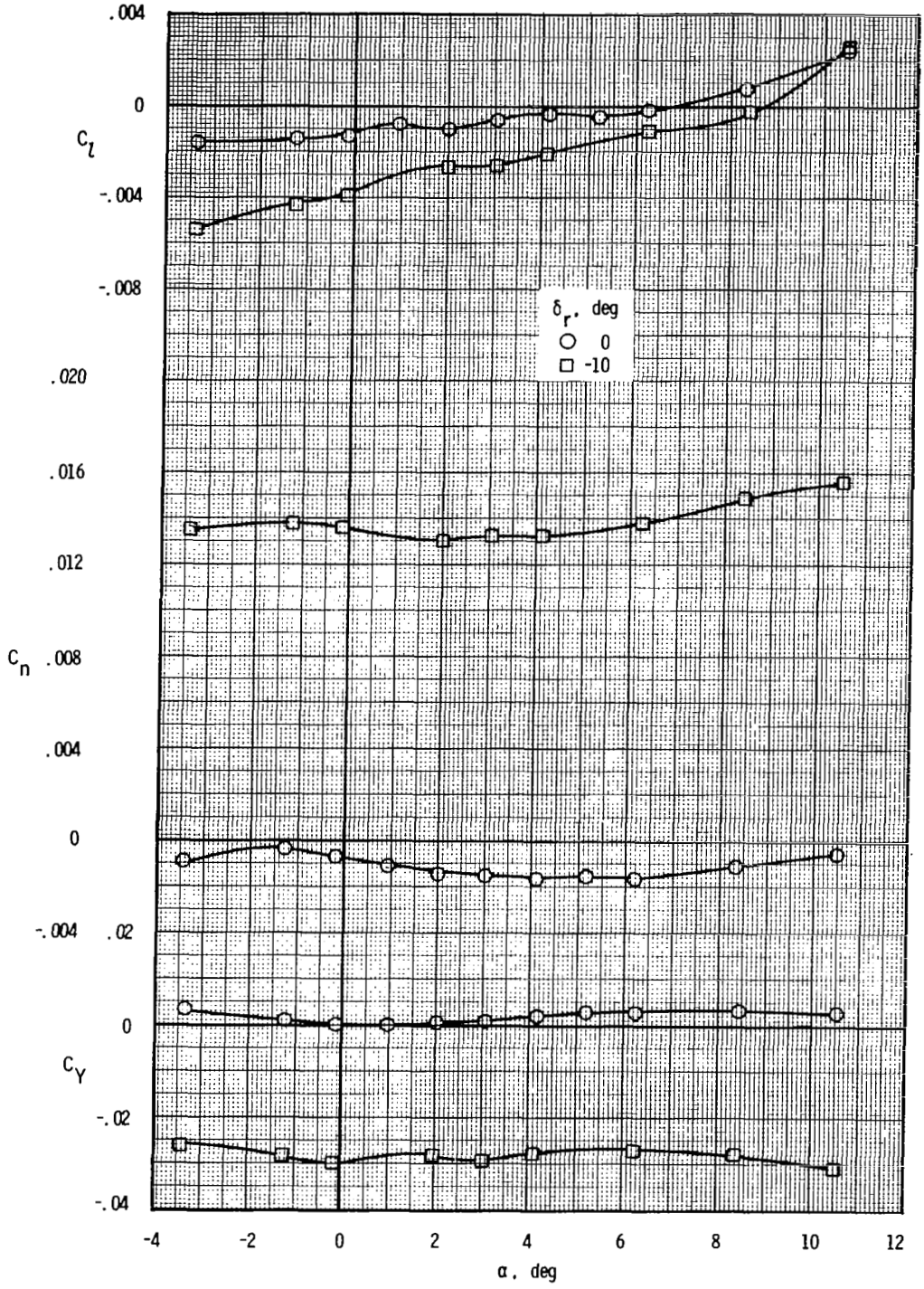

(a) M = 0.400.

Figure 29.- Effect of rudder deflection on lateral-directional aerodynamic characteristics. $\beta = 0^{\circ}$.

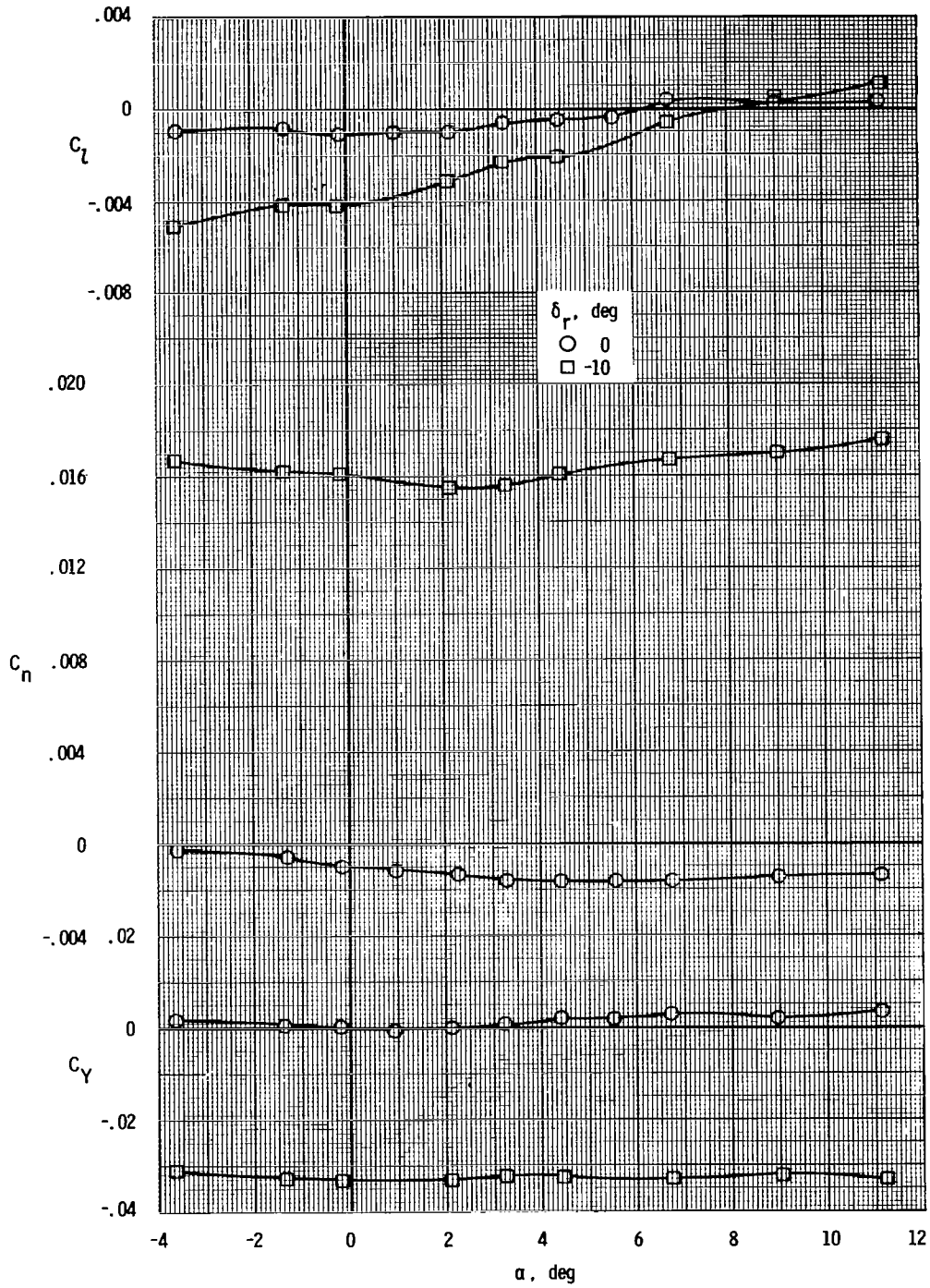

(b) M = 0.800.

Figure 29.- Continued.

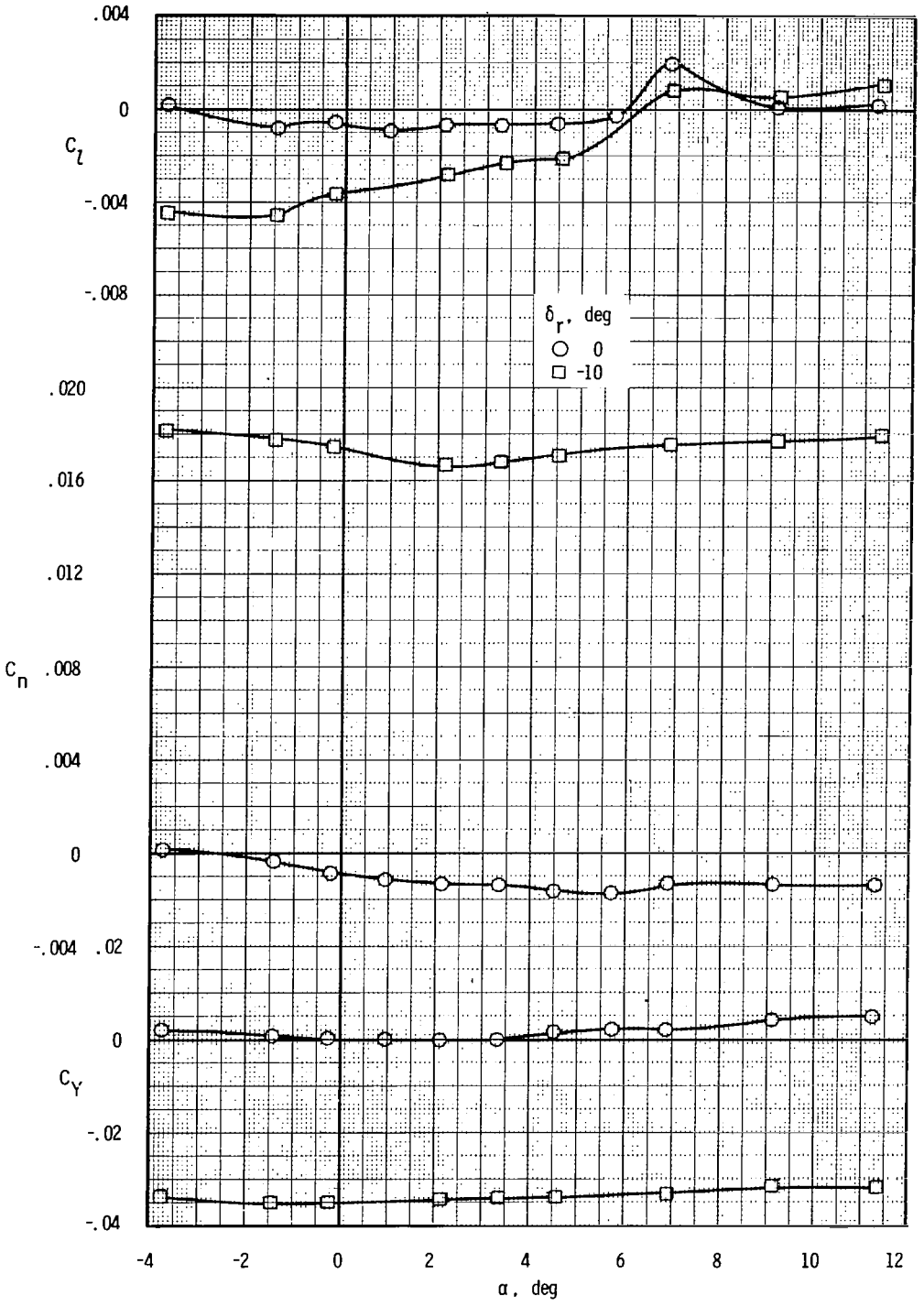

(c) M = 0.900.

Figure 29.- Continued.

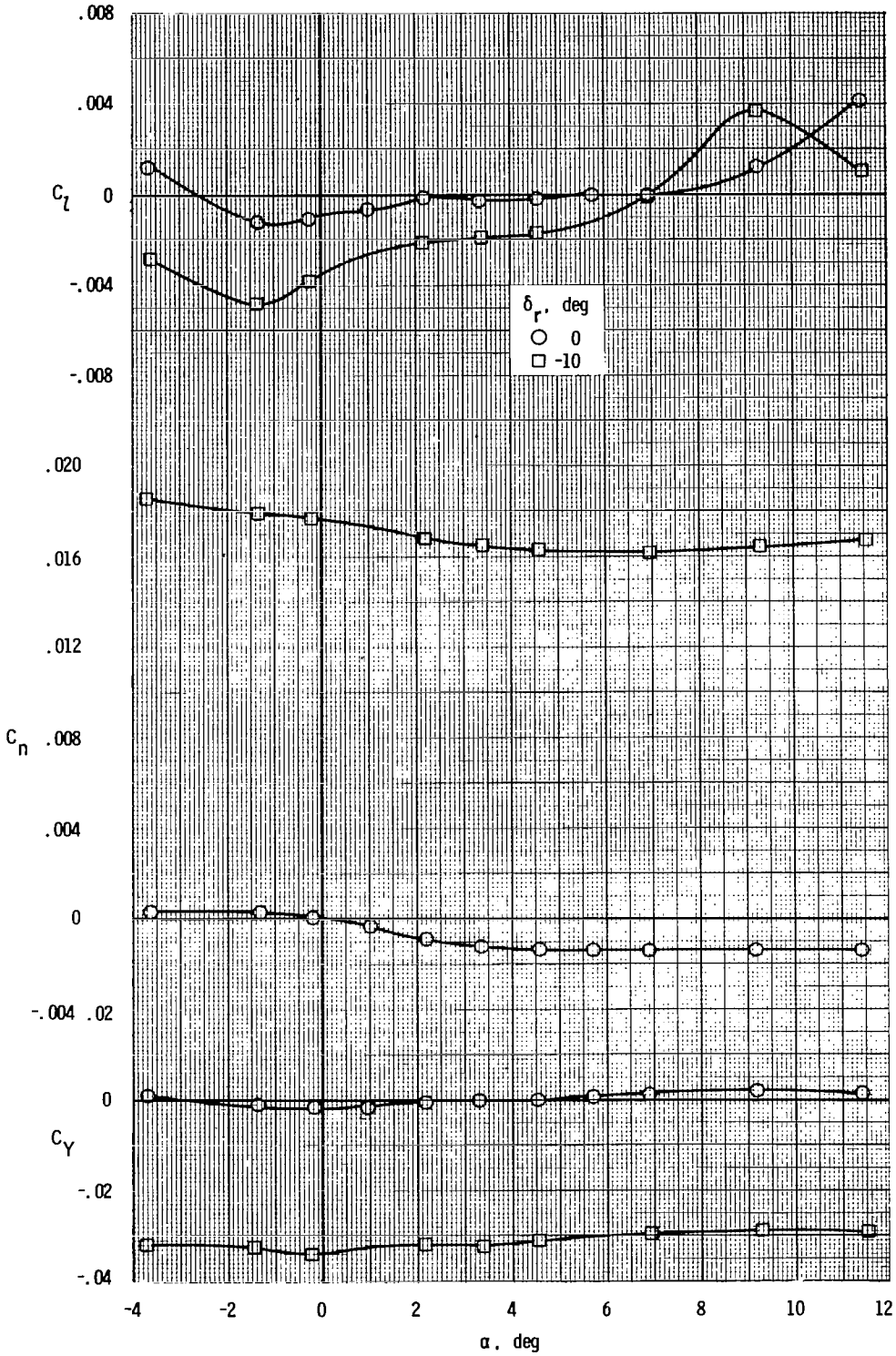

(d) M = 0.980.

Figure 29.- Concluded.

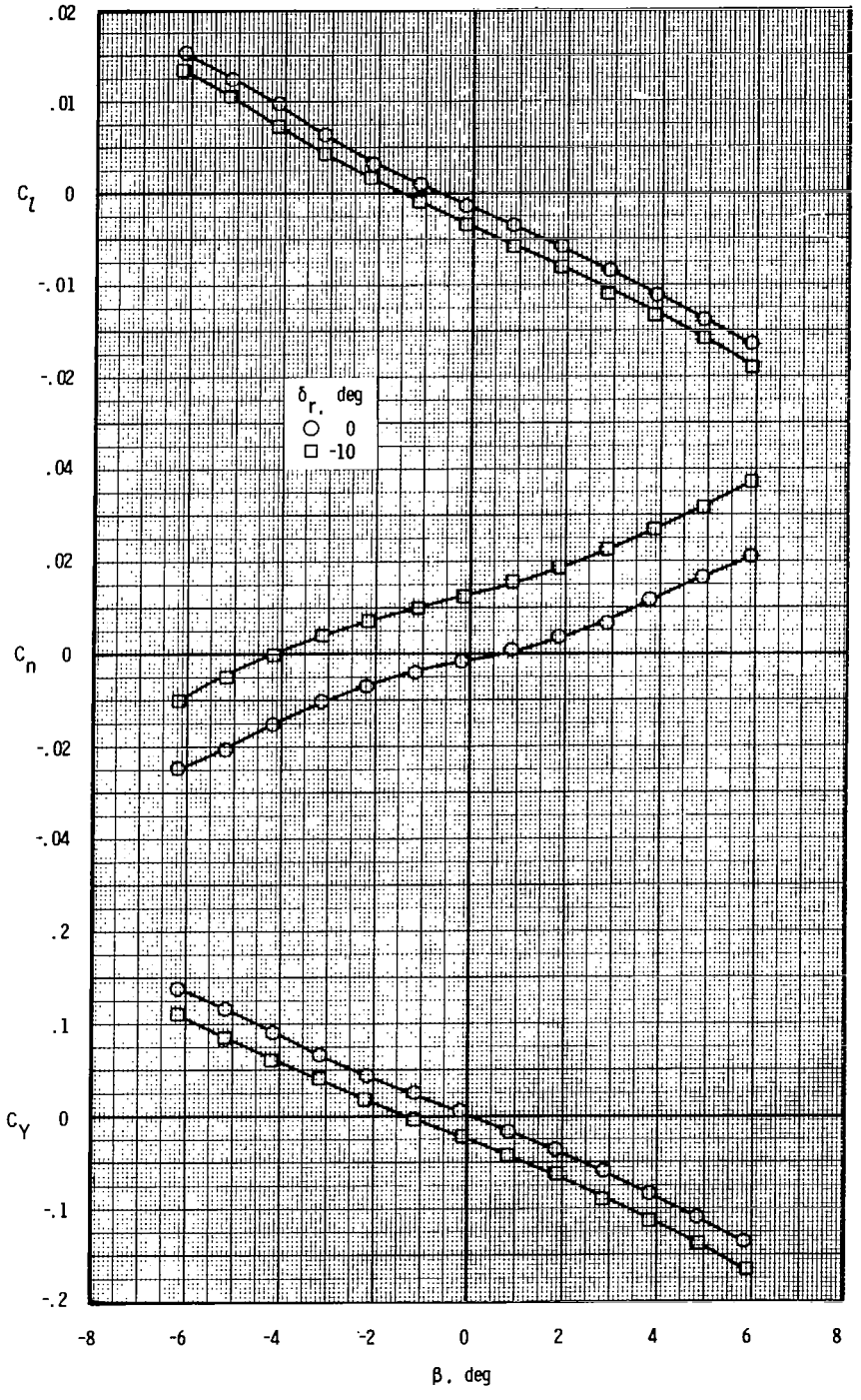

(a) M = 0.400.

Figure 30.- Effect of rudder deflection on lateral-directional aerodynamic characteristics. $\alpha = 2.2^{\circ}$.

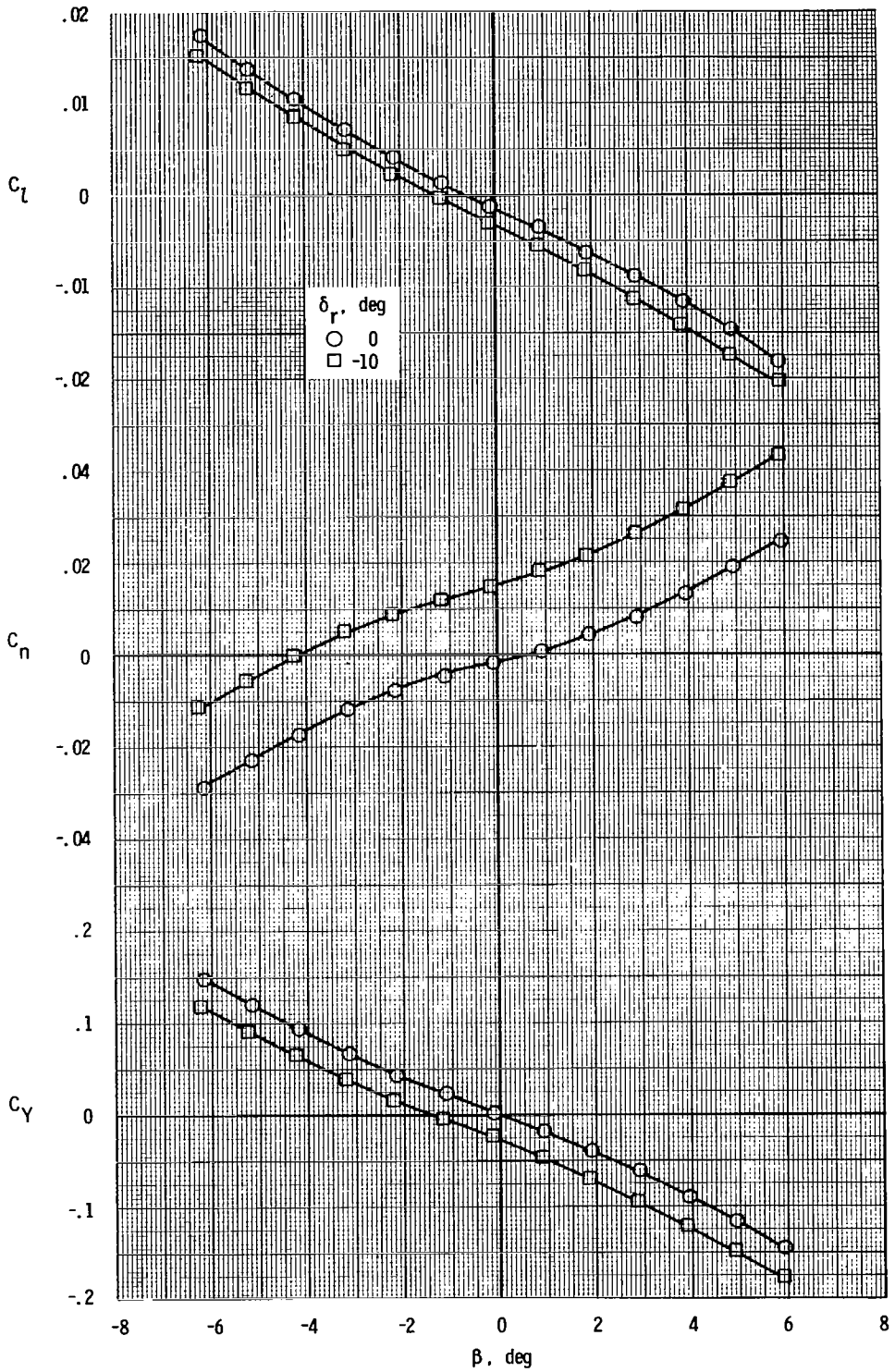

(b) M = 0.800.

Figure 30.- Continued.

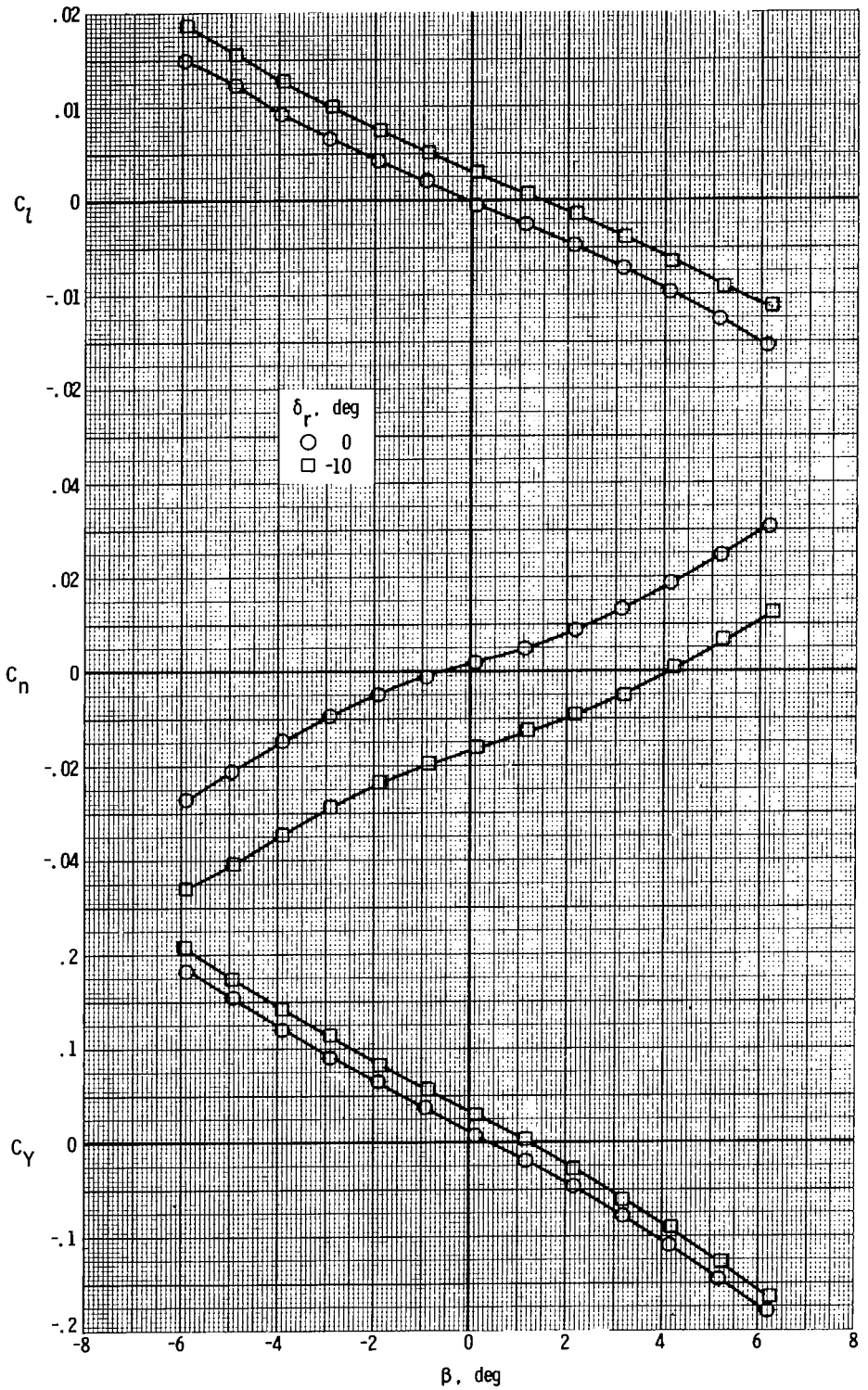

(c) M = 0.900.

Figure 30.- Continued.

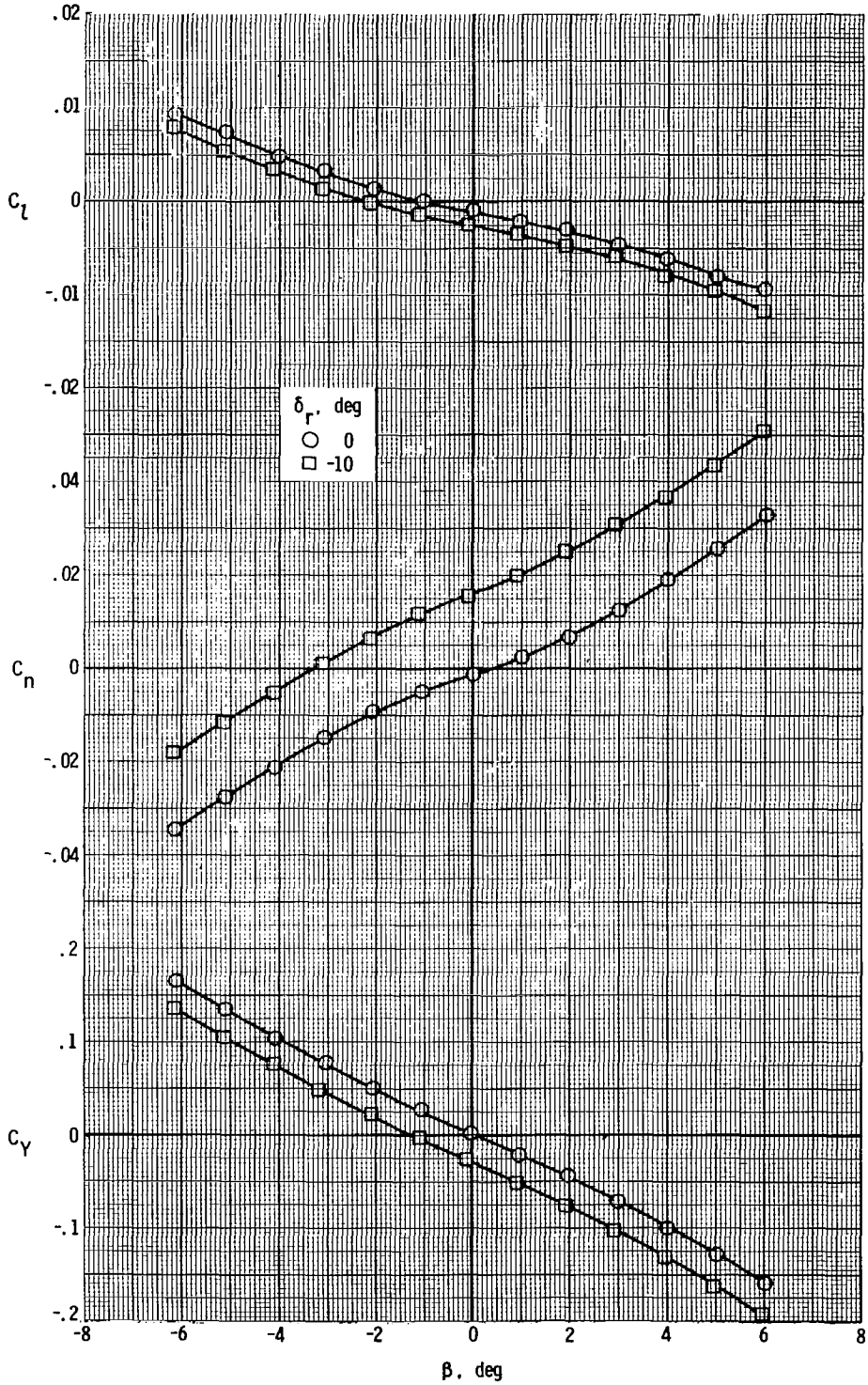

(d) M = 0.980.

Figure 30.- Concluded.

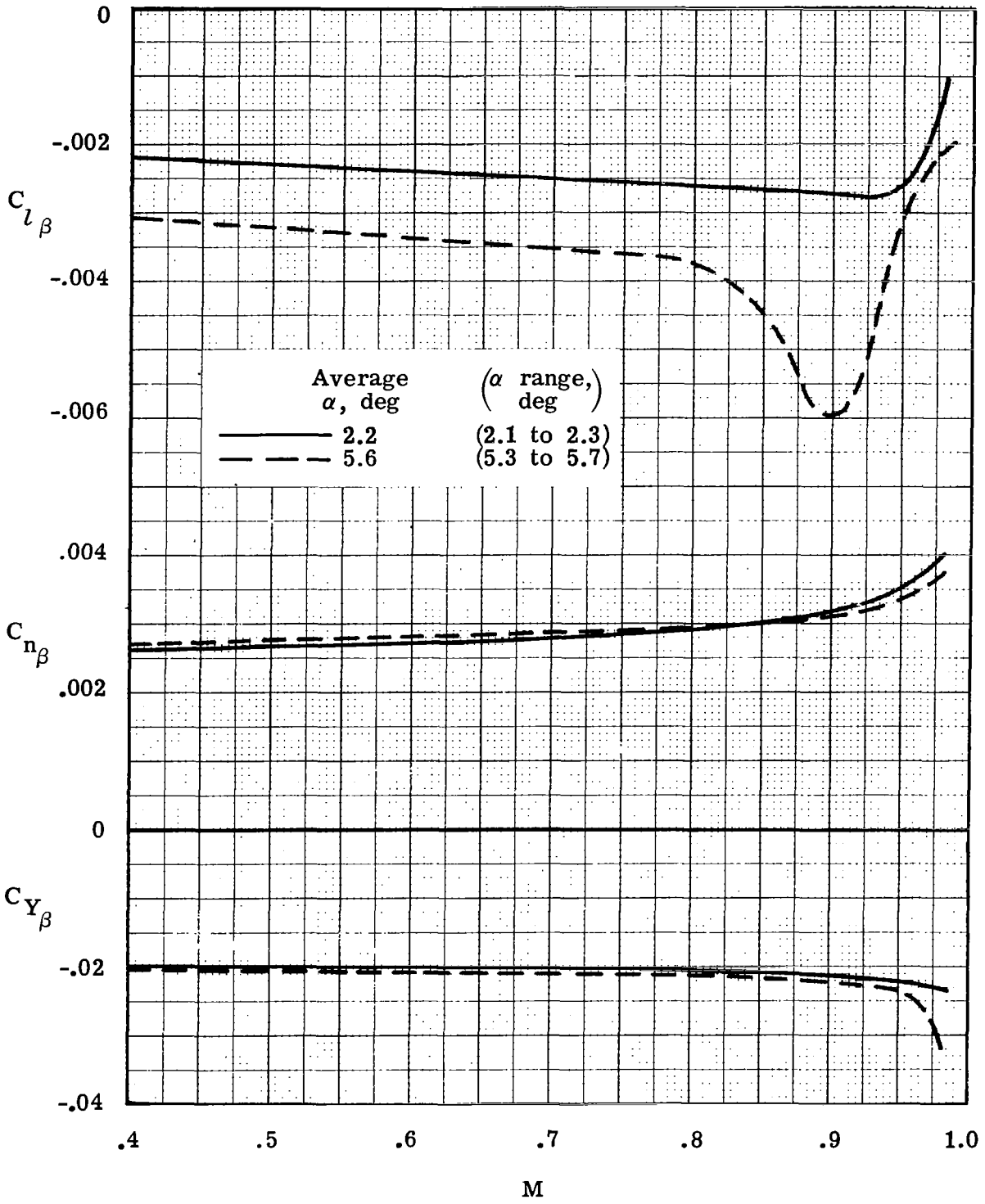

Figure 31.- Variation of lateral-directional stability characteristics with Mach number for two angles of attack.

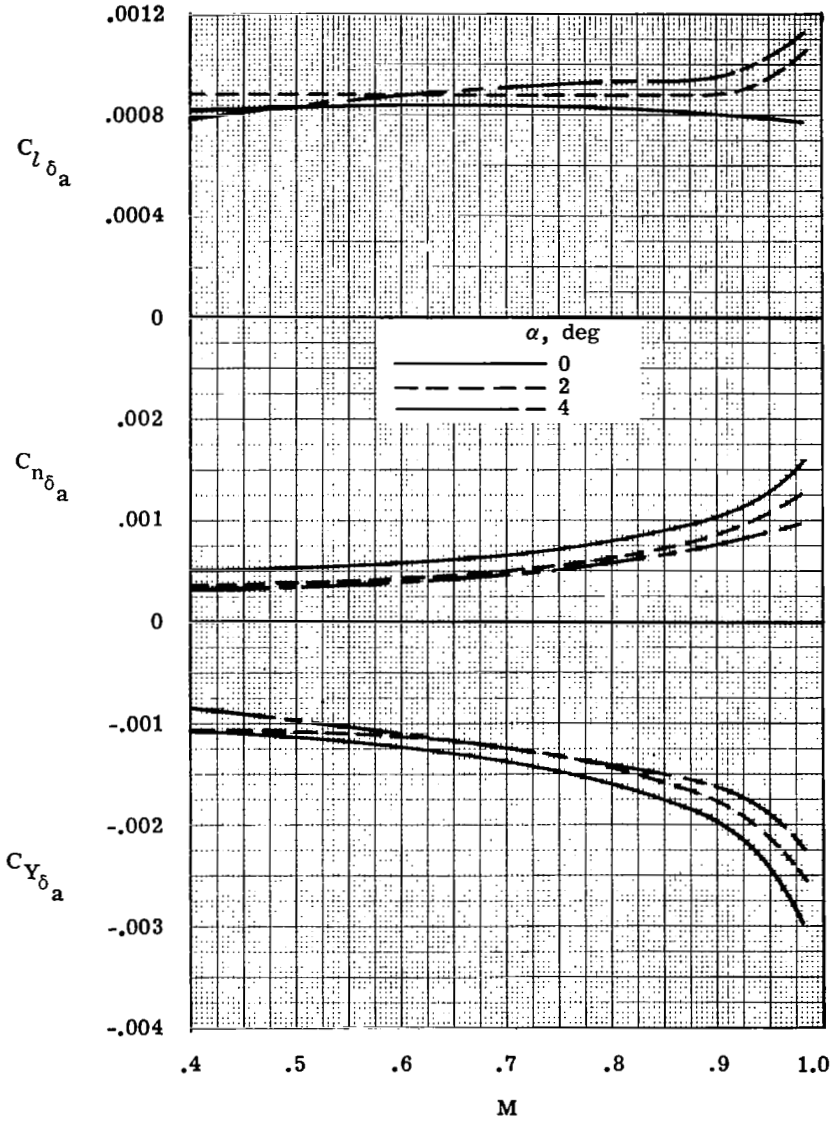

Figure 32.- Variation of roll-control derivatives (asymmetric elevon) with Mach number for three angles of attack. $\beta = 0^{\circ}$.

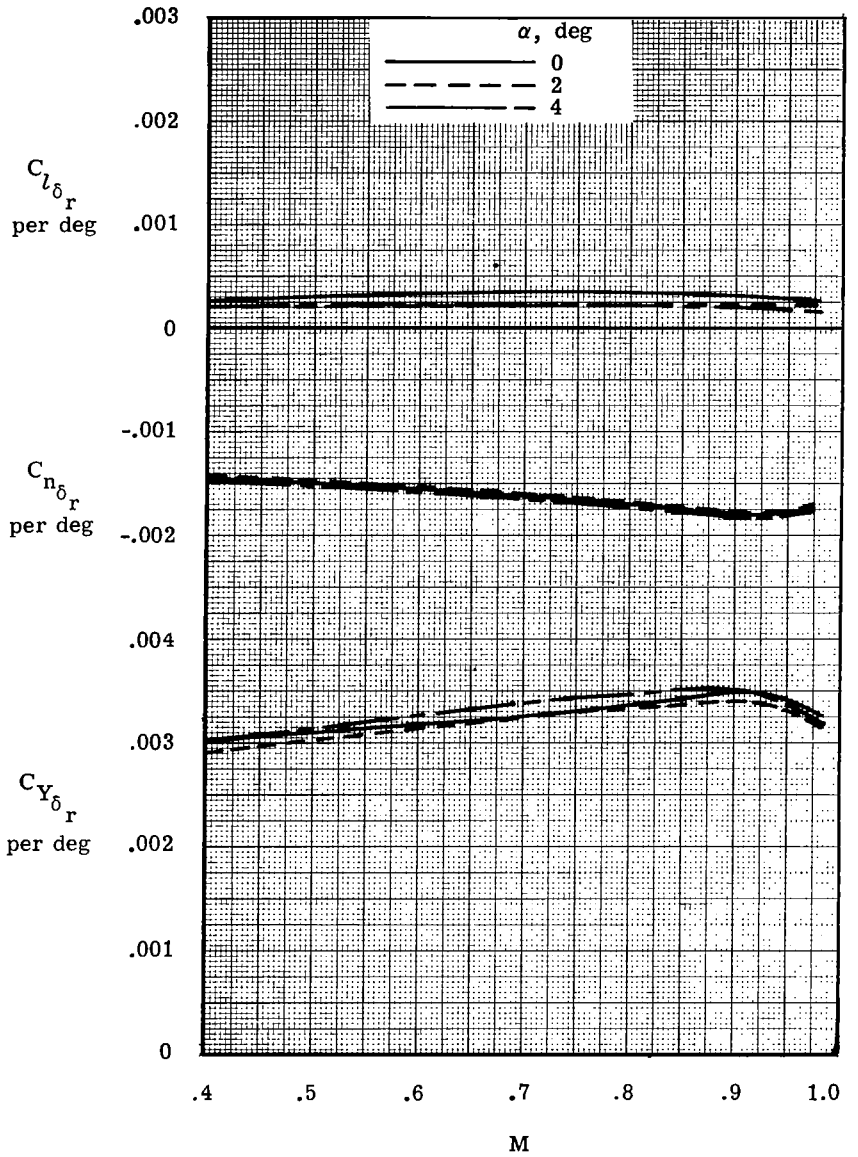

Figure 33.- Variation of lateral-directional rudder-control derivatives with Mach number for three angles of attack.

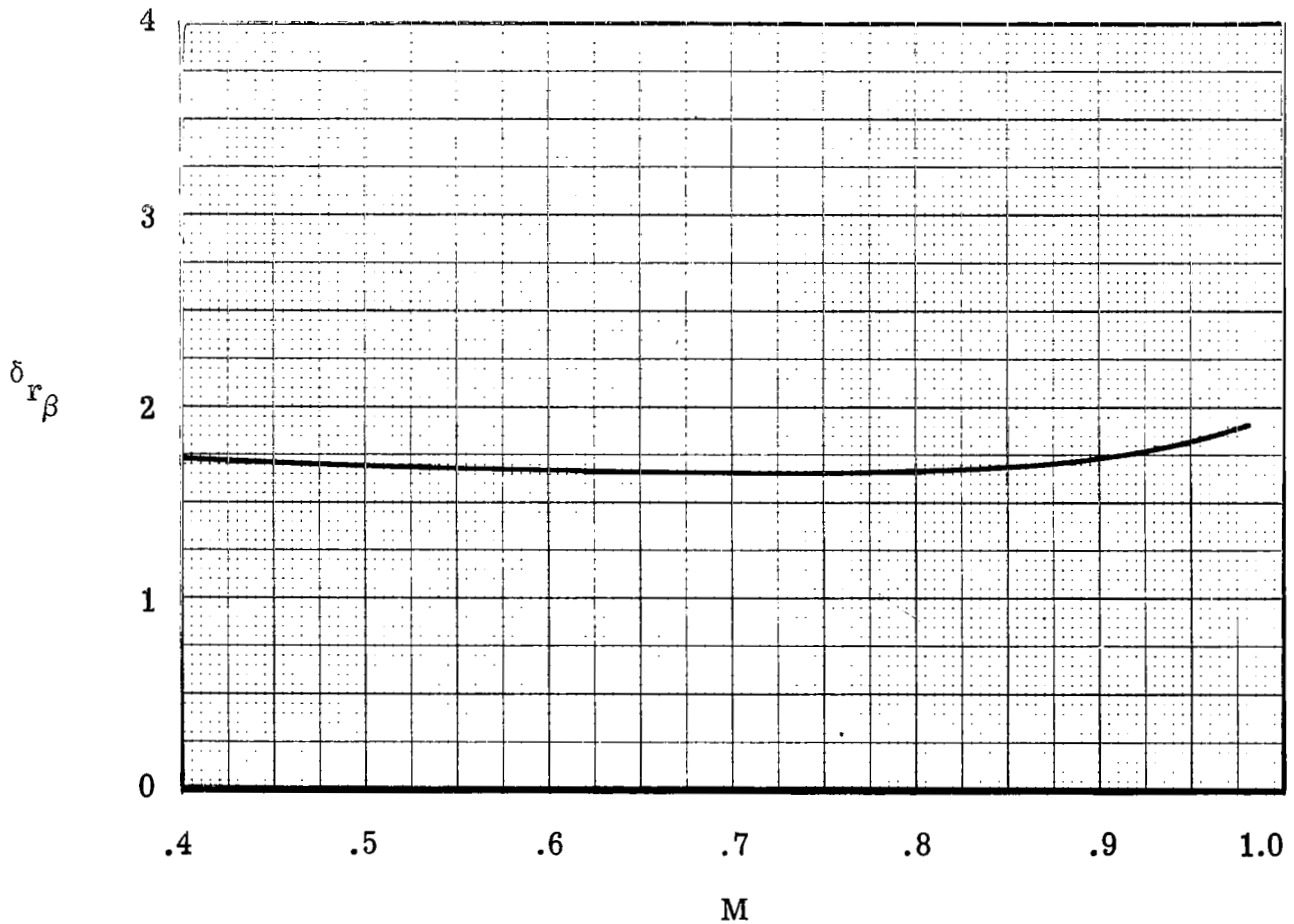

Figure 34.- Variation of rudder-control sensitivity with Mach number. Average α, 2.2°.

1. Report No.	2. Government Accession No.	3. Recipient's Catalog No.
NASA TP-1360		

4. Title and Subtitle	5. Report Date
LONGITUDINAL AND LATERAL STATIC STABILITY AND CONTROL CHARACTERISTICS OF A 1/6-SCALE MODEL OF A REMOTELY PILOTED RESEARCH VEHICLE WITH A SUPERCRITICAL WING	May 1979
	6. Performing Organization Code
7. Author(s)	8. Performing Organization Report No.
Thomas A. Byrdsong and James B. Hallissy	L-12059
9. Performing Organization Name and Address	10. Work Unit No.
NASA Langley Research Center Hampton, VA 23665	505-02-23-02
	11. Contract or Grant No.
12. Sponsoring Agency Name and Address	13. Type of Report and Period Covered
National Aeronautics and Space Administration Washington, DC 20546	Technical Paper
	14. Sponsoring Agency Code

15. Supplementary Notes

16. Abstract

An investigation has been conducted in the Langley 8-foot transonic pressure tunnel to determine the longitudinal and lateral-directional static stability and control characteristics of a 1/6-scale force model of a remotely piloted research vehicle. The model was equipped with a supercritical wing and employed elevons for pitch and roll control. Test conditions were as follows: Reynolds number of about 6.6×10^6 per meter, variations of sideslip from -6° to 6°, elevon deflection angle (symmetrically and asymmetrically) from -9° to 3°, and rudder deflection angle from 0° to -10°. The model was longitudinally statically stable at angles of attack up to about 7°, which is significantly greater than the angle of attack for the cruise condition (approximately 4°). In the range of test Mach numbers, the model was directionally stable and had positive effective dihedral, sufficient pitch control, and positive effectiveness of roll and yaw control.

17. Key Words (Suggested by Author(s))	18. Distribution Statement
Stability and control characteristics Supercritical aerodynamics	FEDD Distribution Subject Category 08

19. Security Classif. (of this report)	20. Security Classif. (of this page)	21. No. of Pages	22. Price
Unclassified	Unclassified	115	

Available: NASA'S Industrial Application Centers

NASA-Langley, 1979